University of Veterinary Medicine Hannover

Institute of Zoology

CSN, Center for Systems Neuroscience Hannover

Input-Output Functions of Sensory Neurons in the Central Nervous System with Focus on the Physiological Basis underlying Information Transfer in the VNLL

THESIS

Submitted in partial fulfilment of the requirements for the degree

Doctor rerum naturalium
(Dr. rer. nat.)

awarded by the University of Veterinary Medicine Hannover

by

Linda Fischer

born in Hamburg

Hannover, Germany 2020

Supervisor: **Prof. Dr. Felix Felmy**

Supervision group: Prof. Dr. Felix Felmy
Prof Dr. Anaclet Ngezahayo
Prof. Dr. Evgeni Ponimaskin

1st evaluation: **Prof. Dr. Felix Felmy**
Institute of Zoology
Division of Neurophysiology and Neuroinfectiology
University of Veterinary Medicine Hannover
Bünteweg 17, 30559 Hannover

Prof. Dr. Anaclet Ngezahayo
Leibniz University Hannover
Institute of Cell Biology and Biophysics
Herrenhäuser Straße 2, 30419 Hannover

Prof. Dr. Evgeni Ponimaskin
Institute of Neurophysiology
Division of Cellular Neurophysiology
Center of Physiology
Hannover Medical School
Carl-Neuberg-Straße 1, 30625 Hannover

2nd evaluation: **PD Dr. Conny Kopp-Scheinpflug**
Ludwig-Maximilians-University Munich
Department for Biology II
Division of Neurobiology
Grosshaderner Straße 2, 82152 Planegg-Martinsried

Date of final exam: 27.03.2020

Listed components of this thesis have been published previously in:

- Fischer, L., et al. (2017). "Intrinsic frequency response patterns in mechano-sensory neurons of the leech." Biol Open **6**(7): 993-999. DOI: 10.1242/bio.023960

- Fischer, L., et al. (2018). "Resonance Properties in Auditory Brainstem Neurons." Front Cell Neurosci **12**: 8. DOI: 10.3389/fncel.2018.00008

Sponsorship:
The VNLL project was financed by the grant FE 789/6-1 (AOBJ: 622960) awarded by the DFG within the priority program 1608 “Ultrafast and temporally precise information processing: normal and dysfunctional hearing”.

Fundraising:

Prof. Dr. Felix Felmy
Institute of Zoology
Division of Neurophysiology and Neuroinfectiology
University of Veterinary Medicine Hannover
Bünteweg 17, 30559 Hannover

Prof. Dr. Christian Leibold
Department Biology II
Ludwig-Maximilians-University Munich
Grosshaderner Str. 2, 82152 Planegg-Martinsried

CONTENTS

List of Figures..... **v**

List of Abbreviations..... **vi**

Summary..... **ix**

Zusammenfassung..... **xi**

Introduction **1**

Neuronal Signalling..... 1

Biophysical Properties of Neuronal Membranes..... 3

Synaptic Transmission in Central Processing..... 6

Animal Models to Investigate Sensory Processing..... 8

Invertebrate Animal Model *H. medicinalis*..... 8

Vertebrate Animal Model *M. unguiculatus*..... 10

Hearing Range..... 10

Mammalian Hearing System..... 11

Mammalian Auditory Brainstem..... 11

Neuronal connections in the auditory brainstem..... 12

The Superior Olivary Complex..... 12

The Lateral Lemniscus..... 14

The Ventral Nucleus of the Lateral Lemniscus (VNLL)..... 16

Physiology of VNLL Neurons..... 17

Mechanisms of Excitatory Postsynaptic Current (EPSC) Kinetics at the VNLL Endbulb..... 19

Glutamatergic Signalling..... 19

Short-Term Plasticity..... 21

Aims..... 21

Publications **23**

Intrinsic Frequency Response Patterns in Mechano-Sensory Neurons of the Leech..... 23

Resonance Properties in Auditory Brainstem Neurons..... 25

Manuscript **27**

Author Contributions…… 27

Synaptic Mechanisms underlying Temporally Precise Information Processing in the VNLL 28

Discussion…… **61**

Conclusion…… **68**

Outlook…… **69**

References…… **70**

Affidavit…… **80**

Acknowledgements…… **81**

LIST OF FIGURES

Fig: 1	Schematic acute brain slice of the auditory brainstem……	16
Fig. 2	EPSC recording at the mature VNLL endbulb……..	19
Fig. 3	AMPA- and NMDARs drive synaptic EPSCs at the VNLL endbulb……	34
Fig. 4	AMPA- and NMDAR mediated short-term plasticity (STP) is frequency dependent.	37
Fig. 5	Boltzmann fit for NMDAR mediated currents……	38
Fig. 6	Decomposing AMPA- and NMDA component……	39
Fig. 7	NMDAR mediated currents promote firing at high stimulation frequencies……..	41
Fig. 8	Action potential (AP) generation depends on input conductance……	42
Fig. 9	AP generation at 400 Hz stimulation frequency is feasible……..	43
Fig. 10	Temporal precision depends on input conductance and history……..	46
Fig. 11	Pseudorandomly distributed frequency stimulation (PrDF) I: Stimulation intensity and NMDA impact temporal precision……..	48
Fig. 12	PrDF II: Frequency and intensity in concert impact AP generation……	51
Fig. 13	AP integration in paired-pulse stimulation arrangement depends on stimulation frequency and –intensity, not on NMDA mediated currents……..	53

LIST OF ABBREVIATIONS

ACh	Acetylcholine
AFS	Afferent Fibre Stimulation
AMPA	α-Amino-3-Hydroxy-5-Methyl-4-Isoxazoleprionic Acid
ANF	Afferent Nerve Fibre
AP	Action Potential
AVCN	Antero-Ventral Cochlear Nucleus
BC	Bushy Cell
c	contralateral
CC	Current-clamp
C_m	Membrane Capacitance
CN	Cochlear Nucleus
CNS	Central Nervous System
d	dorsal
DCN	Dorsal Cochlear Nucleus
DNLL	Dorsal Nucleus of the Lateral Lemniscus
E_m	Resting Potential
EPSC	Excitatory Postsynaptic Current
GABA	*γ*-Aminobutyric Acid
GC	Conductance-clamp
GluR	Glutamate Receptor
HCN	Hyperpolarisation-activated Cyclic Nucleotide Cation Channel
i	Ipsilateral
IC	Inferior colliculus
I_h	Hyperpolarisation-activated nonspecific cation conductance
ILD	Interaural Level Difference
INLL	Intermediate Nucleus of the Lateral Lemniscus
IPSC	Inhibitory Postsynaptic Current
ITD	Interaural Time Difference
ISI	Inter Stimulus Interval
KA	Kainate
K_v	Voltage-gated Potassium Channel
LL	Lateral Lemniscus
LNTB	Lateral Nucleus of the Trapezoid Body
LSO	Lateral Superior Olive
MGB	Medial Geniculate Nucleus
MNTB	Medial Nucleus of Trapezoid Body
MSO	Medial Superior Olive
Na_v	Voltage-gated Sodium Channel
NMDA	N-Methyl-D-Aspartate
OC	Octopus Cell
OCA	Octopus Cell Area
PSC	Postsynaptic Current
PVCN	Posterior-Ventral Cochlear Nucleus
R	Receptor
R_f	Resonance Frequency
R_m	Membrane Input Resistance
SOC	Superior Olivar Complex

SPN	Superior Paraolivary Nucleus
STD	Short-Term Depression
STF	Short-Term Facilitation
STP	Short-Term Plasticity
τ_m	Membrane Time Constant
τ_s	Steady State Membrane Time Constant
v	ventral
VC	Voltage-Clamp
VNLL	Ventral Nucleus of the Lateral Lemniscus
ZAP	Impedance Amplitude Profile

SUMMARY

University of Veterinary Medicine Hannover
Center for Systems Neuroscience (CSN)
Institute of Zoology

Doctor rerum naturalium
(Dr. rer. nat.)

Input-Output Functions of Sensory Neurons in the Central Nervous System with Focus on the Physiological Basis underlying Information Transfer in the VNLL

by Linda Fischer

This thesis pursued two objectives, comprising first the demonstration of the universality of intrinsically tuned input-output functions of neurons in the central nervous system (CNS) involved in sensory information processing. The second objective targeted the detailed examination of the physiological basis underlying temporally precise information transfer in one selected neuron population located in the ventral part of the mammalian ventral nucleus of the lateral lemniscus (vVNLL), which is involved in auditory processing.

Neuronal intrinsic tuning to specific stimulus characteristics is a widely distributed feature for central filtering of incoming sensory information, for example on the level of intrinsic frequency tuning. This feature enables the generation of frequency filter banks allowing for accurate central segregation and processing of sensory inputs. In order to show the universality of neuronal intrinsic frequency tuning across vertebrates and invertebrates and across different sensory systems, intracellular recordings were performed in three types of mechano-sensory neurons of the leech segmental ganglia as well as whole-cell patch-clamp recordings in a selection of neuron populations located in the mammalian auditory brainstem comprising neurons of the medial and lateral superior olive (MSO and LSO) and of the vVNLL. All perform different tasks of auditory information processing. Frequency tuning was evaluated on the sub- and supra-threshold level, in the form of subthreshold membrane potential resonance in mammalian neurons and action potential (AP) generation rates in leech neurons. Membrane potential resonance defines a well-studied intrinsically tuned dynamical feature to amplify specific input frequencies on the basis of subthreshold membrane potential oscillations. Neurons exhibiting membrane depolarising subthreshold resonance respond stronger to stimuli close to their resonance frequency (R_f), and weaker to stimuli that differ from their R_f.

The results reveal neuronal intrinsic frequency tuning in both animal models: for the first time mechano-sensory neurons in leech were characterised according to their frequency excitability profile revealing low-, band- and high pass filter profiles. Furthermore, mammalian auditory brainstem neurons revealed population specific R_f. Together with intrinsic intensity tuning, R_f seems to be

important for central stimulus processing in the mammalian CNS. In all tested neuron types, the high frequency membrane depolarising R_f only depended on one single fit parameter β, which is traced to the membrane leakiness. R_f is apparently mandatory in neurons with leaky membranes and fast membrane decay times as they occur in the tested mammalian auditory brainstem neurons. The study shows the physiological basis for membrane resonance in MSO and LSO neurons, which is attributed to the activity of hyperpolarisation-activated cyclic nucleotide cation (HCN) channels for the low frequency membrane hyperpolarising R_f. The high frequency membrane depolarising R_f, on the other hand, is most likely mediated by potassium channels. Importantly, it is the first time that HCN channels have been shown to be involved in subthreshold resonance in juvenile MSO neurons.

The second objective of this thesis investigated the physiological basis of synaptic information transfer. In the VNLL there is a large somatic synapse formed by axons emerging from octopus cells of the cochlear nucleus, and projecting to globular VNLL neurons. At the VNLL endbulb, excitatory postsynaptic currents (EPSCs) decay fast, rendering this synapse an optimal target structure for the investigation of synaptic mechanisms mediating temporally accurate information processing.

Supra-threshold responses in VNLL neurons are locked to the stimulus onset and can transition into high firing rates during ongoing amplitude modulated (AM) stimulation. Somatic whole-cell patch-clamp recordings revealed the physiological basis for this firing behaviour, verifying a bi-exponentially decaying EPSC mediated by alpha-amino-3-hydroxy-5-methyl-4-isoxazolepropionate receptors (AMPARs) and N-methyl-D-aspartate receptors (NMDARs). These excitatory synaptic currents were hypothesised to be a key feature for rapid and precise information transfer at the VNLL endbulb. Obtained results point towards the assumption that frequency dependent short-term plasticity (STP) of these EPSCs, which is manifested in short-term facilitation (STF) for paired pulses followed by a persistent short-term depression (STD) phase, ensures temporally precise postsynaptic AP generation in VNLL neurons at physiologically relevant levels. Thereby, STF supports faithful onset inhibition provided by VNLL neurons to neurons in the downstream inferior colliculus, whereas STD supports the filtering out of high frequency inputs. Prolonged inhibition to downstream structures during ongoing stimulation is supported by NMDAR mediated build-up currents counteracting STD. In correspondence with identified low R_f values in VNLL neurons this outcome suggests that VNLL neurons are involved in information transmission of low frequency AM stimulus envelope structures, as they occur in conspecific vocalisation. The research conducted within this thesis yielded two publications and one manuscript, describing the detailed experimental procedures, obtained results, data analyses and interpretations.

ZUSAMMENFASSUNG

Tierärztliche Hochschule Hannover
Zentrum für Systemische Neurowissenschaften (ZSN)
Institut für Zoologie

Doctor rerum naturalium
(Dr. rer. nat.)

Eingangs-Ausgangs Beziehungen sensorischer Neurone des Zentralen Nervensystems, mit dem Schwerpunkt auf der physiologischen Basis für Informationstransfer im VNLL

von Linda Fischer

Diese Thesis behandelte zwei Aspekte: erstens die Universalität intrinsisch abgestimmter Eingangs-Ausgangsfunktionen von Neuronen des zentralen Nervensystems (ZNS), welche an der sensorischen Informationsverarbeitung beteiligt sind. Zweitens die detaillierte Untersuchung der physiologischen Basis von zeitlich präziser Informationsweitergabe, anhand einer ausgewählten Neuronenpopulation im ventralen Teil des Ventralen Kerns des Lateralen Lemniscus‘ (vVNLL) eines Säugers, welche in die auditorische Verarbeitung involviert ist.

Das intrinsische Abstimmen von Neuronen auf bestimmte Stimulus-Charakteristika ist eine weit verbreitete Funktion für das neuronale zentrale Filtern eingehender sensorischer Information, beispielsweise auf der Ebene intrinsischer Frequenzabstimmung. Sie ermöglicht die Einrichtung von Frequenz-Filterbanken, welche die akkurate zentrale Diskriminierung und Verarbeitung sensorischer Eingänge ermöglichen. Um die Universalität neuronaler intrinsischer Frequenzabstimmung über Vertebraten und Invertebraten und über verschiedene sensorische Systeme hinweg zu demonstrieren, wurden intrazelluläre Ableitungen in drei Typen mechano-sensorischer Neurone in Segmentganglien des Blutegels, sowie Ganz-Zell Patch-Clamp Ableitungen in einer Auswahl von Neuronenpopulationen im auditorischen Hirnstamm von Säugetieren durchgeführt. Letztere umfasste Neurone der medialen und lateralen superioren Olive (MSO und LSO) und des vVNLL, welche unterschiedliche Aufgaben bei der auditorischen Informationsverarbeitung übernehmen. Neuronale Frequenzabstimmung wurde sowohl auf dem unter- als auch auf dem überschwelligen Level untersucht, und zwar in Form von unterschwelliger Membranpotenzialresonanz in Säugetier- und in Form von Aktionspotenzialraten in Blutegelneuronen. Membranpotenzialresonanz ist eine gut erforschte intrinsisch abgestimmte dynamische Funktion zur Amplifizierung spezifischer Eingangsfrequenzen und basiert auf unterschwelliger Membranpotenzialoszillation. Neurone, die membrandepolarisierend unterschwellig resonieren, antworten stärker auf Stimuli nahe ihrer Resonanzfrequenz (R_f) und schwächer auf Stimuli, die sich von ihrer R_f unterscheiden.

Die Ergebnisse zeigen neuronale intrinsische Frequenzabstimmung in beiden Tiermodellen: Zum ersten Mal wurden mechano-sensorische Neurone im Blutegel entsprechend ihrer frequenzabhängigen Erregbarkeitsprofile charakterisiert, welche Tief-, Band- und Hochpassfiltereigenschaften zeigten. Darüber hinaus zeigten Neurone des auditorischen Hirnstamms in Säugetieren populationsspezifische R_f. Zusammen mit intrinsischer Intensitätsabstimmung, scheint die R_f von hoher Wichtigkeit für die zentrale Stimulusdiskriminierung im ZNS der Säugetiere zu sein. In allen hier getesteten Neuronentypen hing die hochfrequente membrandepolarisierende R_f von einem einzigen Parameter β ab, welcher auf die Undichtheit der Membran und auf schnelle Membranzeitkonstanten zurückzuführen ist, wie sie in den getesteten auditorischen Hirnstammneuronen vorkommen. Diese Studie zeigte ferner die physiologische Basis der Membranresonanz in MSO und LSO Neuronen, welche im Falle tieffrequenter membranhhyperpolarisierender R_f aktiven hyperpolarisations-aktivierten zyklischen Nukleotid Kation (HCN) Kanälen beigemessen wurde. Die hochfrequente membrandepolarisierende R_f ist höchstwahrscheinlich Kaliumkanälen zuzuschreiben. Es ist das erste Mal, dass HCN Kanäle im Zusammenhang mit Resonanz bei juvenilen MSO Neuronen nachgewiesen wurden.

Der zweite Aspekt dieser Thesis untersuchte die physiologische Basis des synaptischen Informationstransfers. Im VNLL gibt es eine große somatische Synapse, welche von Axonen geformt wird, die von Oktopus-Zellen des cochleären Nukleus entspringen und welche auf globuläre VNLL Neurone projizieren. An dieser Synapse klingen exzitatorische postsynaptische Ströme (EPSCs) schnell ab, was diese Synapse, die zeitlich akkurate Informationsverarbeitung vermittelt, zu einer optimalen Zielstruktur zur Untersuchung synaptischer Mechanismen macht.

Überschwellige Antworten von VNLL Neuronen erfolgen zu Stimulus Beginn. Darüber hinaus können sie bei anhaltender Amplitudenmodulierter (AM) Stimulation hohe Feuerraten generieren. Somatische Ganz-Zell Patch-Clamp Ableitungen zeigten die physiologische Basis dieses Feuerverhaltens, und verifizierten ein bi-exponentiell abfallendes EPSC, vermittelt von alpha-amino-3-hydroxy-5-methyl-4-isoxazolepropionsäure Rezeptoren (AMPARs) und N-methyl-D-Aspartat Rezeptoren (NMDARs). Es wurde angenommen, dass diese exzitatorischen synaptischen Ströme eine Schlüsseleigenschaft des schnellen und präzisen Informationstransfers an der VNLL Synapse sind. Die erhaltenen Ergebnisse deuten darauf hin, dass die frequenzabhängige Kurzzeitplastizität (STP) der EPSCs, welche sich in Form von Kurzzeitfaszilitierung (STF) für paarige Pulse gefolgt von einer Kurzzeitdepression (STD) ausdrückt, zeitlich präzise Aktionspotentialgenerierung in VNLL Neuronen auf physiologisch relevanten Ebenen sicherstellt. Dabei unterstützt die STF sichere Anfangsinhibition, welche die VNLL Neurone für Neurone des nachgeschalteten Inferioren Colliculus bereitstellen, und die STD das Herausfiltern hochfrequenter Eingänge. Während hochfrequenter Stimulation wird durch die Anhäufung NMDAR vermittelter Ströme anhaltende Inhibition zu nachgelagerten Strukturen bereitgestellt, die der STD

entgegenwirken. Zusammen mit der identifizierten niedrigen R_f, legen die Ergebnisse nahe, dass VNLL Neurone in der Informationsweitergabe tieffrequenter umhüllender Strukturen von AM Stimulationen involviert sind, wie sie bei der intraspezifischen Vokalisation vorkommen. Diese Thesis ergab zwei Publikationen und ein Manuskript, welche die experimentellen Methoden, erhaltenen Ergebnisse, Datenanalysen und –Interpretationen beschreiben.

INTRODUCTION

Every animal is in continuous contact with the environment, perceiving and processing chemical and physical stimuli through sensory systems. Stimulus perception is implemented by specific sensory organs. In vertebrates and bilaterally symmetric invertebrates the received information is transferred via afferent nerve fibres to the central nervous system (CNS) where information is processed and subsequently transferred via efferent nerve fibres to the target organ, leading to an appropriate reaction according to the stimulus. The stimulus-reaction model or stimulus-reaction compatibility has been described several times (Proctor and Vu, 2006; Masaki et al., 2004). Thereby, adequate stimuli excite specific sensory systems. Across vertebrates and invertebrates, the variability of sensory systems is immense, reaching from olfaction, gustation and mechano-sensation in invertebrates and vertebrates (see Ache and Young, 2005 and Hildebrand and Shepherd, 2004 for review; Burrows and Newland, 1994; Burrows and Newland, 1993; French and Sanders, 1981), to somato-sensory systems (e.g. Nelson et al., 1980), such as complex hearing and visual systems in vertebrates (see Pfaff et al., 2018 and Sung and Chuang, 2010 for review). Thus, sensory systems are of high importance for the survival of animals, as they allow the extraction of relevant information from the environment.
Beyond segregation of stimulus characteristics by different sensory systems, additional stimulus processing is carried out by the CNS, leading to detection and discrimination refinement of incoming stimuli. These refining processes are supported by sensory filtering on various levels, such as response tuning for tactile stimulus intensity preferences (Kretzberg et al., 2016; Mar and Drapeau, 1996; Blackshaw et al., 1982; Jansen and Nicholls, 1973; Van Essen, 1973; Baylor and Nicholls, 1969a) or frequency preferences (see Hutcheon and Yarom, 2000 for review; Puil et al., 1986).

1. NEURONAL SIGNALLING

Sensory processing is defined as the processing of incoming sensory information, provided by sensory organs and their afferent nerve fibres to the spinal cord and the brain in vertebrates or to the nerve cord in invertebrates (see Radojcic and Pentreath, 1978 for invertebrate review). The central neural processing of sensory inputs in the brain is based on the input-output functions of the involved neurons. Often the transformation of input to output constitutes a “black box”. From the input a neuron receives until an output is eventually generated, there are numerous parameters involved, rendering the process highly complex. Among the first output-shaping parameters is the quality of the synapse (electrical or chemical) at which the sensory input arrives. This has, for example, been shown in mossy fibres forming different synapse types in the adult rat brain (Toth et al., 2000).

Chemical synaptic transmission enables directed communication between neurons and constitutes the basis for the establishment of neural networks. The chemical synapse per se is the contact zone between neurons (and other cells), divided by a synaptic cleft of widths in the nanometre range, where synaptic transmission takes place from the pre- to the postsynaptic cell via neurotransmitters (see Peters et al., 1996 for review; Pumplin and Reese, 1978). The information arriving at the presynaptic terminal is coded in the form of action potentials (APs), which can roughly be defined as deviations of the membrane potential from the resting potential of the cell (for a more detailed description see below).

In the absence of an AP or a stimulation, the membrane potential is approximately -50 mV in ganglion nerve cells of Aplysia (Camardo et al., 1983), -75 to -65 mV in frog sympathethic neurons (Jones, 1989), -85 to -60 mV in pyramidal neurons (see Bean, 2007 for review) and around -75 mV in mammalian brainstem neurons (Franzen et al., 2015; Ammer et al., 2012). To maintain these potentials at rest, a selectively permeable membrane and an unequal distribution of ions, primarily of potassium (K^+) and sodium (Na^+) across the membrane are required. K^+ dominates in the intracellular medium, whereas Na^+ dominates in the extracellular medium. The maintenance of this unequal distribution is based on the activity of the adenosine triphosphate consuming Na^+/K^+ pump, transporting K^+ in and Na^+ out of the cell, counteracting the continuous outward diffusion of K^+ ions through K^+ channels and inward diffusion of Na^+ ions through Na^+ channels in the membrane (see Kaplan, 2002; Crill, 1996 and Skou, 1965 for review; Skou, 1957). At rest, the chemical driving forces for the respective ion species and the activity of the Na^+/K^+ pump are in balance with the electro-static driving force, the transmembrane voltage. This transmembrane voltage is mainly caused by the efflux of K^+ ions along their chemical gradient, as K^+ ions have the highest conductance across the membrane. Due to this efflux, K^+ locally accumulate on the extracellular side of the membrane, while large, negatively charged organic ions, which cannot cross the membrane, remain inside the cell. As the membrane potential is measured in reference to the extracellular medium, the resting potential is negative and points towards the reversal potential of K^+. However, due to the involvement of other ion species with lower conductance across the membrane, such as Na^+, the resting potential is usually more positive (see Segev, 1992 for review; Deitmer and Schlue, 1981; Hodgin and Huxley, 1952).

In case of a depolarisation under these ionic conditions, the membrane permeability changes, as the depolarisation leads to a fast and brief voltage gated increase in Na^+ conductance, allowing Na^+ ions to flow into the cell, and a slow but more sustained K^+ conductance, allowing K^+ ions to flow out of the cell (Hodgkin and Huxley, 1952). The initial transient increase in Na^+ conductance further depolarises the membrane, recruiting even more voltage gated Na^+ channels, generating a regenerative response. In case the firing voltage threshold of the neuron is reached, an AP is elicited, whereby positive membrane potentials can be achieved due to the immense influx of Na^+ (see Bean, 2007 for review).

Slow but more sustained increase in K^+ conductance together with decreasing Na^+ conductance, as the voltage gated Na^+ channels deactivate over time, repolarises the cell membrane, bringing the membrane potential back to the resting value (Hodgkin and Huxley, 1952).

Synaptic information transfer is dynamic, as synapses vary for instance on the level of excitation-inhibition balance, neuromodulation, plasticity, and strength and efficacy over time. Many parts of neuronal networks undergo developmental changes in the long-term period. This has, for instance, been shown for resting and active membrane properties of neurons in different regions in the auditory brainstem of gerbils (Franzen et al., 2015; Ammer et al., 2012; Scott et al., 2005), and for molecular mediators of K^+ currents of hippocampal neurons in rats (Falk et al., 2003; Spigelman et al., 1992). Such developmental long-term changes play a role in the adjustment and perfection of synaptic strength and integrity (see Turrigiano and Nelson, 2004 for review). Besides long-term changes, dynamics of the neuronal network can also happen in the short-term range of milliseconds and seconds (see Zucker and Regehr, 2002 and Fioravante and Regehr, 2011 for review), affecting computation in neural circuits. Importantly, the described neuronal processing phenomena of synaptic transmission and dynamics are not limited to vertebrates, but also apply to invertebrates.

2. BIOPHYSICAL PROPERTIES OF NEURONAL MEMBRANES

The model of electrical information propagation in neurites is based on the passive cable theory (see Rall, 1959 for review). The time course of the voltage response to a brief current injection at the dendritic tree is affected by various parameters, such as dendritic morphology, ion channel distribution, biophysical membrane properties, and spatial distribution of synapses (see Segev, 1992 for review). Parameters defining the degree of dispersion of the input current from the stimulus location are the membrane time constant τ_m, which means the required time of the membrane potential to reach 63% of its maximal deflection in response to a stimulus, and the membrane length constant λ, meaning the distance the voltage travels until the voltage is declined to 37% of its initial amplitude. Both are determined by the morphology of each cylindrical segment of the dendritic tree (Agmon-Snir, 1995) as well as by the membrane input resistance R_m, reflecting the amount of open and closed channels in the cell membrane.

Biophysical parameters at rest and during activation in concert define the pattern of AP generation in neurons (Franzen et al., 2015; Ammer et al., 2012; Scott et al., 2005). The membrane resting potential (E_m), R_m, τ_m, and the membrane capacity (C_m), which is associated with the cell surface and which, together with R_m, defines the τ_m, all belong to the resting parameters. Thereby, the cell membrane behaves as an RC element, where τ_m equals R_m multiplied by C_m (see Spruston et al., 1994 for review). A change in any of these three parameters can influence synaptic integration. For instance, a reduction

in C_m or R_m, as it can occur during postnatal development, decreases τ_m, shortening the time window for synaptic integration (Franzen et al., 2015). The active membrane parameters comprise attributes for AP phenotyping, such as voltage threshold, peak amplitude, half-width, or after-hyperpolarisation duration and amplitude (Kowalski et al., 2016; Kuo et al., 2012).

Information flow between neurons is based on involved voltage- or neurotransmitter gated ion channels located in the cell membrane. Besides voltage gated presynaptic calcium (Ca^{2+}) channels, which are crucial for the fusion of presynaptic vesicles with the presynaptic membrane (Brown et al., 1936; Dale et al., 1936), there are numerous other ion channels involved in information transfer in the CNS: Voltage gated K^+ channels (K_v) and voltage gated Na^+ channels (Na_v), for instance, in concert, are the main structures mediating AP generation and propagation. Na_v channels drive the initial depolarisation phase (see Catterall et al., 2000 for review) and K_v channels drive the repolarisation phase (see Scheuer et al., 2011 and Rudy et al., 1988 for review).

Na_v channels consist of subunits, which are classified into α- and β-subunits, determining the cellular function of the respective Na_v channel (see Catterall et al., 2000 for review). β-subunits hold modulatory functions, promoting the fast opening and closing of Na_v channels and affecting the size of mediated currents (Schreibmayer et al., 1994; Bennett et al., 1993). Na_v channels can be regulated, by protein kinase A phosphorylation, which has also an effect on the current size mediated by these channels. This has, for example, been shown in frogs and in rat brain cell culture (Gershon et al., 1992; Li et al., 1992). The trigger for Na_v and K_v channel activation is the membrane depolarisation, leading to an outward movement of one to four of the four transmembrane segments, resulting in conformational change and opening of the ion channel pore (Stühmer et al., 1989). In Na_v channels inactivation follows within milliseconds, conveyed by the intracellular inactivation gate (see Scheuer et al., 2011 for review).

Low threshold K^+ channels, for example, are divided into Ca^{2+} activated K^+ channels, inward rectifiers, and K_v channels, which in turn are subdivided into delayed rectifiers (D-type) and “A” current mediators (A-type) (see Rudy, 1988 for review). In general, K^+ channels consist of four α-subunits and are further divided into subfamilies based on genetic similarity (e.g. K_v1-12 for K_v channels (Ranjan et al., 2019)). D-type K_v channels are activated by membrane depolarisation with a delay compared to voltage gated Na^+ channels and drive the repolarisation phase during the AP process (see Rudy, 1988 for review). Compared to the D-type, the A-type K_v channel mediates the faster and more transient “A” current (Miyasho et al., 2001). Low threshold K^+ channels have been identified across species for instance in frog vestibular neurons, in mesencephalic neurons of rats, as well as in different auditory brainstem areas of gerbils (Hsiao et al., 2009; Beraneck et al., 2007; Scott et al., 2005; Svirskis et al., 2002; Barnes-Davies et al., 2004). Ca^{2+} activated K^+ channels depend on the intracellular Ca^{2+} concentration with high Ca^{2+} concentration promoting K^+ channel opening (see Rudy, 1988 for review).

Besides supra-threshold activity, ion channels are also important during subthreshold membrane activity. Hyperpolarisation-activated cyclic nucleotide cation (HCN) channels predominantly mediate Na^+ and K^+ currents and have been identified in various species across vertebrates and invertebrates (Gerard et al., 2012; see Biel et al., 2009 and Pape, 1996 for review). Exemplary, their presence is usually detected by hyperpolarising current injection and the examination of the resulting sag size, which means the rectification of membrane voltage back to more depolarised levels towards E_m (Gerard et al., 2012; Hassfurth et al., 2009). Functionally, HCN channels have been linked to rhythmogenesis in thalamic neurons in guinea pigs (McCormick and Pape, 1990), the stabilisation of the membrane potential in pyramidal and thalamo-corticoid neurons in mice and rats (Meuth et al., 2006; Ludwig et al., 2003; Pape, 1996), a contribution to membrane resonance in the mouse olfactory bulb and the rat cortex (Hu et al., 2016; Boehlen et al., 2013), as well as to a variety of other functions across species (see Biel et al., 2009 for review). Thereby the amount of HCN mediated current differs between cell types, as it has been shown for mechano-sensory neurons in the leech ganglion (Gerard et al., 2012).

One example for subthreshold membrane activity is membrane potential resonance. Resonance is an intrinsically tuned dynamical feature to amplify the cellular response to specific input frequencies. It can affect neuronal behaviour on the basis of membrane potential oscillations, supporting stimulus discrimination.

Generally, resonance is linked to the membrane impedance, which means the frequency domain of R_m. The membrane resonance can be measured by applying a frequency modulated current waveform aiming at impedance amplitude profiles (ZAP) (see Izhikevich, 2001 and Hutcheon and Yarom, 2000 for review; Moore and Buchanan, 1993; Puil et al., 1986). One feasible ZAP stimulus is the sinusoidal input current with increasing stimulation frequency and constant amplitude. Under these conditions, resonant neurons exhibit larger voltage responses to frequencies close to their membrane depolarising resonance frequency (R_f) and weaker responses to frequencies that differ from their R_f (see Izhikevich, 2001 and Hutcheon and Yarom, 2000 for review; Puil et al., 1986). This neuronal response preference to specific frequencies has been shown for vestibular neurons in guinea-pigs, frogs, and chicks (Beraneck et al., 2003; Ris et al., 2001; Av-Ron and Vidal, 1999; du Lac and Lisberger, 1995) and in hippocampal pyramidal neurons of juvenile rats (Zemankovics et al., 2010). Presumably involved membrane channels are low threshold D-type K^+ channels, as it has been described in frog vestibular brain neurons (Beraneck et al., 2007). Further parameters that are associated with membrane potential resonance are the hyperpolarisation-activated nonspecific cation conductance (I_h) mediated by HCN channels, persistent Na^+ currents, currents mediated by N-Methyl-D-Aspartate (NMDA) channels, and high threshold Ca^{2+} currents (Wu et al., 2005; see Hutcheon and Yarom, 2000 for review). All in all, even though resonance phenomena have been investigated numerous times in various

species and brain areas, the details of how neuronal membrane properties determine R_f are still unclear.

3. SYNAPTIC TRANSMISSION IN CENTRAL PROCESSING

Information transfer between neurons in the CNS happens via electrical and chemical synaptic transmission. Electrical synaptic transmission is mediated through gap junctions, consisting of hemi-channels and is attributed to direct transmission of molecules and electrical current (Rash et al., 2013). Electrical synaptic transmission, therefore, is faster compared to synaptic transmission at chemical synapses. Since all target areas investigated in this thesis mainly use chemical synapses for inter-neuronal information transfer, the process of chemical synaptic transmission will be introduced in more detail.

When an AP reaches the presynaptic terminal, voltage gated Ca^{2+} channels open, so that Ca^{2+} enters the presynaptic compartment and promotes the fusion of synaptic vesicles with the presynaptic membrane, releasing neurotransmitters into the synaptic cleft. Neurotransmitters can act excitatory, e.g. in the cases of the acetylcholine (ACh) transmitter at synaptic connections of motor nerves with skeletal muscles (Brown et al., 1936; Dale et al., 1936) or glutamate, which has been shown to be excitatory in mouse mossy fibre synapses (Pinheiro et al., 2012), in cultured cortical, diencephalic, spinal cord, mesencephalic, and striatal neurons in embryonic mice (Johnson and Ascher, 1987; Mayer et al., 1984; Nowak et al., 1984) and in rat pyramidal neurons (Geiger et al., 1995). Beyond that, neurotransmitters, as for example *γ*-Aminobutyric acid (GABA) or glycine, can have inhibitory effects, as it has been reported in the mammalian brainstem (Pollak et al., 2011) as well as in the CNS of the leech (Nicholls and Wallace, 1978). The amount of transmitter that is released into the synaptic cleft is modulated by the presynaptic activity (see Krnjevic, 1974 for review). The quality of synaptic transmission (e.g. excitatory or inhibitory) is, to a large part, influenced by the receptor molecules in the postsynaptic membrane.

In the most direct form of chemical, synaptic transmission, released neurotransmitters bind to binding sites of postsynaptic ionotropic channels, resulting in conformational changes in the ion channels and an increased permeability of the postsynaptic membrane for specific ions through these ion channels. The resulting changes in postsynaptic conductance are then transformed into a postsynaptic current (PSC) by the diffusion of ions through these ion channels. The generated PSCs are then essential for further information propagation in the postsynaptic neuron (see Bean, 2007 for review).

Taken together, resulting PSCs are shaped by the contributing neurotransmitters and postsynaptic changes in conductance via specific, ligand gated ion channels. Beyond that, the PSC amplitude is influenced by synaptic short-term plasticity (STP), according to the stimulus position in a train of

ongoing stimulation, which might affect the processing function of neurons. STP of PSCs has been shown *in vitro* for auditory brainstem neurons in young and mature mice, gerbils, juvenile rats, and embryonic chicken regarding excitatory and inhibitory postsynaptic currents (EPSCs and IPSCs) (Baumann and Koch, 2017; Krächan et al., 2017; Taschenberger et al., 2016; Caspari et al., 2015; Porres et al., 2011; Walcher et al., 2011; Chanda and Xu-Friedman, 2010; Yang and Xu-Friedman, 2009; Wang and Manis, 2008; Cook et al., 2003; Kuba et al., 2002; Taschenberger and von Gersdorff, 2000) and *in vivo* for whisker stimulation in mature rats (Chung et al., 2002). Synaptic STP is expressed via synaptic short-term facilitation (STF), which means an increase in PSC amplitude (Taschenberger et al., 2016; Wang and Manis, 2008; Taschenberger and von Gersdorff, 2000), and synaptic short-term depression (STD), which means a gradual decrease in PSC amplitude over time (Baumann and Koch, 2017; Krächan et al., 2017; Taschenberger et al., 2016; Caspari et al., 2015; Porres et al., 2011; Walcher et al., 2011; Chanda and Xu-Friedman, 2010; Yang and Xu-Friedman, 2009; Wang and Manis, 2008; Cook et al., 2003; Kuba et al., 2002; Taschenberger and von Gersdorff, 2000). Both STF and STD depend on the probability of presynaptic vesicle release.

Regarding the functionality of STF, it is speculated that it boosts the cell response at input frequencies of 50 Hz and above (Taschenberger et al., 2016; Wang and Manis, 2008; Taschenberger and von Gersdorff, 2000) to ensure faithful spiking by bringing the membrane potential closer to its firing threshold and, thus, acting as a high pass filter. More is known about the functional impact of STD. It is suggested to suppress inputs of unnecessarily high activity, and to promote spike adaptation, and filters out transients (Yang and Xu-Friedman, 2009; Chung et al., 2002; Fortune and Rose, 2000). Furthermore, it is thought to improve coincidence detection (Cook et al., 2003; Kuba et al., 2002), or mediate gain control (see Rothman et al., 2009 for review). Altogether, STF and STD together likely provide temporal filters for central processing: STF provides a high pass filter for paired pulses and STD provides low pass filtering during ongoing stimulation (see Fortune and Rose, 2001 and 2002 for review).

4. ANIMAL MODELS TO INVESTIGATE CENTRAL SENSORY PROCESSING

In this project intrinsic frequency tuning properties in neurons were investigated in invertebrate and vertebrate species. The main animal models were: the European medicinal leech (*Hirudo medicinalis*), as a representative of invertebrates, and the Mongolian gerbil (*Meriones unguiculatus*), representing the vertebrate subphylum. They constitute well-established animal models for tactile excitable sensory systems and auditory research, respectively.

4.1 Invertebrate Animal Model *H. medicinalis*

The model organism used in this thesis for the examination of central processing in invertebrates is the European medicinal leech, *H. medicinalis*. The annelid belongs to the class of clitellata and the order of hirudinae. The leech's body wall consists of longitudinal, oblique and circular muscular fibres, enabling undulating movement in standing or slowly flowing water or to move at land by contraction and elongation (Raeside et al., 1964).

The leech nervous system comprises a ventral nerve cord with one ganglion per body segment, whereby every ganglion includes approximately 400 neurons of roughly 200 types (Kristan et al., 2005). The ganglia are classified into three types: the head ganglion (Yau, 1976; Nicholls and Baylor, 1968), 21 nearly identical segmental ganglia, and the tail ganglion. Besides motor neurons (Stuart, 1970), there are sensory neurons in the segmental ganglia and in the head ganglion, classified as nociceptive (N)-, touch (T)-, and pressure (P)-cells (Pinato and Torre, 2000; Yau, 1976). Each cell type can be characterised by distinct locations within the segmental ganglion (Blackshaw et al., 1982; Yau, 1976; Nicholls and Baylor, 1968), certain electrical properties in order to encode mechanical tactile stimuli (Kretzberg et al., 2016; Mar and Drapeau, 1996; Blackshaw et al., 1982; Jansen and Nicholls, 1973; Van Essen, 1973; Baylor and Nicholls, 1969a), and clearly described receptive fields on the skin surface of the leech (Kretzberg et al., 2016; Blackshaw et al., 1982; Blackshaw, 1981; Yau, 1976, Baylor and Nicholls, 1969b; Nicholls and Baylor, 1968).

N-, T- and P-cells differ regarding their tactile stimulus sensitivity and spike pattern. N-cells require strong tactile stimulation of 50 mN to generate APs with, compared to the other two cell types, the most delayed supra-threshold response of 90 ms first spike latency (Kretzberg et al., 2016; Pinato and Torre, 2000). P-cells require an intermediate stimulus intensity of about 20 mN to elicit APs. The cell response happens then with a jitter of 0.5-10 ms (Pinato and Torre, 2000) and a first spike latency of 45 ms (Kretzberg et al., 2016). When stimulated with a 500 ms long tactile stimulation, P-cells fire at stimulus onset, showing low adaptation, making them tonic responders (Kretzberg et al., 2016; Pirschel and Kretzberg, 2016; Lewis and Kristan, 1998). In contrast, T-cells require only 2 mN stimulation intensity for AP generation when the area of touch stimulus application is close to the recorded central ganglion. For adjacent and, therefore, more distant ganglia, the threshold for AP generation is higher. Supra-threshold cell response to tactile stimulation shows a jitter of around 100 µs for the first elicited AP, with less delay compared to the P-cell supra-threshold response (Kretzberg et al., 2016; Pirschel and Kretzberg, 2016; Pinato and Torre, 2000; Nicholls and Baylor 1968). In response to 500 ms long tactile stimulation, T-cells fire at stimulus onset and offset (Kretzberg et al., 2016; Pirschel and Kretzberg, 2016; Lewis and Kristan, 1998). T-cells are fast adapting low threshold tactile receptor cells,

requiring weak stimulations, such as water bubbling, and are suggested to make the animal sensitive to its movement in water or to close objects (Rodriguez et al., 2004).

Despite the described differences in tactile stimulation intensity sensitivity of the three types of mechano-sensory neurons, there is response overlap to intermediate and strong stimulations between N-, P-, and T-cells (Kretzberg et al., 2016; Pirschel and Kretzberg, 2016; Pinato and Torre, 2000; Nicholls and Baylor, 1968). Segregation of these response overlap causing sensory inputs might be encoded either by spike count (rate) or temporal response features. It is suggested, that spike rate primarily encodes stimulation intensity, which might be done by P-cells by the total sum of spikes, while stimulus duration is encoded by the duration of the P-cell response. Temporal response features of the first spikes of the cells with response overlap, especially the relative latency, have been suggested to encode stimulus location. For this, the fast and temporally precise T-cells have been shown to be most effective (Pirschel and Kretzberg, 2016; Thomson and Kristan, 2006). Interestingly, T-cells have also been described to be important for encoding non-static stimulations and have been classified as velocity detectors (Carlton and Mcvean, 1995). Thus, multiplexed coding involving different cell types, likely is one principle for central stimulus discrimination in mechano-sensory neuron populations in the leech.

Besides multiplexed coding, another operating factor for firing behaviour in these neurons might be linked to the contribution of cells, whose response properties are intrinsically tuned to particular frequency ranges of membrane voltage oscillation. Cell populations consisting of differently intrinsically tuned neurons could then generate filter banks to support segregation of sensory inputs and sensory processing. **I**ntrinsically tuned response properties, such as accommodation rates (Schlue, 1976) and temporal precision (Franzen et al., 2015; Ammer et al., 2012), might further support segregation of inputs. Such frequency filter banks have not been described in the leech yet, and their existence is rather hypothetical.

4.2 Vertebrate Animal Model *M. unguiculatus*

The Mongolian gerbil constitutes a well-established model organism for auditory research. The ascending pathways of the gerbil auditory brainstem have frequently been used to investigate input-output functions of neurons involved in the auditory system and provide an optimal model to examine intrinsic tuning properties of neurons in the vertebrate CNS.

The Mongolian gerbil is endemic in steppes of central Asia (see Stürmer et al., 2003 for review), lives in colonies in underground burrows (Agren et al., 1989), and prefers herbivorous diet. As the Mongolian gerbil is comparatively easy to breed and to keep in captivity (Waiblinger and König, 2004),

it became a popular laboratory animal, especially in the fields of auditory (Kraus et al., 1987) and aging research (Chreal, 1986).

4.2.1 Hearing Range

The most noteworthy benefit of the Mongolian gerbil as an animal model for auditory research is the similar hearing range compared to humans. Hearing range in humans extends from around 31 Hz to 17.5 kHz, when referring to audible frequencies at 60 dB SPL, whereby the best hearing range is at 2-4 kHz, since here, the lowest intensity is needed to hear the acoustic stimulus (see Gleich and Strutz, 2012 and Heffner and Heffner, 2007 for review). The gerbil resembles the human audiogram, as it covers both, the high frequency (and ultrasonic) as well as the low frequency range (Ryan, 1976). Other popular laboratory animals, such as rats and mice, on the other hand, lack the low frequency section. Their best hearing range is shifted to higher frequencies, from around 10 to 25 kHz in mice and 6 up to 42 kHz in rats (see Heffner and Heffner, 2007 for review). Thus, a difference to the human hearing range that all three named rodent species have in common is the shift of the high frequency limit of best hearing to higher levels compared to the human audiogram. Nevertheless, the gerbil is the laboratory animal whose audiogram resembles the low frequency parts of humans the most (see Gleich and Strutz, 2012 for review). Interestingly, the high frequency hearing ability in mammals differs from the one in non-mammals, such as land living reptiles or amphibians, where the upper limit varies between 0.5 and 10 kHz, depending on the species (see Heffner and Heffner et al., 2007 for review). This difference might be due to specialisations in the mammalian middle ear, e.g. in form of the three ossicles, which allow the transfer of higher frequencies compared to land living non-mammals, where the middle ear anatomy shows only one ossicle (see Köppl, 2009 for review).

4.2.2 Mammalian Hearing System

The mammalian hearing system transforms physical acoustic stimuli into bioelectrical signals (see Biacabe et al., 2001 for review). Thus, the adequate stimuli are pressure changes in the transmission medium, such as air or water, which are then propagated as “sound” to appropriate morphological structures of the hearing apparatus (Stephen and Bennet-Clark, 1982, Hopson, 1966). While hearing plays a prominent role in the ecology of nocturnal mammals, for which visual information is scarce, it is also crucial for diurnal and crepuscular animals, for instance in predator-prey interactions (see Grothe et al., 2010 for review).

When an acoustic stimulus reaches the ear, the sound waves come upon the tympanum which constitutes a thin membrane, the ear drum, which connects the outside world with the middle ear. Its

low inertia allows vibrations even in response to extremely soft acoustic stimuli. The tympanum performs one-dimensional movements, turning the acoustic into mechanic vibration, which is then passed on by the three lightweight bone ossicles (malleus, incus, and stapes) to the membrane of the fenestra ovalis (Sillar and Picton et al., 2016). The membrane surface ratio between tympanum and fenestra ovalis values approximately 20:1, which supports the impedance matching. Therefore, higher pressure and less mechanical deflection are delivered to the fenestra ovalis compared to the tympanum (Killion and Dallos, 1979). The resulting oscillation of the perilymph in the inner ear is detected by a sensory epithelium along the basilar membrane in the spiral coiled cochlea, the organ of Corti with its hair cells. Neurons downstream to the hair cells are arranged in a tonotopic fashion, with high frequencies being passed on to these neurons from the basal part and low frequencies from the apical part of the basilar membrane (Sillar and Picton et al., 2016; see Pickles, 2015, Grothe at al., 2010 and Biacabe et al., 2001 for review). These afferent mechano-sensory neurons then transmit signals to the auditory brainstem where information is further processed. Thereby the tonotopic arrangement is further maintained in parts of the auditory brainstem (see Kandler et al., 2009 for review). Final computation is carried out in the central auditory system, which involves the brainstem, the thalamus, and the auditory cortex (see Biacabe et al., 2001 for review).

5. MAMMALIAN AUDITORY BRAINSTEM

Input-output functions in neurons of the mammalian central auditory system can be investigated using the ascending pathways of the auditory brainstem. The auditory brainstem consists of regions separated into distinct nuclei, e.g. within the cochlear nucleus (CN), the superior olivary complex (SOC) or the lateral lemniscus (LL). The SOC consists of the lateral and medial superior olive (LSO and MSO), the medial (MNTB) and lateral nucleus of the trapezoid body, the superior paraolivary nucleus, and the ventral periolivary region. The LL is formed by the ventral nucleus of the lateral lemniscus (VNLL) which is further divided into the ventral, medial, and dorsal VNLL, the intermediate (INLL) and the dorsal nucleus (DNLL). Afferent fibres from the SOC project to the LL, which in turn projects to the inferior colliculus (IC) and finally to the medial geniculate nucleus (MGB) and the auditory cortex (see Felmy, 2019 and Pickles, 2015 for review; Caspari et al., 2015; Kelly et al., 2009; Benson and Cant, 2008; Budinger et al., 2000; Covey and Casseday, 1991 and 1986).

The ascending pathways in the auditory brainstem of rodents comprise different morphological types of chemical synapses, each of them probably reflecting the optimal synaptic morphology for specific tasks. For instance, specialised calyciform synapses at the medial nucleus of the trapezoid body (MNTB) and at the ventral nucleus of the lateral lemniscus (VNLL) of juvenile and adult gerbils are believed to transmit well-timed information with high reliability (see Grothe et al., 2010 for review; Berger and

Meyer et al., 2014; Hermann et al., 2007). Apart from synapse morphology, input-output generation in chemical synaptic transmission is influenced by the composition of ion channels involved (Dzubay and Jahr, 1996; Geiger et al., 1995).

5.1 Neuronal Connections in the Auditory Brainstem

When an acoustic stimulus reaches the ear and, thus, the cochlea, information is transferred to the CN of the ipsilateral (i) ear via auditory nerve fibres (ANFs). The CN is subdivided into the antero-ventral (AVCN), posterior-ventral (PVCN) with multipolar and stellate cells (SCs) (Friauf and Ostwald, 1988), and the dorsal (DCN) CN. The AVCN provides information to iLSO and contralateral (c) LSO, cMSO, and cMNTB, the PVCN provides input to the cVNLL, and the DCN provides input to the cDNLL and cIC (see Pickles, 2015 for review).
Within these neuronal connections in the auditory brainstem, there are three giant synapses involved in the processing of acoustic input: the large glutamatergic endbulb in the AVCN formed by ANFs on bushy cells (BCs), which then provide excitatory input to nuclei in the SOC (Ryugo and Sento, 1991). Within the SOC there is the calyx of Held on MNTB neurons, which is formed by excitatory fibres from the cAVCN and provides inhibition to iLSO and iMSO. The third synapse is the endbulb at vVNLL neurons. It receives the main excitatory input from octopus cells (OCs) in the octopus cell area (OCA) of the cPVCN and provides inhibition to the iINLL, iDNLL, and iIC (see Felmy and Künzel, 2014 for review). All three synapses constitute a part of specific auditory brainstem circuits.

5.1.1 The Superior Olivary Complex

The SOC is the first stage in the auditory circuit where binaural computation takes place, comparing inputs from both ears. The LSO and the MSO are the binaural detectors in the SOC. They enable stimulus discrimination in the time as well as in the intensity domain, since they both receive input from both ears, allowing for sound localisation in the horizontal plane using specific cues: The interaural time difference (ITD) which means the difference in arrival time of sound between the two ears, and the interaural level difference (ILD), which means the difference in loudness of sound arriving at the two ears. In contrast, for sound localisation in the vertical plane, monaural cues are used to detect spectral notches (see Grothe and Pecka, 2014 and Grothe et al., 2010 for review). The basic principle of binaural cue usage for horizontal sound localisation is coincidence detection or interaural cross-correlation. Neuronal processing of binaural cues is complex and constitutes an attractive model for the examination of input-output functions of neurons in the mammalian auditory system (see Grothe et al., 2010 for review).

The LSO receives excitatory glutamatergic input from the iCN and inhibitory glycinergic input from the iMNTB, which in turn receives input from the contralateral ear (Beiderbeck et al., 2018). Its main function is the computation of ILDs, by integrating the glutamatergic and glycinergic input for frequencies above 2 kHz (see Grothe and Pecka, 2014; Grothe et al., 2010 and Tollin, 2003 for review; Tollin and Yin, 2005; Goldberg and Brown, 1969; Boudreau and Tsuchitani, 1968). Importantly, LSO neurons function as cross-correlators, meaning that the relative level difference presented to both ears is crucial for ILD detection, rather than the absolute levels (Goldberg and Brown, 1969).

The LSO comprises two cell types, principal neurons for ILD detection and efferent lateral olivochochlear neurons projecting to the cochlea. The main characteristic to distinguish between those two cell types is the activation of I_h currents in response to membrane hyperpolarisation in principal neurons (Leao et al., 2011; Sterenborg et al., 2010). Synaptic currents in both cell types are, among others, mediated by low threshold activated K^+ channels (Barnes-Davies, 2004). The neuronal connection from the CN to the LSO develops during embryogenesis (Kandler and Friauf, 1993). However, innervations to the LSO are not static after birth, but rather dynamic: in rodents it has been shown, that the amount of innervations of MNTB fibres on LSO neurons decreases during postnatal development before hearing onset (Nishimaki et al., 2007; Kim and Kandler, 2003; Sanes and Siverl, 1991), which likely leads to more precise frequency tuning in the mature animal (see Kandler et al., 2009 for review; Kullmann and Kandler, 2008; Gillespie et al., 2005; Nabekura et al., 2004; Kotak et al., 1998).

The second binaural centre in the SOC is the MSO, which mediates temporally precise ITD detection in the microsecond range for frequencies below 2 kHz. MSO principal neurons integrate glutamatergic excitatory input from both CNs and glycinergic inhibitory input from the iMNTB (see Grothe and Pecka, 2014, Grothe et al., 2010 and Grothe, 2003 for review; Encke and Hemmert, 2018; Fischl et al., 2016; Couchman et al., 2010; Grothe and Sanes, 1994). MSO neurons encode ITDs in AP rate. The resulting output is then transferred to the LL (Kelly et al., 2009). Binaural coincidence detection for neuronal ITD detection is highly complex and involves the neurons' characteristic delay lines, characteristic phase, and best frequencies for the ITD sensitivity (see Ashida and Carr, 2011 for review; Fitzpatrick et al., 2000).

Principal cells in the MSO are bipolar and, in gerbils, largely mature around postnatal day (P) 18 (Magnusson et al., 2005; Scott et al., 2005). They receive inputs via A-amino-3-hydroxy-5-methyl-4-isoxazolepionic acid receptors (AMPARs), NMDARs, glycine receptors and $GABA_A$Rs (Couchman et al., 2011). MSO neurons show fast AMPA currents in EPSCs. Furthermore, low and high voltage gated K^+ channels K_v1 and 3 as well as I_h currents have been shown to be involved in AP generation and E_m adjustment (Fischl et al., 2016). During postnatal development, the glycinergic innervations are reduced in their number, but increased in size, affecting ITD detection and probably resulting in a more

precise MNTB-MSO information transfer (Werthat et al., 2008; Chirila et al., 2007; Goldberg et al., 1969). Also during postnatal development, there are experience dependent structural reorganisations after hearing onset at P12 up to P24, improving encoding of auditory cues with great temporal precision and fidelity during the maturation of sound localisation behaviour (Chirila et al., 2007; Magnusson et al., 2005; Scott et al., 2005). Besides EPSC duration, R_m, and τ_m, which decrease with age, also the spike generation mechanisms mature around hearing onset. This is, for instance, reflected in reduced AP amplitude and elevated current thresholds. These alterations are based on changes in low threshold activated K_v1 channel subunits and I_h currents. These changes in channel composition and mediated currents might be the main determinants for postnatal developmental changes in neuronal excitability, rendering mature neurons temporally more precise, as it has, for instance, been shown in gerbil MSO neurons (Khurana et al., 2012; Scott et al., 2005).

A further structure in the SOC involved in the processing of auditory inputs is the MNTB. Neurons in the MNTB receive excitatory input from BCs in the cAVCN, forming the calyx of Held, one of the three giant synapses for temporally precise synaptic transmission, which is vital for processing of binaural sound localisation cues (see Kandler et al., 2009 for review). Inhibitory output from the calyx of Held is then transmitted to the iLSO, the iMSO (see Grothe et al., 2010 for review), the iVNLL, and the iINLL (Kelly et al., 2009). Due to the tonotopic organisation, high frequencies are processed in the medial and low frequencies in the lateral region of the MNTB (Kopp-Scheinpflug et al., 2002; Spangler et al., 1985). As in the MSO, low threshold activated K_v1 and K_v3 channels mediate postsynaptic currents and control timing and faithfulness of postsynaptic activity (Brew and Forsythe, 1995).

5.1.2 The Lateral Lemniscus

The lateral lemniscus is divided into the VNLL, the INLL, and the DNLL, all arranged in a comma-like structure between the SOC and the IC (Caspari et al., 2015; Kelly et al., 2009; Benson and Cant, 2008; Budinger et al., 2000; Covey and Casseday, 1991 and 1986). Retrograde labelling of rat INLL neurons in acute brain slices revealed input from the cCN, the iSOC, the iVNLL, and, interestingly from the iIC. Excitatory and most likely glutamatergic output is transferred to the iDNLL and the iIC (Ito et al., 2011; Kelly et al., 2009). The morphology of INLL neurons is highly diverse comprising elongated, globular, and multipolar, loosely packed neurons (Benson and Cant, 2008; Covey and Casseday, 1986). First spike latency is not outstandingly short compared to the short latencies found in VNLL neurons, which will be described later. INLL neurons show variable frequency tuning curves and both, monaural and binaural activation. Frequency preferences are not documented so far (Covey and Casseday, 1991). Probably the INLL serves as an integrating station across different frequencies on the population level.

Compared to the INLL, the DNLL is a well-studied nucleus of the ascending auditory pathway. Cell morphology reveals mostly elongated cells (Covey and Casseday, 1986). They receive excitation from both ears via the LSO and provide inhibition, with GABA mediated by $GABA_A$Rs, to the cDNLL via the commissure of Probst for binaural interaction, and to the iIC (Ammer et al., 2015 and 2012; Kelly and Kidd, 2000). In rodents, glutamate currents are sensitive to NMDA- and non-NMDAR antagonists (Siveke et al., 2018; Kelly and Kidd, 2000) and are, thus, mediated by AMPA- and NMDARs (Siveke et al., 2018; Ammer et al., 2012; Porres et al., 2011; Kelly and Kidd, 2000; Fu et al., 1997; Wu and Kelly, 1996), with NMDAR mediated currents supporting firing at specific frequencies (Siveke et al., 2018; Ammer et al., 2012; Porres et al., 2011; Kelly and Kidd, 2000; Fu et al., 1997; Kelly et al., 1997). Neuronal biophysical properties vary across cells and change during postnatal development, decreasing the integration time window (Ammer et al., 2012). The excitation coming from the LSO accelerates and AP width decreases, which is probably one factor for improving the speed and precision of signal integration in the DNLL. This in turn constitutes the basis for high spiking rates during ongoing stimulation and fits to the high temporal precision already existing in upstream structures of the SOC and the LL (Ammer et al., 2015 and 2012). In response to long current injections, DNLL neurons show sustained firing with no or low adaptation and with higher maximal firing rates in mature compared to juvenile animals (Ammer et al., 2012; Porres et al., 2011). In mature rats, neurons show a small amount of I_h currents at hyperpolarised membrane potentials (Fu et al., 1997).

The main downstream projection structure of nuclei in the LL is the IC (Kelly et al., 2009; Nayagam et al., 2005; Tanaka et al., 1985; Willard and Martin, 1983; Zook and Casseday, 1982). The IC functions as an integration station, or a switchboard, where integration of multimodal sensory perception takes place. In the IC, NMDAR activation has been reported to play an important role in auditory information processing (Sanchez et al., 2007). Target tissue of IC neurons is the MGB and, finally, the auditory cortex (Pickles et al., 2015 for review).

6. THE VENTRAL NUCLEUS OF THE LATERAL LEMNISCUS (VNLL)

The structure of the LL most relevant for this thesis is the VNLL. Whereas the VNLL in bats is the most distinct nucleus, with clearly defined borders, containing densely packed neurons (Covey and Casseday, 1986), in rodents, only the vVNLL is clearly separated from neighbouring structures. Across different mammals, the neuronal morphology of the VNLL is heterogeneous, with globular neurons located in the vVNLL of rodents and humans or the columnar region in bats and other morphological neuron types located dorsally to the vVNLL (Mylius et al., 2013; Budinger et al., 2000; Adams, 1997; Schofield and Cant, 1997; Covey and Casseday, 1986). The difference in morphological appearance of VNLL neurons is one criterion for the division of the VNLL into a dorsal part (dVNLL) and the vVNLL.

Further criteria are differences in the intrinsic neuronal properties like E_m, τ_m or R_m and the concomitant firing patterns, suggesting different roles in sound processing (Caspari et al., 2015).

Neurons in the vVNLL receive their main excitatory input from OCs and multi-stellate cells in the OCA, which is located in the cPVCN (Friauf and Ostwald, 1988; Zook and Casseday, 1987). Axons form large somatic synapses on globular neurons of the cvVNLL (Caspari et al., 2015; Berger and Meyer et al., 2014; Smith et al., 2005; Adams, 1997; Schofield and Cant, 1997; Friauf and Ostwald, 1988; Covey and Casseday, 1986). Inhibitory glycinergic input is provided by the iMNTB (Kelly et al., 2009; Irfan et al., 2005). VNLL neurons in mammals can be excited monaurally by contralateral stimulation (Recio-Spinoso and Joris, 2014; Batra et al., 2006; Covey and Casseday, 1986). Synaptic output is then fed forward to the iINLL, iDNLL, and iIC (Moore and Trussell, 2017; Kelly et al., 2009; Saint-Marie et al., 1997; Zook and Casseday, 1987 and 1982; Tanaka et al., 1985; Willard and Martin, 1983) and possibly to neurons within the dVNLL (Nayagam et al., 2005) (Fig. 1).

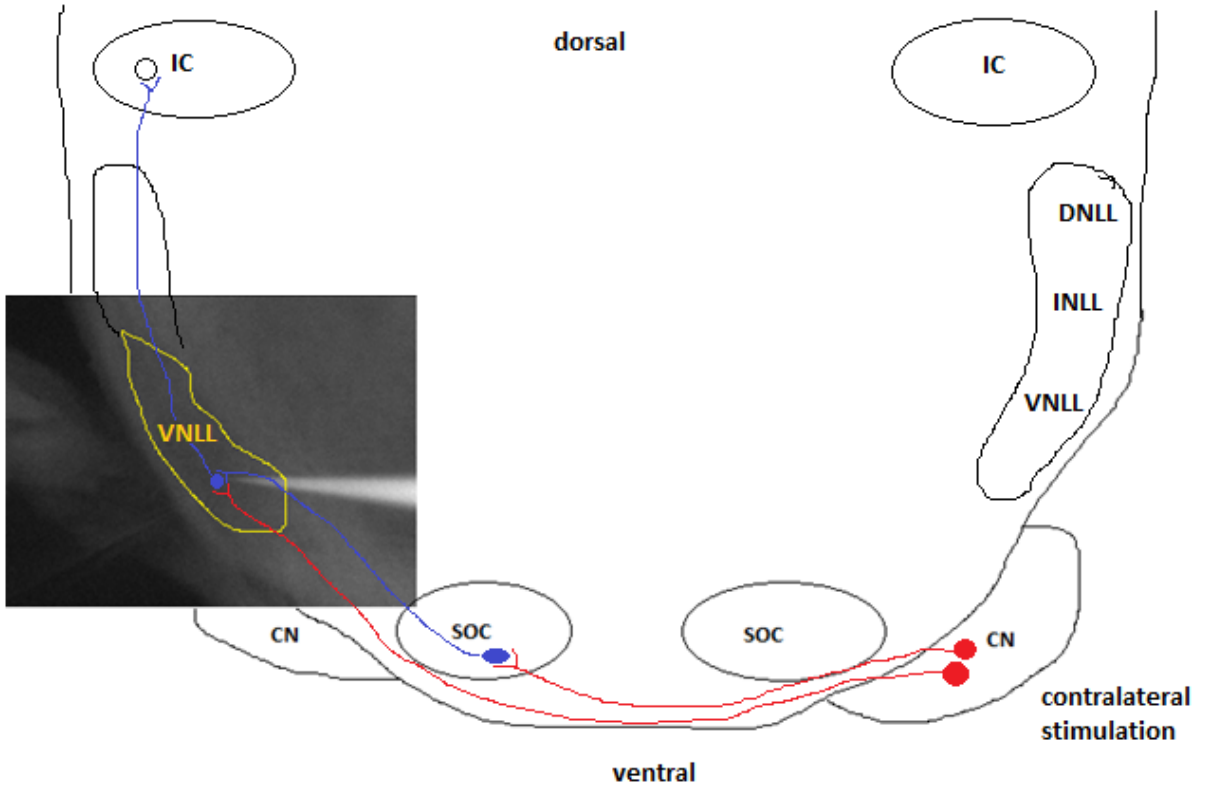

Fig. 1: Schematic drawing of an acute brain slice of the auditory brainstem in a Mongolian gerbil, with integrated photograph of the VNLL region (yellow highlight) under the light microscope with patch electrode (white structure). In response to monaural, contralateral stimulation, vVNLL globular neurons receive excitatory glutamatergic input from the cCN and input from the iMNTB in the SOC. The excitatory input is then converted into inhibitory output and fed forward to the iINLL, iDNLL, and iIC. CN = cochlear nucleus, SOC = superior olivary complex, VNLL = ventral nucleus of the lateral lemniscus, INLL = intermediate nucleus of the lateral lemniscus, DNLL = dorsal nucleus of the lateral lemniscus, IC = inferior colliculus. *Red* = excitatory fibres, *blue* = inhibitory fibres.

6.1 Physiology of VNLL Neurons

The VNLL endbulb synapse rapidly converts excitatory glutamatergic input into inhibitory output, which is transmitted to the iIC (Moore and Trussell, 2017; Berger and Meyer et al., 2014; Kelly et al., 2009; Benson and Cant, 2008; Saint-Marie et al., 1997; Zook and Casseday, 1987 and 1982; Tanaka et al., 1985; Willard and Martin, 1983) via co-release of glycine and GABA (Moore and Trussell, 2017; Saint-Marie et al., 1997). Postsynaptic integration is further mediated by $K_v1.1$ channels in the columnar region in bats (Rosenberger et al., 2003) and by HCN channels in gerbils (Caspari et al., 2015). Thereby channel expression differs within the VNLL, expanding the heterogeneity aspect of VNLL neurons from the morphology to the protein level.

Input-providing cells in the OCA spike at the stimulus onset with high temporal precision for frequencies up to 800 Hz when stimulated with click trains (Smith et al., 2005; Rhode et al., 1983). The temporal precision is maintained in VNLL neurons: *In vivo*, supra-threshold responses reveal extremely low latencies of 3-8 ms across species, with a jitter of around 200 µs for onset spikes. Onset spikes are, over a wide range, invariant to stimulation frequency and SPL (Liu et al., 2014; Recio-Spinoso and Joris, 2014; Zhang and Kelly, 2006a and b; Covey and Casseday, 1991 and 1986), rendering VNLL cells temporally reliably locked to the stimulus onset. In general, two firing types have been documented in the mammalian VNLL, an onset type and a sustained firing type (Liu et al., 2014; Recio-Spinoso and Joris, 2014; Zhang and Kelly, 2006a and b; Adams, 1997). Thereby onset type neurons can merge into sustained firing behaviour when stimulated with ongoing amplitude modulated (AM) tones. Therefore, it is likely that VNLL neurons preserve timing information of the sound structure onset and additionally can generate high firing rates during ongoing AM sounds (Zhang and Kelly, 2006a; Covey and Casseday, 1986). Modulation of the AM sound envelope reveals modulation transfer functions with low bandwidth and high vector strength at frequencies between 40 and 300 Hz. In rats, VNLL neurons follow frequencies up to 400 Hz, probably making them optimal processors for low- and intermediate frequency sound structures (Zhang and Kelly, 2006a). Frequency tuning across species shows, for instance, broadly tuned V-shaped tuning curves in columnar neurons in bats that broaden with increasing SPL (Covey and Casseday, 1991 and 1986). Tuning curves of mouse and cat VNLL neurons depend on the respective characteristic frequency (CF) of the neuron, which is defined as the frequency where a neuron requires the smallest amount of SPL in order to spike. Neurons with low CFs reveal wider tuning curves (Liu et al., 2014; Recio-Spinoso and Joris, 2014).

Tonotopically arranged frequency representation has been shown in bats, with low frequencies in the dorsal- and high frequencies in the ventral part of the VNLL (Covey and Casseday, 1986). Furthermore, retrograde labelling of different frequency bands in the IC in cats revealed cluster-like topographic

organisation of neurons in the ventral complex of the lateral lemniscus throughout the dorsoventral axis (Malmierca et al., 1998).

In juvenile gerbils, globular VNLL neurons can be innervated by more than one axon. They require multiple inputs in a short time window to be activated for supra-threshold integration (Berger and Meyer et al., 2014). During postnatal development, intrinsic membrane properties change with age (Franzen et al., 2015), and excitatory inputs increase regarding their current peak amplitude as it has been shown, for instance, in VNLL neurons of mice (Baumann and Koch, 2017). ACh supports these changes, enhances the synaptic excitability and, thus, promotes faithful one-to-one connection in mature animals (Baumann and Koch, 2017).

Based on these physiological characteristics, VNLL neurons are thought to provide fast and broadband onset inhibition to the iIC. The IC is the main centre of the auditory midbrain, where incoming information from all brainstem nuclei are processed and sent, via the thalamus, to the auditory cortex. On the level of the IC, input provided by VNLL neurons could enhance the contrast to excitatory inputs reaching the iIC and to suppress sound frequencies of spectral splatter at the level of the iIC (Spencer et al, 2015; Nayagam et al., 2005). Thus, VNLL input to the iIC might enhance the dynamic range of excitatory integration and might reduce the threshold for physiologically relevant stimuli, rendering IC neurons more excitable. Since VNLL neurons process the envelope of sound structures by relaying sound transients, as they occur in gerbil vocalisation, temporally precisely (Ter-Mekaelian et al., 2012) and since they are monaurally driven, they might be implicated in the processing of conspecific vocalisation.

6.2 Mechanisms of EPSC Kinetics at the VNLL Endbulb

From the above given background information the question arises: what is the physiological basis for the firing behaviour of VNLL neurons, i.e. the generation of APs with extreme precision to the stimulus onset and the generation of high firing rates during ongoing AM stimulation. One basis for the firing behaviour of these neurons might be linked to the glutamatergic synaptic transmission at the VNLL endbulb (Caspari et al., 2015; Berger and Meyer et al., 2014; Adams, 1997; Schofield and Cant, 1997; Friauf and Ostwald, 1988; Covey and Casseday, 1986).

6.2.1 Glutamatergic Signalling

EPSCs at the VNLL mediate rapid signalling during sound processing. Compared to the structurally very similar calyx of Held at the MNTB, excitation at the VNLL endbulb is remarkably shorter. This is probably due to differences in the synaptic morphology, allowing fast glutamate diffusion out of the synaptic

cleft at the VNLL endbulb. Furthermore, VNLL neurons are temporally more precise, due to lower R_m, allowing faster membrane charging (Berger and Meyer et al., 2014). At the mature gerbil VNLL endbulb, EPSCs decay bi-exponentially, starting with a fast and followed by a slow component (Fig. 2).

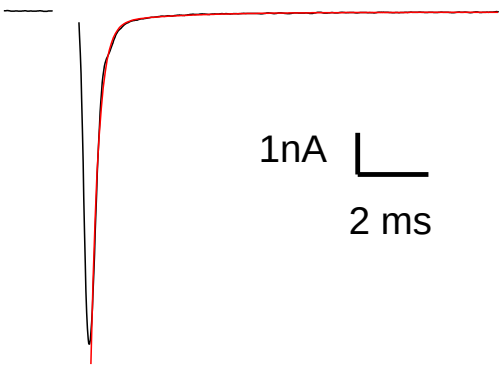

Fig. 2: EPSC at the mature VNLL endbulb. Currents were recorded in voltage-clamp mode at -63 mV holding potential. For better visualisation, the typically occurring recording artefact before the actual EPSC is blanked out. *Red*: EPSC decay fitted with a bi-exponential function.

This bi-exponential EPSC shape is not limited to the VNLL, but has also been documented at the endbulb of Held in the AVCN in mice (Chanda and Xu-Friedman, 2010) and at the calyx of Held at the MNTB in rats (Yamashita et al., 2003). Thereby, the stimulus time course is crucial for synaptic integration (Franzen et al., 2015). However, the role of the two EPSC components for postsynaptic AP generation has not been elucidated yet. One hypothesis suggests that both components together define the current threshold for AP generation. The basis for the crucial bi-exponential shape of EPSC decays might be linked to the types of postsynaptic ligand gated ion channels involved. In the mammalian CNS, glutamate receptors (GluRs) are widely distributed, mediating synaptic transmission and comprising three subtypes of postsynaptic ionotropic GluRs (Pinheiro et al., 2012; Geiger et al., 1995; Johnson and Ascher, 1987; Mayer et al., 1984; Nowak et al., 1984): AMPARs for rapid glutamatergic signalling (Geiger et al., 1995), NMDARs for slow glutamatergic signalling (Dzubay and Jahr, 1996) and kainate receptors (KAR) (Cossart et al., 2002). All three subtypes are heteromers consisting of different subunits: GluR1-4 for AMPARs, GluN1, GluN2A-D and GluN3A-B for NMDARs and GluK1-5 for KARs (see Furukawa, 2012 for a review; Lu et al., 2009). Thereby, the subunit composition of receptors and the mediated currents change during postnatal development (Pliss et al., 2009; Irfan et al,. 2005; Caicedo and Eybalin, 1999). Both non-NMDARs and NMDARs are activated by the binding of glutamate and mainly mediate Na^+ influx and K^+ efflux. In contrast to the non-NMDARs, the NMDARs require a certain degree of membrane depolarisation in addition to the binding of glutamate to overcome the voltage dependent magnesium (Mg^{2+}) block (Mayer et al., 1984; Nowak et al., 1984). The different receptor subtypes apparently do not work separately, but rather in concert

with each other as it has been described for the interaction of AMPA- with NMDARs (see Caporale and Dan, 2008 and Lisman, 1989 for review): The opening of NMDARs depends on previous AMPAR activation, leading to Na^+ influx, which in turn depolarises the membrane and supports the overcome of the voltage dependent Mg^{2+} block of NMDARs. Since NMDARs are permeable for Ca^{2+} and are ideal for slow glutamatergic signalling, they can drive plasticity switch and persistent signalling. Thus, intracellular Ca^{2+} mediates widespread and lasting changes in the postsynaptic neuron by triggering a series of signal transduction cascades involving kinases and phosphatases to activate enzymes, opening channels or expressing genes (see Lüscher and Malenka, 2012; Caporale and Dan, 2008 and Lisman, 1989 for review).

6.2.2 Short-Term Plasticity (STP) in the VNLL

As stated before, synaptic transmission is not constant, but varies according to the stimulus history. Synaptic transmission at the VNLL is affected by frequency dependent STP for excitatory currents *in vitro* in young and adult VNLL neurons in mice (Baumann and Koch, 2017; Caspari et al., 2015). Whereas STF in the VNLL has mostly not been observed in previous studies, STD is the better-studied synaptic phenomenon. STD increases with stimulation frequency during ongoing stimulation (Baumann and Koch, 2017; Caspari et al., 2015) and oppresses high activity signals with temporally less accurate information (Yang and Xu-Friedman, 2009). Effects of STD on the AMPAR mediated EPSC amplitude might be counteracted by the NMDAR mediated current proportion in EPSCs, which increases due to the formation of a frequency dependent NMDAR mediated build-up current during ongoing stimulation. This has been documented in the AVCN in mice and *in vivo* for inhibitory currents in the gerbil DNLL. This accumulation occurs during stimulation frequencies of 100 Hz and above (Pliss et al., 2009). Regarding postsynaptic spike generation, build-up currents probably support long-lasting activation to downstream neurons by increasing the amount of elicited APs (Siveke et al., 2018; Porres et al., 2011; Pliss et al., 2009; Harsch and Robinson, 2000). For the temporal precision of supra-threshold responses in the VNLL, latency and jitter increase during ongoing stimulation (Baumann and Koch, 2017). This is probably mediated by presynaptic changes or by a change in postsynaptic input conductance during ongoing stimulation (Chanda and Xu-Friedman, 2010; Yang and Xu-Friedman, 2009). Taken together, although much research has been done on synaptic glutamatergic signalling across species and regions within the mammalian auditory brainstem, the mechanisms underlying temporally precise processing at the VNLL endbulb and its function within the circuit of ascending auditory pathways are still not well understood.

7. AIMS

This thesis aims to investigate neuronal intrinsic tuning across invertebrates and vertebrates in order to point out the universality of this feature for central stimulus discrimination in the CNS. Beyond that, this thesis intends to investigate the physiological basis for temporally precise information processing in VNLL neurons, which are involved in central auditory processing. Therefore, the following three objectives were set for this project:

1. **Frequency filter banks in invertebrates.** As a well-studied model organism, the medicinal leech *Hirudo medicinalis* was used as a representative of invertebrates to examine intrinsic frequency tuning in mechano-sensory neurons. Therefore, somatic intracellular current-clamp recordings were performed in different sensory neuron types of segmental ganglia.

2. **Membrane resonance in vertebrates.** Subthreshold membrane potential resonance in the auditory brainstem is a well described feature in vertebrates for stimulus discrimination. To show the universality of this phenomenon across nuclei in the mammalian ascending auditory pathway, whole-cell current-clamp recordings were performed in five different neuronal populations: neurons of the MSO of young and mature Mongolian gerbils *Meriones unguiculatus*, the LSO of mature B57Bl6/6N mice and Brown Norway rats, and the VNLL of mature gerbils. Hence, the sample comprises neurons that perform auditory computations in the low- and high frequency range and which are involved in the processing of temporal information of acoustic stimuli.

3. **Synaptic mechanisms for temporal precision.** To further examine temporal processing in the vertebrate, mammalian auditory brainstem, synaptic information transfer and supra-threshold current integration at the VNLL endbulb was studied, performing whole-cell voltage- and current-clamp recordings of VNLL neurons in acute brain slices of hearing Mongolian gerbils *Meriones unguiculatus*. The investigation of stimulus discriminability of postsynaptic response patterns and the role of EPSC components on AP generation and precision was conducted using a combination of whole-cell conductance-clamp recordings of VNLL neurons and computational modelling provided by M.R. and C.L.

PUBLICATIONS

Intrinsic frequency response patterns in mechano-sensory neurons of the leech

Linda Fischer, Frank Scherbarth, Boris Chagnaud, Felix Felmy (2017)

Fischer, L., et al. (2017). "Intrinsic frequency response patterns in mechano-sensory neurons of the leech." Biol Open **6**(7): 993-999. DOI: 10.1242/bio.023960
https://www.ncbi.nlm.nih.gov/pubmed/28546342

Author contributions:

F.F. raised funding, project administration and supervision.
F.F., B.C. and L.F. designed experimental study.
L.F. performed electrophysiological recordings.
B.C. provided fluorescent labelled leech ganglion for Fig. 1a.
F.F. and B.C. provided concept for analysis.
L.F., F.S., B.C. and F.F. analysed data.
L.F., F.S., B.C. and F.F. interpreted results.
L.F., F.S. and F.F. prepared the figures.
L.F., F.S. and F.F. wrote the first version of the manuscript.
L.F., B.C. and F.F. reviewed and edited the manuscript.

ABSTRACT

Animals employ mechano-sensory systems to detect and explore their environment. Mechano-sensation encompasses stimuli such as constant pressure, surface movement or vibrations at various intensities that need to be segregated in the central nervous system. Besides different receptor structures, sensory filtering via intrinsic response properties could provide a convenient way to solve this problem. In leech, three major mechano-sensory cell types can be distinguished, according to their stimulus sensitivity, as nociceptive, pressure and touch cells. Using intracellular recordings, we show that the different mechano-sensory neuron classes in *Hirudo medicinalis* differentially respond supra-threshold to distinct frequencies of sinusoidal current injections between 0.2 and 20 Hz. Nociceptive cells responded with a low-pass filter characteristic, pressure cells as high-pass filters and touch cells as an intermediate band-pass filter. Each class of mechano-sensory neurons is thus intrinsically tuned to a specific frequency range of voltage oscillation that could help segregate mechano-sensory information centrally.

Key words: Input-output function, Sensory filter, Neuronal excitability, Sensory integration, Medicinal leech

Resonance properties in Auditory Brainstem Neurons

Linda Fischer, Christian Leibold, Felix Felmy (2018)

Fischer, L., et al. (2018). "Resonance Properties in Auditory Brainstem Neurons." Front Cell Neurosci **12**: 8. DOI: 10.3389/fncel.2018.00008
https://www.ncbi.nlm.nih.gov/pubmed/29416503

Author contributions:

F.F. raised funding.
F.F. and C.L. designed experimental study.
L.F. performed electrophysiological recordings in mice and rats. F.F. performed electrophysiological recordings in gerbils.
C.L. designed the mathematical model.
F.F. and C.L. provided concept for analysis.
L.F., C.L. and F.F. analysed data.
L.F. and F.F. prepared Fig. 1-3 and 5. C.L. prepared Fig. 4 and 6.
C.L. and F.F. wrote the paper.

ABSTRACT

Auditory signals carry relevant information on a large range of time scales from below millisecondstoseveralseconds.Differentstagesintheauditorybrainstemarespecialized to extract information in specific frequency domains. One biophysical mechanism to facilitate frequency specific processing are membrane potential resonances. Here, we provide data from three different brainstem nuclei that all exhibit high-frequency subthreshold membrane resonances that are all most likely based on low-threshold potassium currents. Fitting a linear model, we argue that, as long as neurons possess active subthreshold channels, the main determinant for their resonance behavior is the steady state membrane time constant. Tuning this leak conductance can shift membrane resonance frequencies over more than a magnitude and therefore provide a flexible mechanism to tune frequency-specific auditory processing.

Key words: membrane resonance, auditory brainstem, MSO, LSO, VNLL

MANUSCRIPT

Author contributions:

F.F. and C.L. designed the study, wrote the funding application and received the DFG grant FE 789/6-1 (AOBJ: 622960) within the DFG priority program 1608 “ultrafast and temporally precise information processing: normal and dysfunctional hearing”.
L.F. and N.K. performed electrophysiological experiments. L.F. performed voltage-clamp recordings for Fig. 3 and 4, current-clamp recordings for Fig. 9, conductance-clamp recordings for Fig. 6-8, 11, 12 and for Fig. 10 regarding stimulation at threshold. N.K. performed conductance-clamp recordings for Fig. 10 regarding stimulation at steady firing and for Fig. 13. N.K. fitted data with the Boltzman function in Fig. 5.
L.F. and N.K. created templates for conductance-clamp train experiment of distinct frequencies. M.R. created pseudorandomly distributed frequency templates.
L.F., N.K., F.F., and C.L. analysed data. L.F. and N.K. wrote macros in Igor Pro software for wave analysis. F.F. provided concept for analysis of Fig. 1-8, 10 and 11. C.L. provided concept for analysis of Fig. 9.
L.F., N.K., F.F., and C.L. interpreted results of experiments. L.F. and F.F. interpreted results of Fig. 3, 4, 9 and 11. L.F., N.K., and F.F. interpreted results of Fig. 6-8, 10 and 13. L.F., F.F., and C.L. interpreted results of Fig. 12.
L.F., N.K., and F.F. prepared figures. L.F. and F.F. prepared Fig. 3, 4, 6-9, 11 and 12. L.F., N.K., and F.F. prepared Fig. 8. N.K. and F.F. prepared Fig. 13. N.K. prepared Fig. 3.
L.F. and F.F. wrote the first version of the manuscript.

Synaptic Mechanisms underlying Temporally Precise Information Processing in the VNLL

Fischer Linda,[1,2], Rebhan Michael,[3] Kladisios Nikolaos,[1,2] Leibold Christian,[4] Felmy Felix[1]

[1]*Institute of Zoology, University of Veterinary Medicine Hannover*
[2]*Hannover Graduate School for Veterinary Pathobiology, Neuroinfectiology, and Translational Medicine (HGNI)*
[3]*Department Biology II, Ludwig-Maximilians-University Munich*
[4]*Bernstein Center for Computational Neuroscience Munich*

Corresponding address for reprint requests and other correspondence: F. Felmy, Institute of Zoology, Division of Neurophysiology and Neuroinfectiology, University of Veterinary Medicine Hannover, Bünteweg 17, 30559 Hannover (e-mail: felix.felmy@tiho-hannover.de).

Fischer L, Rebhan M, Kladisios N, Leibold C, Felmy F. Synaptic Mechanisms underlying Temporally Precise Information Processing in the VNLL. - Neurons in the ventral nucleus of the lateral lemniscus (VNLL) show highly precise temporal discharge patterns locked to the sound onset, which can transition into ongoing firing during amplitude modulated (AM) sound stimulation. At the VNLL endbulb fast relay of sign inverted information is taking place, turning excitatory glutamatergic input into inhibitory output. Glutamatergic excitatory postsynaptic currents (EPSCs) at this endbulb decay bi-exponentially, revealing a slow and a fast component. During ongoing AM stimulation, EPSCs undergo short-term plasticity. In general, EPSC shape is crucial for synaptically driven output generation and might therefore contribute to high precision and high firing rates in VNLL neurons. Here we show the physiological basis and role of the biphasic EPSC shape for precise ongoing output generation performing electrophysiological recordings of VNLL neurons in hearing gerbils (*M. unguiculatus*). Results reveal exclusive contribution of Alpha-amino-3-hydroxy-5-methyl-4-isoxazolepropionate- (AMPA) and N-methyl-D-aspartate receptor (NMDAR) mediated currents in EPSCs at the VNLL endbulb. Furthermore, this study elucidates the effect of frequency dependent short-term plasticity and NMDAR mediated currents on precise ongoing output generation, providing evidence that the generated inhibitory output at the VNLL endbulb supplies fast onset inhibition to ascending structures, to sharpen the cell response to broadband noise.

Key words: auditory system; ventral nucleus of the lateral lemniscus; endbulb synapse; synaptic transmission; glutamatergic signalling; temporal precision

Information transfer at auditory synapses happens with high temporal precision (Krächan et al., 2017; Liu et al., 2014; Recio-Spinoso and Joris 2014; Zhang and Kelly 2006; Covey and Casseday, 1991 and 1986). There are three large glutamatergic, somatic synapses of nearly the same morphology and input-output function in the ascending pathway of the mammalian auditory brainstem: The endbulb of Held at the anteroventral cochlear nucleus (AVCN), the calyx of Held at the medial nucleus of the trapezoid body (MNTB) and the endbulb at the ventral nucleus of the lateral lemniscus (VNLL). For all three synapses, alpha-amino-3-hydroxy-5-methyl-4-isoxazolepropionate receptor (AMPAR) mediated synaptic excitatory postsynaptic currents (EPSCs) consist of two components and decay bi-exponentially, as, e.g., already shown for the endbulb of Held in mice (Chanda and Xu-Friedman, 2010), for the calyx of Held in rats (Yamashita et al., 2003) and in a comparative analysis for the calyx of Held and the VNLL endbulb in juvenile gerbils (Berger and Meyer et al., 2014). Here, we use the VNLL endbulb to examine the source and impact of EPSC shape on postsynaptic action potential (AP) generation.

The VNLL is located in the lateral lemniscus (LL) between the superior olivary complex (SOC) and the inferior colliculus (IC) (Mylius et al., 2013; Budinger et al., 2000). When an acoustic stimulus reaches the ear, information is conveyed to cells in the octopus cell area (OCA) located in the posterioventral cochlear nucleus (PVCN), from where main excitatory glutamatergic input for contralateral VNLL (cVNLL) neurons emerges. Octopus- and multistellate cells send their axons to the cVNLL where they form large somatic synapses (Schofield and Cant, 1997; Friauf and Ostwald, 1988). Thereby, several large somatic inputs can converge on single VNLL neurons in juvenile animals (Berger and Meyer et al., 2014). At the mature VNLL endbulb, fast relay of sign inverted information is taking place: The generated output is inhibitory, mediated by glycine and γ-Aminobutyric acid (GABA) (Moore and Trussell, 2017; Saint Marie et al., 1997), and fed forward to the IC (Mylius et al., 2013). Since VNLL neurons code for sound transients and are monaurally driven by stimulation of the contralateral ear (Zhang and Kelly, 2006; Covey and Casseday, 1991), they are thought to be implicated in processing conspecific vocalisation (Oertel et al., 2000).

Within the VNLL, various cell types have been identified (Mylius et al., 2012; Convey and Casseday, 1986). In the ventral VNLL (vVNLL), globular neurons dominate (Berger and Meyer et al., 2014; Caspari et al., 2015). They show highly precise temporal discharge patterns locked to the sound onset, when stimulated with short sound bursts, with a jitter of around 200 µs, short latencies and integration times of supra-threshold responses, suggesting that VNLL neurons maintain extremely precise timing information concerning the stimulus onset (Liu et al., 2014; Recio-Spinoso and Joris, 2014; Zhang and Kelly, 2006; Covey and Casseday, 1991). Thereby, onset timing is invariant to stimulation sound pressure level and frequency (Liu et al., 2014; Recio-Spinoso and Joris, 2014; Zhang and Kelly, 2006; Covey and Casseday, 1991). Onset firing can transition into high firing rates during ongoing amplitude modulated (AM) sounds, whereby the cell response is highly synchronised to sound envelopes of maximal 300 Hz and narrowly tuned to modulation rates (Zhang and Kelly, 2006).

Here out the question concerning the cellular basis for firing properties arises. During rapid information transfer at the VNLL endbulb, the synaptic EPSC time course is crucial for synaptically evoked supra-threshold output (Franzen et al., 2015, Ammer et al., 2012, Axmacher and Miles, 2004). The bi-exponential EPSC might be conducted by rapid glutamate signalling at the VNLL synapse. There are three subtypes of postsynaptic ionotropic glutamate receptors in the mammalian central nervous system (CNS) (Pinheiro et al., 2012; Geiger et al., 1995; Johnson and Ascher, 1987; Mayer et al., 1984; Nowak et al., 1984): AMPARs for rapid (Geiger et al., 1995), N-methyl-D-aspartate receptors (NMDARs) for slow glutamatergic signalling (Dzubay and Jahr, 1996) and Kainate receptors (KARs).

Moreover, synaptic short-term plasticity (STP) might influence synaptic transmission and, for example, improve coincidence detection (Cook et al., 2003; Kuba et al., 2002), contribute to spike adaptation (Chung et al., 2002), and mediate gain control (see Rothman et al., 2009 for review). Conductance-clamp (GC) recordings revealed an impact of the degree of STD on response probability and timing (Yang and Xu-Friedman, 2009). Also in the VNLL of adult mice, AMPA- and NMDAR mediated signalling has been shown to undergo frequency dependent STP (Caspari et al., 2015).

Based on this background, we hypothesised that dual components of EPSCs and the STP are key features for precise ongoing output generation. To test this, we quantitatively described dynamics of afferent synapses and examined their supra-threshold current integration using a combination of electrophysiological recordings of VNLL neurons of hearing Mongolian gerbils *M. unguiculatus* and computational modelling. Taken together, we demonstrate an activity dependent role of STP and postsynaptic AMPA- and NMDAR mediated currents on AP generation.

MATERIALS AND METHODS

Animals and housing. Recordings were made in male and female Mongolian gerbils (*M. unguiculatus*) of average postnatal age (P) 23.53 ± 0.4 days of own breeding of the Institute of Zoology at the University of Veterinary Medicine, Hannover. Animals were kept monogamous in breeding pairs together with appropriate litters in Makrolon Type IV cages, with dimensions of 59x38x20 cm (LxTxH), 1.815 cm^2 floor area, enriched with bedding, a wooden house (self-made), tissue for nesting material, food pellets and water ad libitum. The temperature of 22°C, the humidity of 35-44% and the 12 hours dark-light-cycle (7-19 o'clock light phase wintertime), were constantly monitored.

Slice Preparation. All experiments were performed in accordance with institutional guidelines and regional laws. Animals were deeply anesthetised using an isoflurane (1ml/ml, cp-pharma) filled desiccator. Animals were decapitated using scissors, the skullcap was removed, connections to the brain were cut using scalpel and tweezers and the brain was taken out. Cerebellum and prefrontal cortex were removed so that the remaining parts of the brain could be superglued (UHU GmbH & Co. KG) in a slice chamber filled with slice solution containing (mM) 120 D-Saccharose, 25 NaCl, 25 $NaHCO_3$, 1.25 NaH_2PO_4, 2.5 KCl, 25 D-Glucose, 0.4 L-Ascorbic acid, 3 Myo-Insositol, 2 Na-pyruvate, 3 $MgCl_2$, 0.1 $CaCl_2$, pH=7.4 when oxygenated with 95% O_2 and 5% CO_2. The brain was cut into 200 µm thick slices containing the VNLL using a vibratome (Leica VT1200, Leica Microsystems GmbH, Germany). Slices were transferred into recording solution containing (mM) 125 NaCl, 25 $NaHCO_3$, 1.25 NaH_2PO_4, 2.5 KCl, 25 D-Glucose, 0.4 L-Ascorbic acid, 3 Myo-Inositol, 2 Na-Pyruvate, 1 $MgCl_2$, 2 $CaCl_2$ for voltage-clamp (VC), 1.2 $CaCl_2$ for GC, pH=7.4 when oxygenated with 95% O_2 and 5% CO_2 and incubated for at least 45 min at 34.2°C in a universal stirred water bath (Type BWT-U No. 010404-120-0095, Version V.1AA, Kirkser Biothech GmbH&Co. KG). For VC experiments, (µM) 10 SR 95531 hydrobromide and 1 Strychnine (Stry) were added to the recording solution to suppress inhibitory inputs. (µM) 10 (R)-CPP, 50 GYKI 53655, 99.9% (latter diluted in dimethylsulfoxid) or 20 6,7-dinitroquinoxaline-2,3-dione (DNQX) respectively were applied to block NMDA-, AMPA-, and KAR mediated currents.

Electrophysiology in VC and GC. Slices were transferred into a recording chamber integrated into an upright microscope (VC: BX51, 0WI; Olympus, Center Valley, PA; GC: BCXT1WI; Olympus) which was continuously perfused with bubbled recording solution using a pump (ISMATEC, a unit of IDEX Corporation, model ISM796B and ISM796C), and heated to a physiologically relevant level of 34.57 ± 0.1°C using a dual automatic temperature controller (TC-344, Warner Instrument Cooperation, HARVARD Apparatus). Electrophysiological recordings were performed using PatchMaster software on a computer connected to a patch-clamp EPC 10/2 USB amplifier (HEKA, Lambrecht/Pfalz, Germany). For GC, an additional computer and DA board interface (BNC-2090A, National Instruments) were used. Visualisation was conducted using a camera (VC: TILL-Imago VGA, Retiga 2000DC; GC: SCMS PCO.edge 3.1m) integrated into the microscope, which in turn was connected to a computer, controlled by TILLvisION imaging system for VC (FEI Munich GmbH, Munich, Germany) and Camware64 imaging system for GC experiments. Cells were recorded in whole-cell configuration using glass capillaries (0.86x1.50x100 mm; Harvard Apparatus Ltd., Edenbridge, Kent, UK) which were pulled with 5.31 ± 0.4 MΩ average tip resistance using an electrode horizontal DMZ-Universal Puller (DMZ-Universal Puller Model P87, Zeitz Instruments, Martinsried, Germany and Flaming/Brown Micropipette puller Model P-97). Glass electrodes were then filled with intracellular solution containing for VC (mM) 130 Cs-Gluconate, 10 HEPES, 20 TEA-Cl, 4 MgATP, 0.3 NaGTP, 5 Na-Phosphocreatine, 5 Cs-EGTA, 5 Qx 314, 0.1 Spermin, 0.05 Alexa and for GC (mM) 4.5 KCl, 145 K-Gluconate, 15 HEPES, 2 Mg-ATP, 2 K_2-ATP, 0.3 Na_2GTP, 7 Na_2-Phosphocreatine, 0.5 K-EGTA, 0.05 Alexa and mounted onto the pipette holder (EPC10 usb GND, HEKA). Micromanipulators (Scientifica, models: U1-1000-I, ACCI UI and ACCiUI) were

used for electrode positioning under the microscope. For afferent fibre stimulation (AFS), the stimulation electrode was filled with recording solution.

VC recordings were performed at -50 mV holding potential. The liquid junction potential (LJP) of -13 mV in VC experiments was adjusted offline, whereas in GC LJP of -16 mV was corrected online. Throughout VC recordings, the series resistance was compensated by a constant residual of 2 MΩ. Throughout GC recordings bridge balance was set to 100%, and throughout all experiments the capacitance of electrodes and cells were compensated. Sampling interval was set to 20 µs/50 kHz. For GC recordings, V_{rev} for AMPAR mediated currents was set to 0 mV. NMDAR mediated currents were defined using the Boltzmann fit, with V_{rate} = 23.046 and V_{half} = -24.282 (calculation described below).

Experimental protocols: In VC, when the VNLL cell was patched and the stimulation electrode was brought onto the presynaptic fibre the stimulation intensity was adjusted to faithfully elicit one EPSC. In order to investigate input-output functions of synaptic components at the endbulb, cells were stimulated with one input, mimicking the arrival of an AP at the synapse, at different step potentials. Pharmacological treatment was conducted to characterise contributing EPSC components.

For investigating activity dependent STP, 20 pulses of various frequencies (1, 10, 50, 100, 250, 333, 400 Hz) were injected into the cells. Applying these protocols in combination with pharmacological treatment aimed for the examination of frequency dependent kinetics of EPSC components.

Results of the VC train experiment were used to create templates required for GC experiments. Therefore, recorded current responses were averaged for every frequency, and then transformed into one average conductance template for 1, 10, 50, 100, 333 and 400 Hz for AMPA- and NMDA currents respectively. For EPSC conversion into templates, the following formulas were used for AMPA: $(I/(V_{hold}*1000))$ and NMDA: $(I*(1+\exp((V_{half}-(-V_{hold}))/V_{rate})))/(V_{hold}*1000)$, with V_{half} and V_{rate} resulting from the Boltzman equation $I = A[V_{hold}(t)-V_{rev}]/[1+\exp(V_{half}-V_{hold})/V_{rate}]$. The created templates allowed the separate investigation of activity dependent effects of EPSC components on postsynaptic AP generation and precision for different stimulation frequencies and intensities.

Since during experiments, AP generation throughout 400 Hz train stimulation was not feasible in GC, cells were additionally stimulated with a 400 Hz train in current-clamp (CC), which in contrast to GC templates consisted of pulses of identical size and duration, in order to identify the source for the spike limitation observed under GC protocol conditions.

After the characterisation of EPSCs and their contribution to spiking behaviour under standardised frequency conditions, cells were introduced to a pseudorandomly distributed frequency (PrDF) train stimulus comprising 691 pulses with inter stimulus intervals (ISIs) ranging from 2.32 to 666.82 Hz. Templates were created for AMPA- and NMDAR mediated components with and without STP. These PrDF trains were used to investigate the postsynaptic AP generation in VNLL neurons under more natural conditions. Temporal precision was evaluated by the standard deviation of the time difference between stimulus and spike time t(m,n), for all stimuli using $\sqrt{((\sum m(\sum n(t(m,n)-tau(m))^2))/(N(m))/M)}$ with $tau(m) = \sum n(t(m,n))/N(m)$, whereby variables were defined as m = serial numbering of stimuli in PrDF stimulus train (1-691), M = number of stimuli in PrDF stimulus train (691), n = spikes, N(m) = number of spikes for all repetitions for stimulus m. Additionally, the average latency was calculated using $\sum m(tau(m))/M$. Further, the average spike number per stimulus was calculated using $(\sum m(N(m))/M)/(\text{number of repetitions})$.

To investigate limitations in temporal integration for supra-threshold responses, an additional experiment was performed where cells were stimulated with paired-pulses (PPs) of the same amplitude at different intensities. Thereby ISIs ranged from 10 up to 2000 Hz.

Data analysis. Custom written Igor Pro Version 6.37 (WaveMetrics, Lake Oswego, OR) procedures were used to analyse electrophysiological data, to create conductance templates, and to scale the templates

online during GC experiments. Microsoft Excel 2010 software was used to analyse electrophysiological data. PrDF generation was done by M.R. and C.L., using Matlab. Statistical analysis was done using GraphPad Prism 8.0.1 (244): All data was tested for normal distribution using Kolmogorov-Smirnov test (KS) with the assumption of a 5% α-level. Normally distributed data was further analysed either with paired or unpaired t-test. Not normally distributed data was either analysed with paired two-tailed Wilcoxon matched-pairs rank test (WMP), unpaired Mann-Whitney test (MW) or Friedman test. Data are documented as averages with SEM or as median.

RESULTS

Pharmacological isolation of EPSC components. Synaptic EPSC components at the VNLL endbulb in hearing gerbils of P21.46 ± 0.7 were identified by performing pharmacological VC recordings in acute brain slices. Neurons were held at different voltages during stimulation. These recordings characterised currents contributing to synaptic EPSCs. Inhibitory currents were blocked using SR for GABAR and Stry for glycine receptors, to ensure that solely excitatory currents were recorded.
EPSCs at the VNLL endbulb are mediated exclusively by AMPA- and NMDARs (Fig. 3). Recordings with SR and Stry showed bi-exponentially decaying EPSCs. Pharmacological treatment with CPP, a competitive NMDAR antagonist, eliminates the second component, suggesting that this EPSC part is NMDAR driven (Fig. 3A). The resulting I-V curve shows a small amount of NMDAR mediated current at strongly hyperpolarised potentials of -93 and -83 mV, reaching a negative maximum of -0.28 ± 0.03 nA, at -33 mV and depolarising until it reaches the reversal potential of 0 mV. In contrast, the average AMPAR mediated current behaves linearly at negative step potentials, starting with -8.67 ± 0.3 nA at -93 mV, depolarising monotonically, until it reaches 2.73 ± 0.2 nA at +67 mV. Adding CPP results in the complete elimination of average NMDAR mediated currents (paired two-tailed WMP test or paired two-tailed t-test: at -93 mV HP: W = 28.0, p = 0.016, at -33 mV HP: W = 28.0, p = 0.016, at +67 mV HP: t(6) = 3.01, p = 0.024, n = 7) and in a decrease in average AMPAR mediated currents (paired two-tailed WMP test or paired two-tailed t-test: at -93 mV HP: W = 28.0, p = 0.016, at -33 mV HP: t(6) = 6.94, p = 0.0004, at +67 mV HP: t(5) = 3.13, p = 0.026, n = 7). The median proportion of NMDAR mediated current that is left after CPP treatment values 0.02 nA and ranges from 0.01 to 0.3 nA (Fig. 3B).
To analyse the EPSC timing, decays were fitted bi-exponentially. Two components in the AMPAR mediated current were extracted by determining the fast (τ_1) and the slow decay time (τ_2). τ_1 means the decay of the fast EPSC component of 0.16 ± 0.006 ms to 0.35 ± 0.2 ms, revealing no significant change from step potential -93 mV up to -53 mV under both conditions, with or without CPP (Friedman test: without CPP: F = 9.49, n.s.; with CPP: F = 8.80, n.s, n = 7). T_2 means the decay of the slow EPSC component, which increases significantly with depolarisation level, starting with 2.4 ± 0.4 ms at -93 mV, and increasing continuously to 8.0 ± 0.9 ms at -57 mV (paired two-tailed t-test: τ_2 comparison between -93 mV and -53 mV: t(6) = 4.20, p = 0.006). Blocking NMDARs removes this voltage dependence (paired two-tailed t-test: t(6) = 0.2, n.s., n = 7; Fig. 3C). Fraction analysis reveals voltage dependence of A_1, starting with -6 ± 0.4 nA at -93 mV and increasing continuously to -3.65 ± 0.2 nA at -57 mV (paired two-tailed WMP test: comparison between -93 and -53 mV: W = 26.0, p = 0.031, n = 7), which is unchanged when adding CPP (paired two-tailed WMP test: comparison at -93 mV: W = 14.0, n.s., comparison at -53 mV: W = 20.0, n.s., n = 7). Concerning A_2, currents are voltage- and CPP independent for the most part (paired two-tailed WMP test: comparison between -93 and -53 mV without CPP: W = 2.0, n.s.; difference to A_2 with CPP at -93 mV: W = 14.0, n.s., at -53 mV: W = 16.0, n.s., n = 7; Fig. 3D). Combining decay time constants τ_1 and τ_2 and calculating the weighted tau (τ_w) using $(\tau_1*A_1+\tau_2*A_2)/(A_1+A_2)$ reveals voltage dependence of the second EPSC component: at -93 mV τ_w

values 0.25 ± 0.04 ms. Increasing the potential to -57 mV increases τ_w to 1.12 ± 0.3 ms. Compared to recordings with CPP, where τ_w ranges from 0.24 ± 0.02 to 0.34 ± 0.1, this means a larger τ_w when recorded with NMDA. Thereby the difference in τ_w between both stimulation paradigms becomes significant from -83 mV onwards. The largest difference in τ_w was recorded at -73 mV step potential (paired two-tailed t-test or two-tailed WMP test: -93 mV: t(6) = 0.41, ns; -83 mV: W = -28.0, p = 0.016; -73 mV: t(6) = 2.91, p = 0.027; -63 mV: W = -26.0, p = 0.031; -53 mV: W = -22, p = 0.078, n = 7; Fig. 3E). Overall, results suggest that NMDAR mediated currents influence the EPSC timing at the VNLL endbulb.

After having identified the slow EPSC component and its kinetics, the fast EPSC component was examined by pharmacological treatment with GYKI, a non-competitive AMPAR antagonist. This treatment results in the elimination of the fast component suggesting its exclusive mediation by AMPARs (Fig. 3F). The appropriate I-V curve supports this finding, revealing the linearity of the average peak current amplitude and complete current elimination in the presence of GYKI (paired two-tailed t-test: at -93 mV HP: t(5) = 15.02, p<0.0001; at -33 mV HP: t(5) = 18.05, p<0.0001, at +67 mV HP: t(5) = 10.51, p<0.0001, n = 6 for all step potentials). The rectification index (RI) emphasises the linearity of the AMPAR mediated currents. It takes the average current amplitudes of all 13 cells recorded in this experiment into account, and was obtained by applying a linear fit to the average peak current amplitude from -93 mV to -3 mV step potential, which reflects the step potential range where the current is not rectified. Coming from the linear fit, the deviation of the first and last three averaged average peak currents in the I-V curve was calculated under the assessment, that a value of 1 reflects a perfectly linear course of the I-V curve. The average RI values 0.41 ± 0.03, ranging from 0.30 to 0.67 across cells (Fig. 3G). This RI suggests a reduced amount of the edited AMPAR subunit GluR2 in the mature AMPARs, in which presence, the current-voltage relationship would progress linearly. The inward rectification at positive step potentials in the presented data probably rather originates from the voltage dependent block of AMPARs by intracellular, endogenous polyamines (see Isaac et al., 2005 for review). Taken together, results show that EPSCs at the VNLL endbulb are mediated by two synaptic receptor types, AMPARs mediating the fast, and NMDARs mediating the slow component.

Frequency dependent STP. After having identified AMPA- and NMDARs as mediators of synaptic EPSCs at the VNLL endbulb, activity dependent short-term plasticity of synaptic transmission was investigated. This experiment aimed at two objectives: first, the examination of STP of AMPA- and NMDAR mediated synaptic currents under physiologically relevant conditions. The second objective was to characterise NMDAR mediated build-up currents which shape the second EPSC component. Therefore, trains with 20 pulses of 1, 10, 50, 100, 250 and 333 Hz at -63 mV holding potential were applied to the cells.

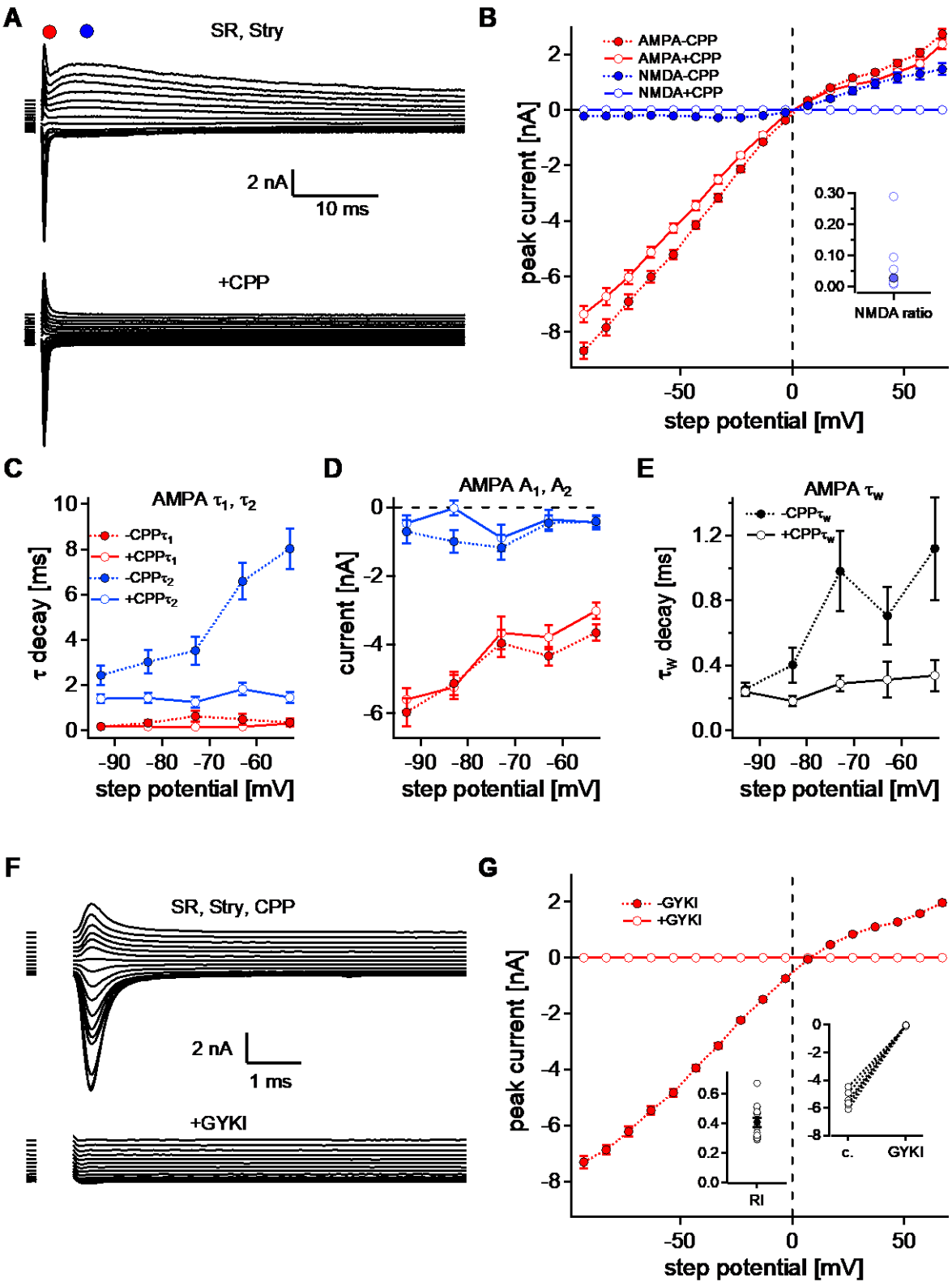

Fig. 3: AMPA- and NMDARs drive synaptic EPSCs at the VNLL endbulb**. A-E:** slow EPSC component is driven by NMDARs. **A**: Synaptic EPSCs in response to different step potentials with extracellular [mM] 2 $CaCl_2$ and 1 $MgCl_2$, with SR, Stry (*top*), revealing a fast (*red marker*) and a slow component (*blue marker*), and with CPP (*bottom*). **B:** Average peak current amplitude [nA] as a function of the step potential [mV] for NMDA- (*blue*) and AMPAR mediated currents (*red*) when recorded with (*white dots, solid lines*) or without CPP (*filled dots, dashed lines*). *Inset*: Single cell NMDAR mediated current amplitude ratio between recordings before and after CPP treatment at +67 mV step potential. **C:** average fast (τ_1, *red*) and slow (τ_2, *blue*) decay time [ms] of the AMPAR mediated currents when recorded with (*white dots, solid lines*) or without CPP (*filled dots, dashed lines*) plotted against

step potential [mV]. **D**: average AMPAR mediated current [nA] as a function of step potential [mV] for the fractions A_1 (*red*) and A_2 (*blue*) when stimulated with (*white dots, solid lines*) or without CPP (*filled dots, dashed lines*). **E:** average weighted decay time τ_w [ms] plotted against step potential [mV] when stimulated with (*white dots, solid lines*) or without CPP (*filled dots, dashed lines*). n = 7 cells. SEM. **F-G:** fast EPSC component is driven by AMPAs. **F:** Recordings in presence of extracellular SR, Stry and CPP (*top*) and with additional GYKI (*bottom*). **G:** average peak current amplitude [nA] plotted against step potential [mV] in absence (*filled dots*) or presence of GYKI (*white dots*). *Inset, left*: Single cell (*white dots*) and average RI (*filled dot*) for pharmacologically isolated AMPAR mediated currents. n=13. *Inset, right*: Comparison of peak current amplitudes recorded in absence (*c.*) or in presence of GYKI (*GYKI*) at -63 mV step potential for single cells. n = 6. SEM. All graphs LJP corrected. LJP: liquid junction potential; RI: rectification index.

EPSCs at the VNLL endbulb show frequency dependent STP (Fig. 4). At 1 Hz, EPSC size remains stable throughout the train stimulus. At higher frequencies, such as 333 Hz, the EPSC shows synaptic facilitation, revealing increased peak current amplitude compared to the first EPSC, followed by a depression phase until the end of the train (Fig. 4A). Under physiological conditions the median initial EPSC size was -5.20 nA ranging from -1.81 to -9.98 nA (Fig. 4B). Normalisation of EPSC amplitudes to the initial EPSC size quantifies the frequency dependence of the EPSC amplitude during the train stimulus. At 100 Hz and above, the 2nd and optionally two more following EPSCs show facilitation, followed by a depression phase. EPSCs in response to lower stimulation frequencies show no facilitation and a lower degree of depression (Fig. 4C). For facilitation, the pair pulse ratio (PPR) was calculated, meaning the change in average peak current amplitude from the 1st to the 2nd EPSC under the assumption that a PPR value of 1 means identical amplitudes for both peak currents. Results reveal frequency dependent change in PPR: For low frequency stimulations from 1 to 50 Hz, the 2nd average EPSC peak current amplitude was rather smaller or indifferent compared to the 1st EPSC peak (paired two-tailed t-test or two-tailed WMP test: 1 Hz: 1.01 ± 0.05, t(10) = 0.27, ns, n = 11; 10 Hz: 0.81 ± 0.02, t(4) = 4.54, p = 0.011, n = 5; 50 Hz: 0.95 ± 0.03, W = -8.0, ns., n = 7). With increasing stimulation frequency, the average PPR value increases significantly up to 1.34 ± 0.1 in response to a 333 Hz stimulus (two-tailed WMP test: W = 66.0, p = 0.007, n = 12; Fig. 4D).

Depression quantification was done by calculating the normalised average steady state (st.st.) peak current amplitude from the last three pulses. As for the facilitation, depression is frequency dependent. Depression was present in response to all stimulation frequencies, but its degree increased with stimulation frequency, revealing lowest depression at 1 Hz where 90 ± 1.8% of the initial EPSC size are still present in st.st., and strongest depression at 333 Hz where only 39.18 ± 2.2% current size are maintained (1 to 333 Hz: unpaired two-tailed MW test: U = 14.0, p = 0.0007, 10 Hz: n = 11, 333 Hz: n = 12). Blocking NMDARs with CPP has no significant effect on the degree of depression (unpaired two-tailed MW test or paired two-tailed t-test: 1 Hz: U = 46, ns., n = 11; 10 Hz: t(4) = 0.16, ns., n = 5; 50 Hz: t(6) = 0.59, ns., n = 7; 100 Hz: t(5) = 0.07, ns., n = 6; 250 Hz: t(6) = 0.18, ns., n = 7; 333 Hz: t(11) = 1.86, ns., n = 12; Fig. 4E). In order to examine the frequency dependent impact of NMDAR mediated currents on EPSC decay timing, the last EPSC of the train was fitted bi-exponentially to extract τ_w for all frequencies with and without NMDA (Fig. 4F). Results indicate a continuous increase in τ_w with stimulation frequency, starting with 0.2 ± 0.02 ms at 1 Hz, and increasing up to 0.9 ± 0.09 ms at 333 Hz (unpaired two-tailed t-test: t(21) = 4.98, p<0.0001, 1 Hz: n = 11, 333 Hz: n = 12). Blocking NMDARs decreases decay times, whereby the significance is limited to 333 Hz stimulation frequency (paired two-tailed t-test: 1 Hz: t(10) = 0.41, ns., n = 11; 10 Hz: t(4) = 0.46, ns., n = 5; 50 Hz: t(6) = 1.23, ns., n = 7; 100 Hz: t(5) = 1.87, ns., n = 6; 250 Hz: t(6) = 2.10, ns., n = 7; 333 Hz: t(11) = 2.83, p = 0.016, n = 12; Fig. 4G). Taken together, results indicate that EPSCs at the VNLL endbulb undergo frequency dependent STP, which is probably mediated by frequency dependent contribution of NMDAR mediated currents.

In order to investigate the influence of NMDAR mediated currents on the EPSC kinetics, and to analyse their frequency dependent build-up currents, they were pharmacologically isolated in three more cells. Synaptic EPSC trains of various frequencies were recorded at different holding potentials, applying SR and Stry to block inhibitory currents, and the AMPA antagonist DNQX to block the fast EPSC component. The following analysis was conducted on the basis of recordings at +37 mV (similar to analysis in Pliss and Xu-Friedman, 2009; Berger and Meyer et al., 2014), since peak current amplitudes at this potential were higher than at negative holding potentials and, thus, more suitable concerning kinetics evaluation.

NMDAR mediated currents show frequency dependent build-up. At 1 Hz the EPSC shape appears to be invariant to the stimulus position in the train. At 333 Hz, the EPSC shows a clearly visible build-up current throughout the train stimulus (Fig. 4H). Average 20-80 rise time of the 1st EPSC values 1.3 to 1.5 ms across frequencies, with a median of 1.25 ms (Fig. 4I). For the EPSC decay times, the last EPSC in the train stimulus was fitted exponentially, extracting τ, which clearly increases with stimulation frequency from 23.4 ± 6.1 ms at 1 Hz to 27.0 ± 7.5 ms at 10 Hz, 38.4 ± 5.2 ms at 50 Hz, to 40.6 ± 6.5 ms at 100 Hz, reaching a plateau. Further increase in stimulation frequency to 250 and 333 Hz reveals τ of 38.5 ± 7.2 and 43.5 ± 5.8 ms. Due to the low sample size (n = 3 for all stimulation frequencies), statistical analysis was not feasible (Fig. 4J). Taken together, results reveal that the slow NMDAR mediated EPSC component is frequency dependent.

Impact of distinct synaptic properties on output generation. So far, synaptic currents mediating EPSCs at the VNLL endbulb have been identified and quantitatively estimated. The obtained results from VC experiments were used to design templates for GC experiments in order to dissect the contribution of the different EPSC components for AP generation. For the template creation, average EPSCs of 1, 10, 50, 100 and 333 Hz trains from the previous VC experiment were used to calculate the average conductance a VNLL neuron receives at these frequencies. For the NMDA component, average NMDA peak current amplitudes of the first I-V experiment were fitted with a Boltzmann fit, identifying V_{half} = -24.282 and V_{rate} = 23.046, which were then inserted into appropriate formulas (see methods; formulas taken over from Yang et al., 2015; Fig. 5). For both, AMPA- and NMDAR mediated component, one template per frequency was obtained, which was used to inject an appropriate amount of current (I_{dc}) into the cell, taking the membrane- and the reversal potential of each stated conductance into account.

The general procedure intended to examine frequency dependent supra-threshold response patterns in VNLL neurons in GC. Therefore, cell responses to stimulation trains containing 20 pulses of 1, 10, 50, 100 and 333 Hz were recorded at various intensities. Thereby, stimulation intensity refers to the first pulse in the AMPA template.

Cell responses are linked to stimulation intensity, -frequency and the EPSC composition (Fig. 6). Low stimulation intensities elicit fewer APs than high intensities. At 50 Hz less intensity is needed to make cells fire throughout the train stimulus compared to higher frequencies. For the EPSC composition, the participation of NMDAR mediated currents on top of AMPA, resulted in a build-up current at high stimulation frequencies, which in turn impact the neuronal firing behaviour (Fig. 6A). First quantitative analysis revealed that the number of elicited APs increases with initial input conductance, as shown in an exemplary cell. Adding up NMDA, results in an increased number of APs. The number of elicited APs increases consistently with input conductance until it reaches steady firing when stimulated with 55.3, 49.1, 38.3 and 77.6 nS at 10, 50, 100 and 333 Hz with both EPSC components. Eliminating the slow component slightly shifts required conductance for steady firing to higher values.

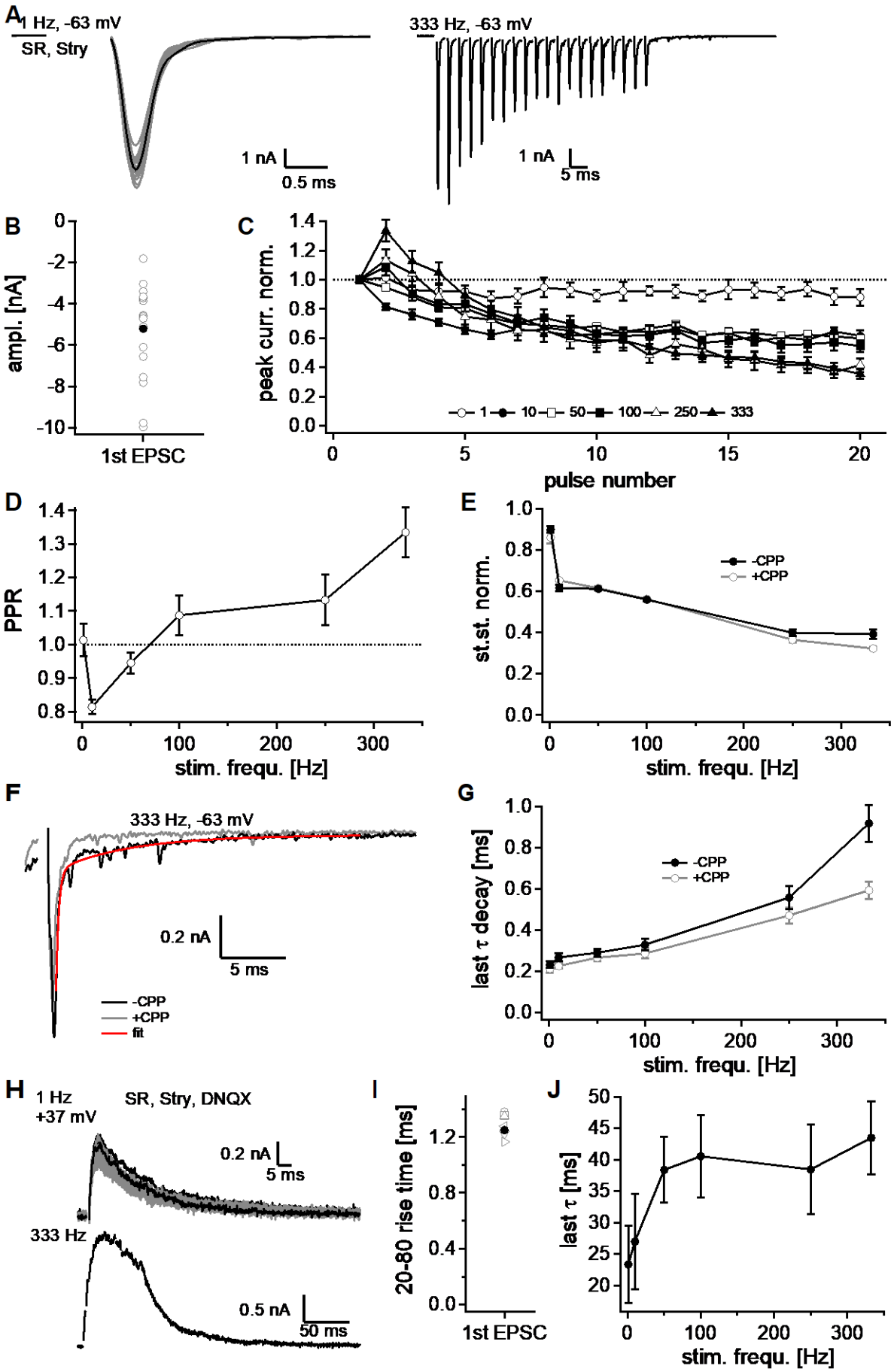

Fig. 4: AMPA- and NMDAR mediated STP is frequency dependent. **A-E:** Synaptic facilitation and depression. **A:** EPSCs recorded at -63 mV holding potential with SR and Stry in extracellular solution containing [mM] 1.2 $CaCl_2$

and 1 $MgCl_2$, in response to 20 pulses, at 1 Hz (*left, black: 1st and 20th EPSC, trials in between grey*) and 333 Hz (*right*). **B:** Single cell peak current amplitude [nA] of the 1st EPSC in response to a 10 Hz stimulus (*circled, grey*) and median (*filled, black*). **C:** average peak current amplitude normalised to the 1st EPSC plotted against pulse number for 1, 10, 50, 100 and 333 Hz trains. **D:** average PPR as a function of stimulation frequency [Hz]. *Dashed line*: value of 1 means identical peak current amplitudes for 1st and 2nd EPSC. **E:** average steady state values (mean of the three last EPSC peak current amplitudes in the train) of peak current amplitudes plotted against stimulation frequency [Hz] in absence (*filled, black*) or in presence of CPP (*circled, grey*). **F+G:** frequency dependent impact of NMDAR mediated currents on EPSC timing. **F:** 20th EPSC in response to a 333 Hz stimulus with (*grey*) and without CPP (*black*) recorded at -63 mV holding potential fitted with a bi-exponential function (*red*). **G:** average τ_w of 20th EPSC [ms] as a function of stimulation frequency [Hz] with (*circled, grey*) and without CPP (*filled, black*). **H-J:** NMDAR mediated STP is frequency dependent. **H:** Isolated NMDAR mediated EPSCs in response to 20 pulses at 1 Hz (*top, black: 1st and 20th EPSC, trials in between grey*) and 333 Hz (*bottom*) at +37 mV holding potential with SR, Stry and DNQX. **I:** Average 20-80 rise time [ms] of 1st EPSC for all frequencies [Hz] across cells (*grey, differently shaped markers*) and median (*black*). **J:** average last τ_w [ms] as a function of stimulation frequency [Hz]. For B-E, G: 1 Hz: n = 11, 10 Hz: n = 5, 50 Hz: n = 7, 100 Hz: n = 6, 250 Hz: n = 7, 333 Hz: n = 12. For H-J: n = 3. PPR: pair pulse ratio. SEM.

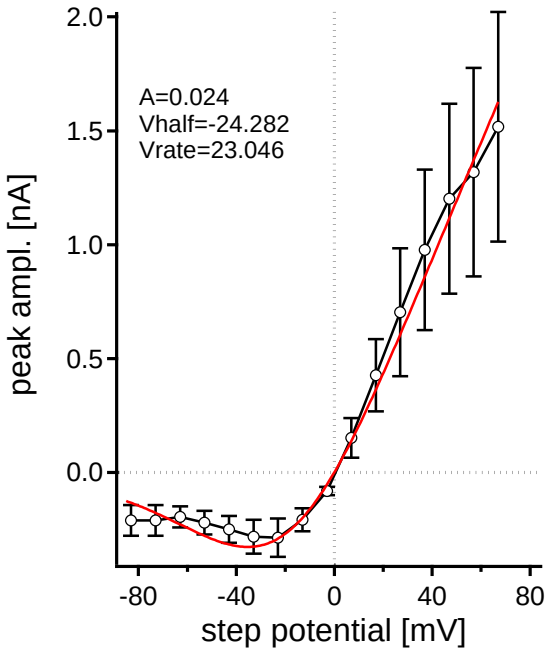

Fig. 5: Boltzmann fit (*red*) for NMDAR mediated currents. Average EPSC peak amplitude [nA] recorded in VC with 1.2 mM extracellular $CaCl_2$, plotted against step potential [mV] with V_{half} and V_{rate}. A = initial value. n = 16. SEM.

Data of all cells were fitted with a sigmoid function (Fig. 6B), exposing maximal growth rate, which means the linear slope of the fit around the inflection point xhalf, and xhalf itself (data not shown). Both parameters rate and xhalf will be described in later analyses. Taken together, results point towards an impact of stimulation frequency, -conductance and the involved synaptic currents on output generation.

For detailed investigation of NMDA-, stimulation intensity and -frequency impact on postsynaptic AP generation, the average amount of elicited APs per train stimulus was determined for defined stimulation intensity ranges. Thereby every intensity range contained an average of at least two cells. Moreover, the average amount of APs across the stimulus train for each stimulation frequency at approximately 100% stimulation intensity was analysed. Results are reported for stimulation with both EPSC components and with AMPA alone, according to the pulse number.

Results indicate an impact of stimulation intensity and -frequency on postsynaptic output generation Additionally, NMDAR mediated currents apparently promote AP generation at high stimulation frequencies (Fig. 7). Considering the firing behaviour at 333 Hz, the amount of elicited APs increases with stimulation intensity and decreases with pulse number. When stimulated with both EPSC components, the lowest stimulation intensity results in median values of 0 to 10% AP generation for the first two pulses, whereby cells cease firing from the third pulse number on. Intermediate stimulation intensities of 51-56% elicit steady firing for the first five pulses. Subsequent pulses trigger fewer APs, until no APs are elicited anymore. Stimulation with AMPA alone elicits fewer APs from the fifth pulse on. Stimulation intensities exceeding an average input make cells fire steadily, until including pulse number 17 or 14 when stimulated with both components, or with AMPA alone.

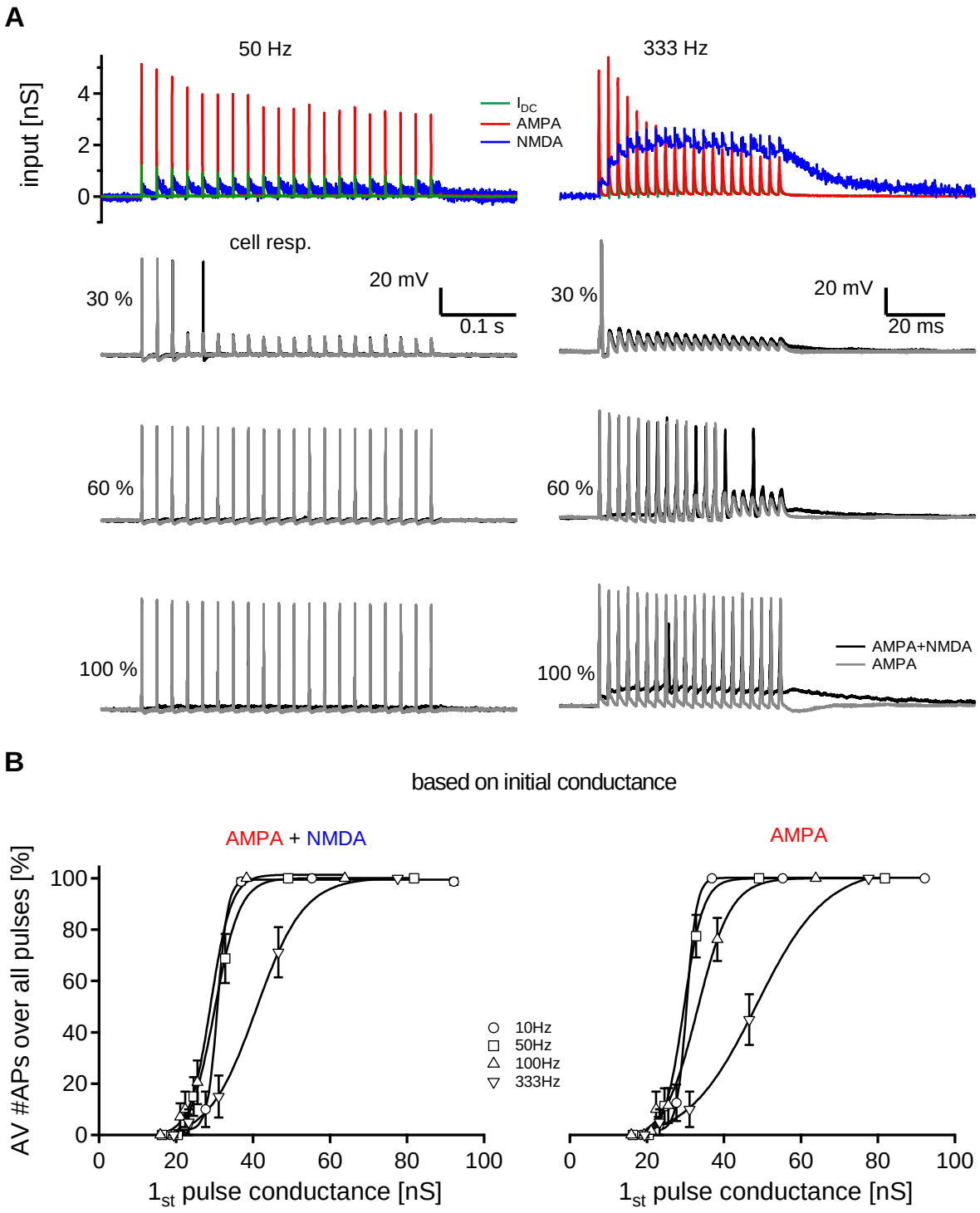

Fig. 6: Decomposing AMPA and NMDA component. **A:** *Top:* calculated exemplary conductance templates [nS] for AMPA (*red*), and NMDA (*blue*) with calculated output dynamic current I_{DC} (*green*) for 50 and 333 Hz. Appropriate cell response for both frequencies [mV] to low (*upper middle)*, intermediate (*lower middle*) and high intensities [%] (*bottom*), when stimulated with AMPA alone (*grey*) or with AMPA and NMDA together (*black*). **B:** Average number of elicited APs over all pulses [%] fitted with a sigmoid function in dependence of applied conductance [nS] for 10, 50, 100, and 333 Hz when stimulated with AMPA and NMDA together (*left*) or with AMPA alone (*right*). Conductance was calculated from the initial conductance in the AMPA template. SEM.

Regarding the firing behaviour at intensities which approximate one input, the quantity of evoked APs decreases with both, increasing stimulation frequency and pulse number. At 10 and 50 Hz, cells fire

steadily to all pulses no matter the EPSC component contribution. At 100 Hz cells fire steadily until and including pulse number 15, but the amount of elicited APs in response to subsequent pulses is consistently higher when stimulated with both components compared to when stimulated with AMPA alone. Increasing the stimulation frequency to 400 Hz makes the cell fire faithfully for the first five pulses for both stimulation paradigms. During train continuation, the number of APs decreases until it reaches a steady state median value of 50% APs when stimulated with both components, or ceases firing when stimulated with AMPA alone (Fig. 7A).

In the following, both stimulation intensity and -frequency were combined and examined together with involved EPSC components regarding their collective impact on AP generation. In general, amount of elicited APs increases with stimulation intensity and decreases with stimulation frequency. When stimulated with both EPSC components, AP generation is initiated at 41.4 to 64% stimulation intensity across frequencies, eliciting 62.5, 100, 100, 81.25 and 25% APs at 10, 50, 100, 333 and 400 Hz. An increase in stimulation intensity increases the amount of evoked APs until it reaches steady firing. For steady firing, low frequencies of up to 100 Hz require less intensity to make cells fire for all 20 pulses compared to higher frequencies. At frequencies up to 50 Hz, EPSC component contribution does not alter the required stimulation intensity to make cells fire steadily. At 100 Hz the required intensity is 1.2 fold increased when stimulated with AMPA alone. For 333 Hz, in both stimulation scenarios more than 70% are required to make cells spike faithfully. Interestingly, at 400 Hz results reveal no steady firing for both stimulation paradigms (Fig. 7B). Taken together, this experiment shows first that stimulation intensity and -frequency in concert influence postsynaptic output generation and second that NMDAR mediated currents promote firing at high stimulation frequencies. Furthermore, one average input seems to be sufficient to make cells fire steadily to frequencies up to 100 Hz.

So far, GC analysis was based on the conductance peak of the first AMPA pulse. To receive information concerning conductance driving output generation during ongoing stimulation, the following analysis involved the conductance of every pulse in the AMPA template.

AP generation depends on input conductance (Fig. 8). Quantitative analysis reveals an increased percentage of pulses evoking an AP with increasing input conductance, as shown in the exemplary cell: when stimulated with AMPA and NMDA together the conductance threshold for AP generation ranges from 15.4 nS at 333 Hz to 21.1 nS at 50 and 100 Hz. When stimulated with AMPA alone, threshold increases by 9.1 nS to 24.5 nS at 333 Hz. For remaining frequencies, threshold difference is not notable. Faithful spiking is reached at 23.3 nS for 100 and 333 Hz and at slightly higher levels for lower frequencies. Involvement of EPSC components has no noteworthy effect on required conductance for faithful firing. For further analysis data of all cells were fitted with a sigmoid function (Fig. 8A). Comparison of consequential maximal growth rate and inflection point xhalf within stimulation frequencies reveals a significant decrease in xhalf at 100 and 333 Hz when stimulated with both synaptic components compared to the AMPA stimulation (paired two-tailed WMP test or paired two-tailed t-test: rate: 10 Hz: W = -27.0, ns.; 50 Hz: t(8) = 0.36, ns.; 100 Hz: t(8) = 1.28, ns.; 333 Hz: W = -3.0, ns.; xhalf: 10 Hz: t(8) = 2.1, ns.; 50 Hz: t(8) = 0.98, ns.; 100 Hz: t(8) = 4.72, p = 0.002; 333 Hz: t(8) = 3.59, p = 0.007; all frequencies n = 9; Fig. 8B). Comparison between frequencies reveals significant increase in rate from 10 to 333 Hz, when stimulated with both components, indicating that the slope becomes less steep with increasing frequency (paired two-tailed WMP test or paired two-tailed t-test: 10 to 50 Hz: 50 Hz: t(8) = 0.08, ns.; 10 zu 100Hz: t(8) = 1.1, ns.; 10 to 333 Hz: W = 37.0, p = 0.027; for all frequencies n = 9). In contrast, xhalf remains unaffected by stimulation frequency (paired two-tailed t-test: 10 to 50 Hz: t(8) = 0.97, ns.; 10 to 100 Hz: t(8) = 0.98, ns.; 10 to 333 Hz: t(8) = 0.08, ns; for all frequencies n = 9; Fig. 8B).

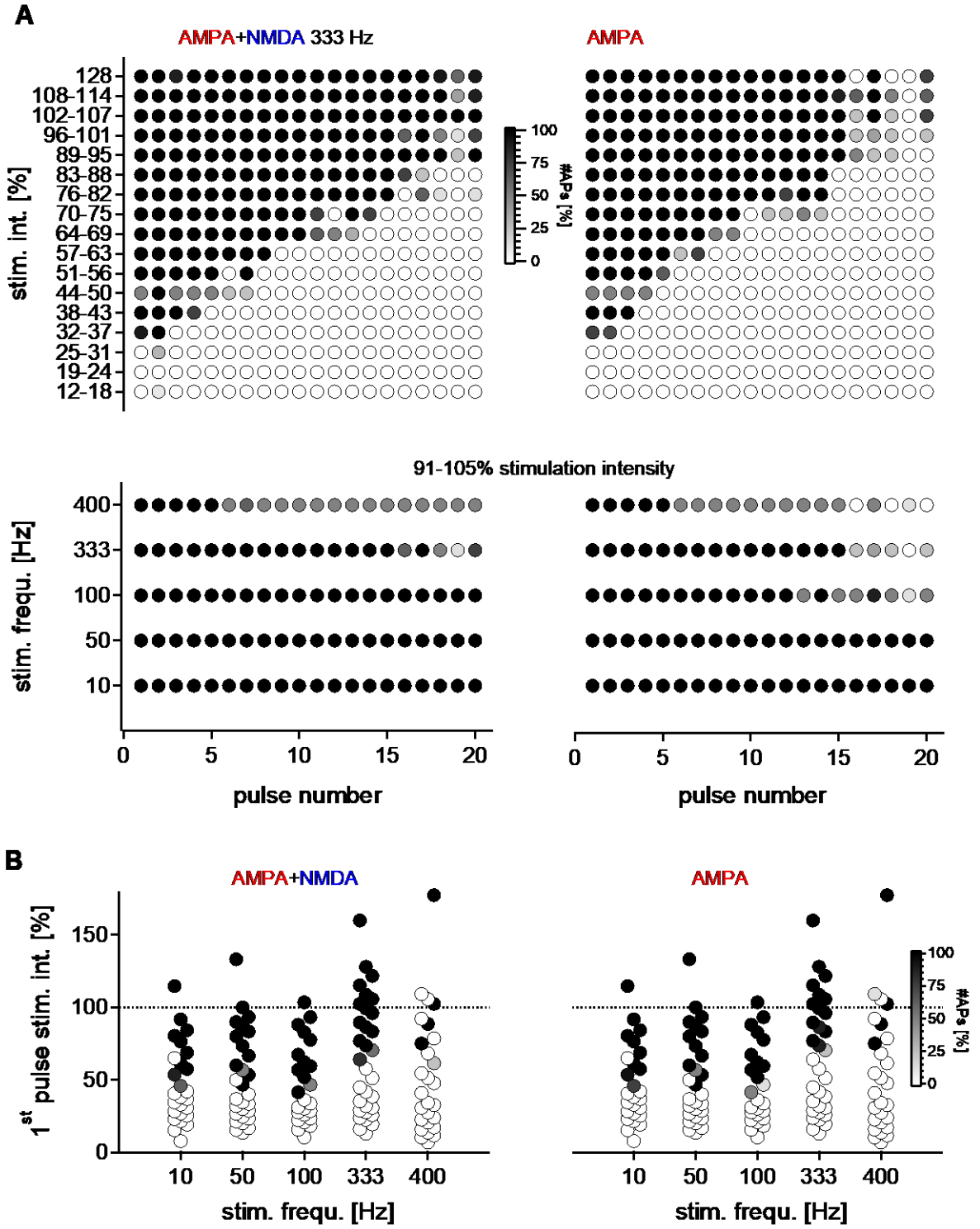

Fig. 7: NMDAR mediated currents promote firing at high stimulation frequencies. **A:** median amount of elicited APs (*grey level coded,* [%]) as a function of initial stimulation intensity [%] at 333 Hz (*top),* and stimulation frequency [Hz] at approximately 100% stimulation intensity (*bottom*), in both cases according to pulse number when stimulated with AMPA and NMDA together (*left*) or with AMPA alone (*right*) (12-18%: n = 2, 19-24%: n = 7, 25-31%: n = 14, 32-37%: n = 12, 38-43%: n = 15, 44-50%: n = 2, 51-56%: n = 13, 57-63%: n = 3, 64-69%: n = 19, 70-75%: n = 3, 76-82%: n = 10, 83-88%: n = 3, 89-95%: n = 7, 96-101%: n = 8, 102-107%: n = 5, 108-114%: n = 4, 128%: n = 2). **B:** Median amount of elicited APs (*grey level coded,* [%]) as a function of initial stimulation intensity [%] according to stimulation frequency [Hz] when stimulated with AMPA and NMDA together (*left*) or with AMPA alone (*right*). *Dashed line:* Average input to VNLL neuron (10 Hz: n = 16, 50 Hz: n = 17, 100 Hz: n = 19, 333 Hz: n = 20, 400 Hz: n = 13). Median.

Taken together, results point towards an effect of input conductance on postsynaptic output generation. Thereby, NMDA supports postsynaptic firing at high frequencies from 100 Hz on, which is reflected in the frequency specific change in xhalf. Results suggest that there is no synaptically independent effect of stimulation frequency on AP generation.

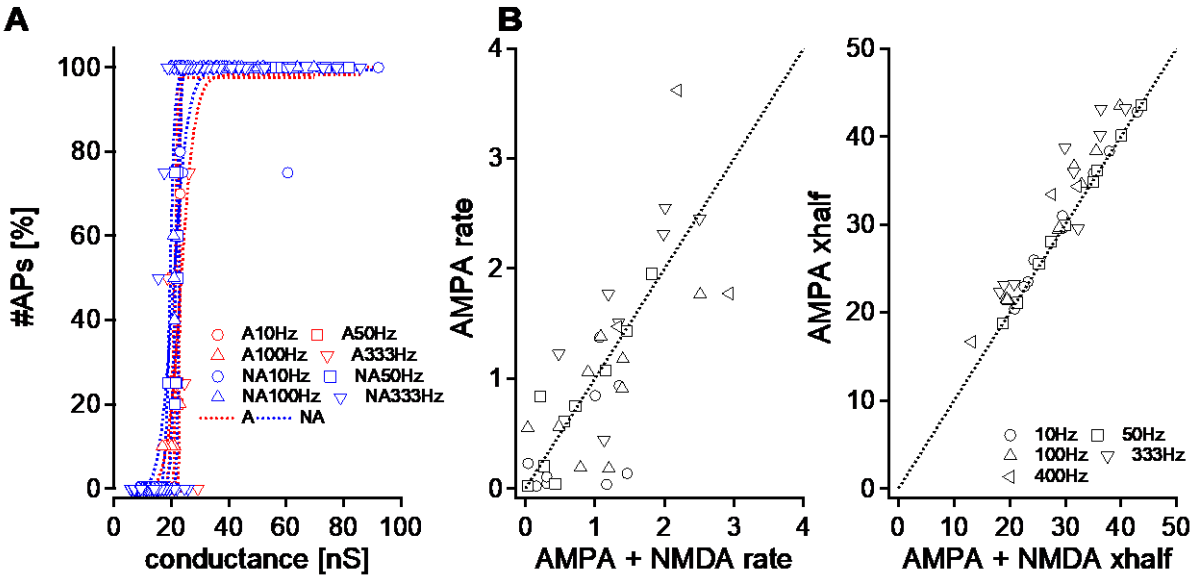

Fig. 8: AP generation depends on input conductance. **A:** Amount of APs [%] fitted with a sigmoid function plotted against input conductance [nS], exemplary for one cell for frequencies 10, 50, 100 and 333 Hz when stimulated with AMPA and NMDA together (*blue markers*) or with AMPA alone (*red markers*). Conductance refers to every single pulse number within AMPA stimulation train. **B:** Calculated rate (*left*) and xhalf (*right*) for all recorded cells when stimulated with AMPA alone or with AMPA and NMDA together plotted against each other at the same conductance level respectively, for all frequencies (10 Hz: n=9, 50 Hz: n=9, 100 Hz: n=9, 333 Hz: n=9, 400 Hz: n=3). *Dashed lines:* unity lines.

Functionality of the spike generator at 400 Hz. Results presented so far were partly limited to a maximum of 333 Hz stimulation frequency. In fact, only a low amount of VNLL neurons followed faithfully for 20 repetitions at 400 Hz in both AFS and GC experiments. Interestingly, both experimental settings, AFS and GC, involve integration processes e.g. STP, which might somehow make faithful spike generation at high frequencies difficult. Nevertheless, the postsynaptic spike generator itself might be able to follow these frequencies.

To test this, a CC experiment was performed, applying a 400 Hz stimulus of 20 pulses, each of the same amplitude and duration. During the experimental procedure, the current square pulse amplitude was varied for the different trials. Results reveal an effect of input intensity on AP generation and spike precision (Fig. 9) and demonstrate the capability of VNLL neurons to spike faithfully to a 400 Hz train (Fig. 9A). Thereby the average number of elicited APs per train increases with stimulation intensity, and decreases with pulse number: The 1st pulse elicits 32.22 ± 17.2% APs at 0.8-0.9 nA stimulation intensity and up to 100 ± 0% APs at 1.4-1.5 nA. For the last pulse, the amount of elicited APs was reduced (Fig. 9B). For the temporal precision, both average jitter and latency decrease with stimulation intensity, making the cell response more accurate, and increase with pulse number (Fig. 9C and D). Taken together, results suggest the functionality of the postsynaptic spike generator at 400 Hz. Moreover, AP generation and temporal precision are affected by stimulation history and -intensity.

Temporal precision depends on stimulation frequency. After having quantified the AP generation in dependence of various stimulation parameters, temporal precision of these supra-threshold responses was evaluated. Temporal precision was examined in three experimental train stimulus arrangements in GC: First, cells were stimulated with both components or with AMPA alone with STP in order to

investigate the effect of the input conductance and NMDA component on temporal precision. Second, cells were stimulated with AMPA alone with STP at low intensity to approximate physiologically relevant inputs close to firing threshold. Finally, cells were stimulated with AMPA alone without STP, where the stimulus strength was adjusted to elicit steady spiking throughout the train stimulus. The omission of STP and the NMDA template allowed exclusive examination of the pulse number impact on the temporal precision.

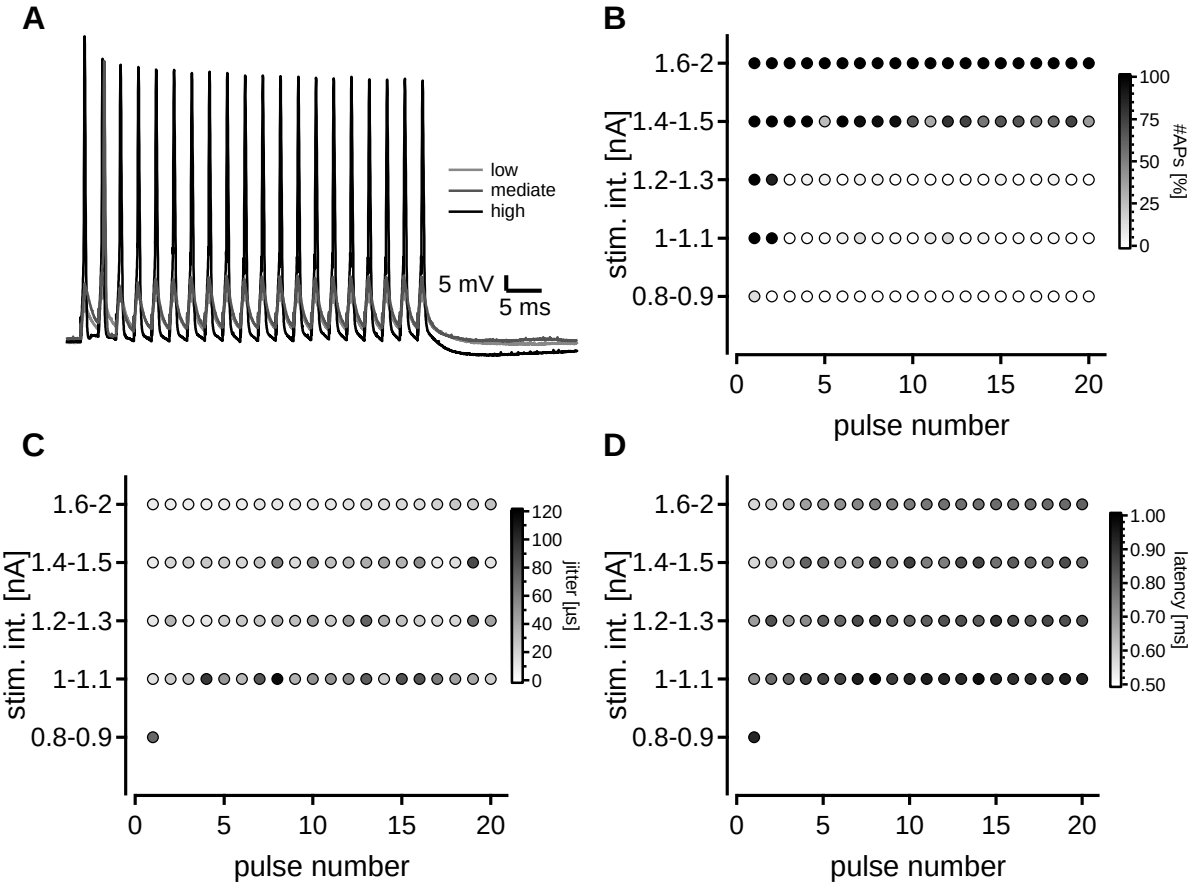

Fig. 9: AP generation at 400 Hz stimulation frequency is feasible. **A:** Voltage response to 20 pulses of 400 Hz of low (*light grey*), mediate (*dark grey*) and high stimulation intensity (*black*) recorded in CC at 1.2 mM extracellular $CaCl_2$, exemplary shown for one cell. **B, C and D:** Grey level coded amount of elicited APs (*B*), average jitter (*C*) and latency [%] (*D*) as a function of stimulation intensity [%] and of pulse number (0.8-0.9 nA: n = 1, 1-1.1 and 1.6-2 nA: n = 3, 1.2-1.3 and 1.4-1.5 nA: n = 5). Median.

Results reveal that temporal precision is history- and input conductance dependent (Fig. 10). Data incorporating STP and NMDA (Fig. 10A), plotted against input conductance bins of 0.5 nS over all frequencies reveal a decrease in both latency and jitter with input conductance. Data reveal significant change in average latency and partly in average jitter when stimulated with AMPA and NMDA together or with AMPA alone for both stimulation paradigms at threshold or at steady firing (paired two-tailed WMP test: latency at threshold: W = 4801.0, p<0.0001, n = 13; steady firing: W = 3285.0, p<0.0001, n = 8; jitter at threshold: W = 1596.0, ns., n = 13; steady firing: W = -1905, p = 0.0003, n = 8; Fig. 10B). Yet, despite the here stated significant change in case of NMDA contribution, results must be treated with caution. The impact of NMDA on AP precision must be differentiated between low and high input conductance and thus it must be considered in dependence of the stimulus history.

In order to investigate the influence of stimulus history on AP precision, trains were applied with STP and AMPA alone, at intensities close to firing threshold and evaluated as a function of pulse number

(Fig. 10C). Appropriate cell responses reveal an increase in average latency and jitter with pulse number. For the response to the 1st pulse, average latency ranges from 0.31 to 0.48 ms across frequencies. For all frequencies, the average latency increases significantly until the average value of the last five pulse numbers (paired two-tailed WMP test or paired two-tailed t-test: 10 Hz: W = 66.0, p = 0.001, n = 11; 50 Hz: t(10) = 11.06, p<0.0001, n = 11; 100 Hz: t(11) = 9.25, p<0.0001, n = 10; 333 Hz: t(6) = 7.82, p = 0.0002, n = 7). The average of the last five pulse numbers was chosen since the sample size is variable from 3-11 cells across frequencies for these pulses, due to stimulation close to firing threshold. The course of the average jitter resembles the average latency, starting at 0.02 ± 0.005 µs at 10 Hz, 0.01 ± 0.002 µs at 50 Hz, 0.01 ± 0.002 µs at 100 Hz and 0.008 ± 0.001 µs at 333 Hz for the 1st pulse and increasing significantly until the average value of the last five pulse numbers for all frequencies (paired two-tailed WMP test or paired two-tailed t-test: 10 Hz: W = 66.0, p = 0.001, n = 11; 50 Hz: W = 55.0, p = 0.002, n = 10; 100 Hz: W = 36.0, p = 0.008, n = 8; 333 Hz: t(4) = 4.38, p = 0.01, n = 5; Fig. 10D).

In order to extract the effect of stimulus history on AP precision, cells were stimulated without STP and with AMPA alone at steady firing level (Fig. 10E). Temporal precision is increased significantly, which is reflected in the increased average latency of the last five pulses for all frequencies compared to when cells were stimulated at threshold (unpaired two-tailed MW test or unpaired two-tailed t-test: 10 Hz: t(17) = 3.81, p = 0.001, n = 8 and 11; 50 Hz: t(17) = 3.66, p = 0.002, n = 8 and 11; 100 Hz: U = 8.0, p = 0.003, n = 8 and 10; 300/333 Hz: t(11) = 3.74, p = 0.03, n = 6 and 7), and in the increased average jitter of the last five pulse numbers at all frequencies except 100 Hz, which might be due to large SEM (unpaired two-tailed MW test or unpaired two-tailed t-test: 10 Hz: U = 8.0, p = 0.002, n = 8 and 11; 50 Hz: t(16) = 2.19, p = 0.044, n = 8 and 10; 100 Hz: U = 14.0, ns., n = 8 both; 300/333 Hz: t(9) = 3.55, p = 0.006, n = 6 and 5). Regarding the 1st pulse, the accuracy of the cell response seems to be arbitrarily lower or higher between the two stimulation paradigms (unpaired two-tailed MW test or unpaired two-tailed t-test: latency: 10 Hz: U = 18.0, p = 0.013, n = 8 and 13; 50 Hz: U = 15.0, p = 0.006, n = 8 and 13; 100 Hz: t(19) = 1.36, ns., n = 8 and 13; 300/333 Hz: t(16) = 0.92, ns., n = 6 and 12; jitter: 10 Hz: U = 10.0, p = 0.006, n = 8 and 13; 50 Hz: U = 3.0, p<0.0001, n = 8 and 13; 100 Hz: U = 19.0, p = 0.016, n = 8 and 13; 300/333 Hz: t(16) = 0.27, ns., n = 6 and 12). The difference in the starting value between frequencies for both average latency and jitter stems from the higher amount of required stimulation intensity for steady firing at high frequencies, compared to lower frequencies (Fig. 10F). Taken together, results of this experiment show the dependence of temporal precision on stimulus history and especially on input conductance in train stimuli of distinct stimulation frequencies.

Pseudorandomly distributed frequency stimulation. To stimulate cells more physiologically, PrDF train stimuli were applied. They approximated natural input reaching VNLL neurons and were based on AMPA and NMDA kinetics recorded in previous VC experiments. They contained 691 pulses with an ISI ranging from 2.3 to 666.8 Hz. The stimulus was applied at different intensities and under four stimulation paradigms: AMPA and NMDA with STP, AMPA and NMDA without STP, AMPA alone with STP, AMPA alone without STP.

Ongoing AP generation is affected by STP and only marginally by NMDA contribution (Fig. 11). The experimental template is outlined exemplary for the stimulation setting at 70% intensity for AMPA and NMDA with STP. Resulting voltage responses differ according to stimulation intensity and contribution of the synaptic EPSC components (Fig. 11A).

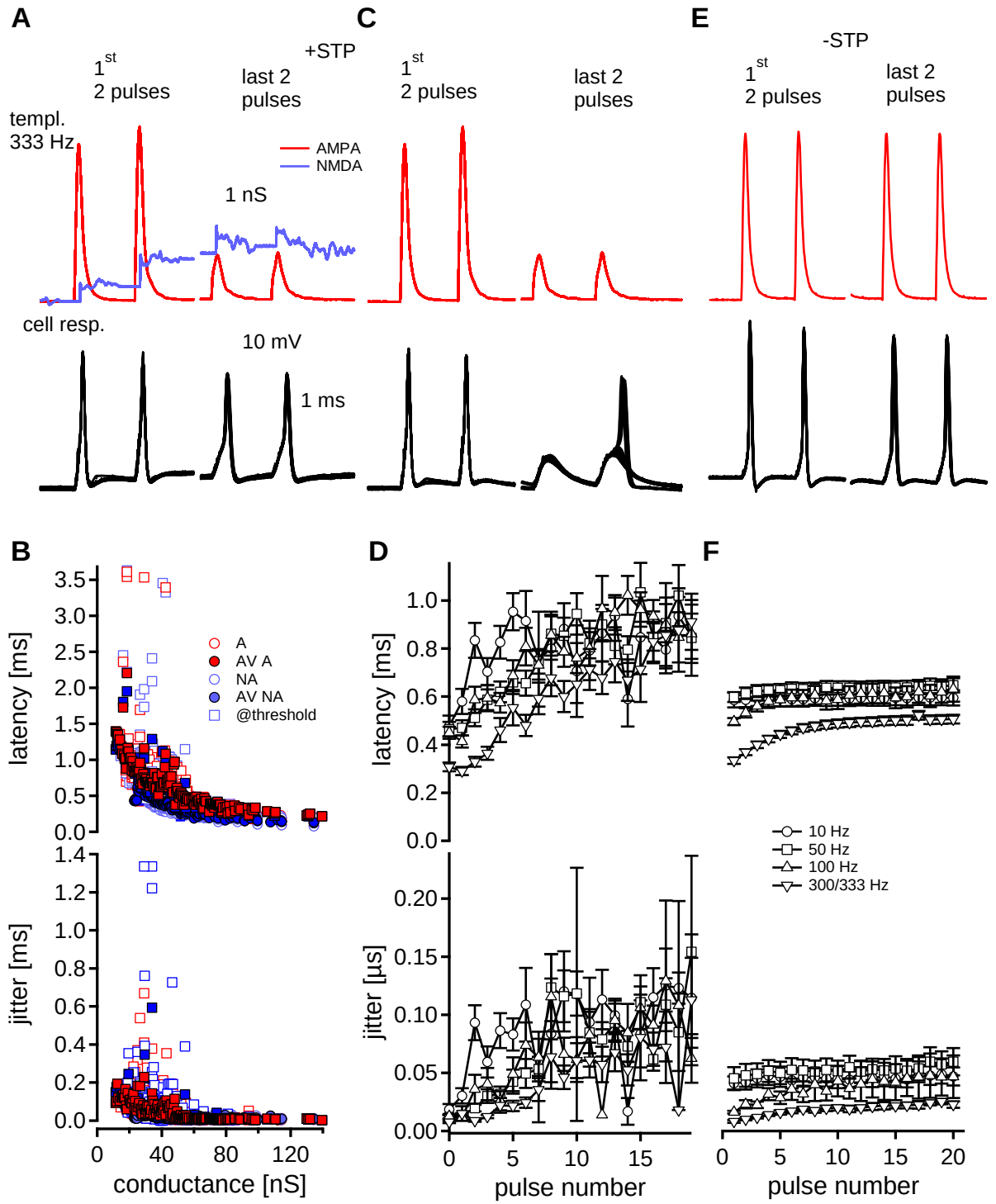

Fig. 10: Temporal precision depends on input conductance and history. **A+C+E:** Exemplary stimulation template (nS, *top*) for AMPA (*red*) and NMDA (*blue*) of 333 Hz with STP (**A+C**) and without STP (**E**) for the first and last two pulses with appropriate cell response (*bottom, black*). **B:** Average latency [ms] and jitter [ms] for single cells (*white markers*) and averages (*filled markers*) when recorded with AMPA and NMDA together (*blue*) or with AMPA alone (*red*), at steady firing (*circles*) or at threshold (*square*), as a function of input conductance bins of 0.5 nS at stimulation frequencies of 10, 50, 100 and 300/333 Hz. **D:** Average latency [ms] and jitter [ms] resulting from stimulation with STP (**D,** n = 13 for all frequencies) and without STP (**F,** 10-100 Hz: n = 8, 300 Hz: n = 6) plotted against pulse number for same frequencies as in B. SEM.

First examination of spiking behaviour in response to 100 and 70% stimulation intensity for one representative cell shows higher amount of generated APs when cells were stimulated with higher intensity. Thereby AP generation appears to slightly increase when stimulated with both components

compared to stimulation with AMPA alone. Furthermore, the cell tends to fire at the onset of individual sequences of relatively dense packed bundles of various frequencies when stimulated with STP (Fig. 11B). Spikes per stimulus, average latency and jitter across the train stimulus were calculated (calculation described in methods) for the temporal precision evaluation. For all cells, analysis reveals an increase in average spike number per stimulus with stimulation intensity from 20% intensity of the first AMPA pulse on. It reaches a maximum of 0.57 to 1 spike per stimulus at 100% intensity, when stimulated without STP. This maximum is decreased when stimulated with STP. Averaged across cells, the increase in APs per stimulus from 20 to 100% intensity was not significant for any condition, which might be due to the low cell number (paired two-tailed WMP test: AMPA and NMDA: W = -10.0, ns.; AMPA alone: W = -10.0, ns.; AMPA and NMDA with STP: W = -10.0, ns.; AMPA with STP: W = -10.0, ns.; n = 4 for all conditions; Fig. 11C). To extract the effect of NMDA contribution on temporal precision, single cell responses to stimuli with AMPA alone were subtracted from those to stimuli comprising both synaptic components. This was done for both paradigms with and without STP. Additionally, to extract the effect of STP on temporal precision, cell responses to stimuli with STP were subtracted from those without STP. This was done for both paradigms with and without NMDA. Results suggest a slight promotion of spiking by NMDA at all intensities. STP absence reduces this promotion at 20, 40 and significantly at 100% intensity, indicating a band-pass filter in this setting (paired two-tailed WMP test or paired two-tailed t-test: 100%: $t(5) = 7.79$, $p = 0.0006$, n = 6; 80%: W = 8.0, ns., n = 4; 70%: $t(5) = 2.34$, ns., n = 6; 60%: W = -5.0, ns., n = 6; 50%: W = 6.0, ns., n = 4; 40%: W = -1.0, ns., n = 4; 20%: W = 5.0, ns., n = 4, Fig. 11D). Furthermore, STP extraction reveals more elicited APs per stimulus in absence of STP than in the presence of STP (Fig. 11E).

Both average latency and jitter decrease with intensity, making cell responses more accurately (ignoring the outlier of 1.3 ms at 100% stimulation intensity). The decrease in average latency from 40 to 100% intensity is statistically insignificant for all conditions (paired two-tailed WMP test: AMPA and NMDA: W = 10.0, ns., n = 4; AMPA alone: W = 10.0, ns., n = 4; AMPA and NMDA with STP: W = 6.0, ns., n = 3; AMPA with STP: W = 10.0, ns., n = 4; comparison was made between 40 and 100% due to small sample size at 20% stimulation intensity Fig. 11F). Interestingly, latency seems to be independent of NMDA contribution (Fig. 11G), but rather seems to depend on STP, revealing increased values in STP presence compared to when STP is absent (Fig. 11H).

The decrease in average jitter, from 60 to 100% intensity is significant when stimulated with both synaptic components (paired two-tailed WMP test or paired two-tailed t-test: AMPA and NMDA: $t(5) = 5.93$, $p = 0.002$, n = 6; AMPA alone: W =10.0, ns., n = 4; AMPA and NMDA with STP: $t(5) = 3.21$, $p = 0.024$, n = 6; AMPA with STP: $t(5) = 1.44$, ns., n = 6; 60% as reference value to 100% was chosen since for 20, 40 and 50% sample size was too small to allow for statistical analysis; Fig. 11I). Thus, jitter seems to be reduced at high stimulation intensities at 60% and above when NMDA contributes (Fig. 11J) and marginally increased by STP (Fig. 9K). Taken together, obtained results point towards an interplay of STP and NMDA influencing temporal precision, STP leading to increased latencies (Fig. 11H) and NMDA component resulting in increased jitter (Fig. 9J) of ongoing supra-threshold responses.

So far, firing behaviour analysis to PrDF stimulation was limited to temporal precision as a function of stimulation intensity in concert with NMDA contribution and STP. The following examination further included the frequency impact on the neuronal firing behaviour.

To do so, stimulation frequency bins of 25 Hz were averaged and the corresponding average number of elicited APs was calculated cell wise for the four stimulation paradigms: AMPA and NMDA with STP, AMPA and NMDA without STP, AMPA alone with STP, AMPA alone without STP.

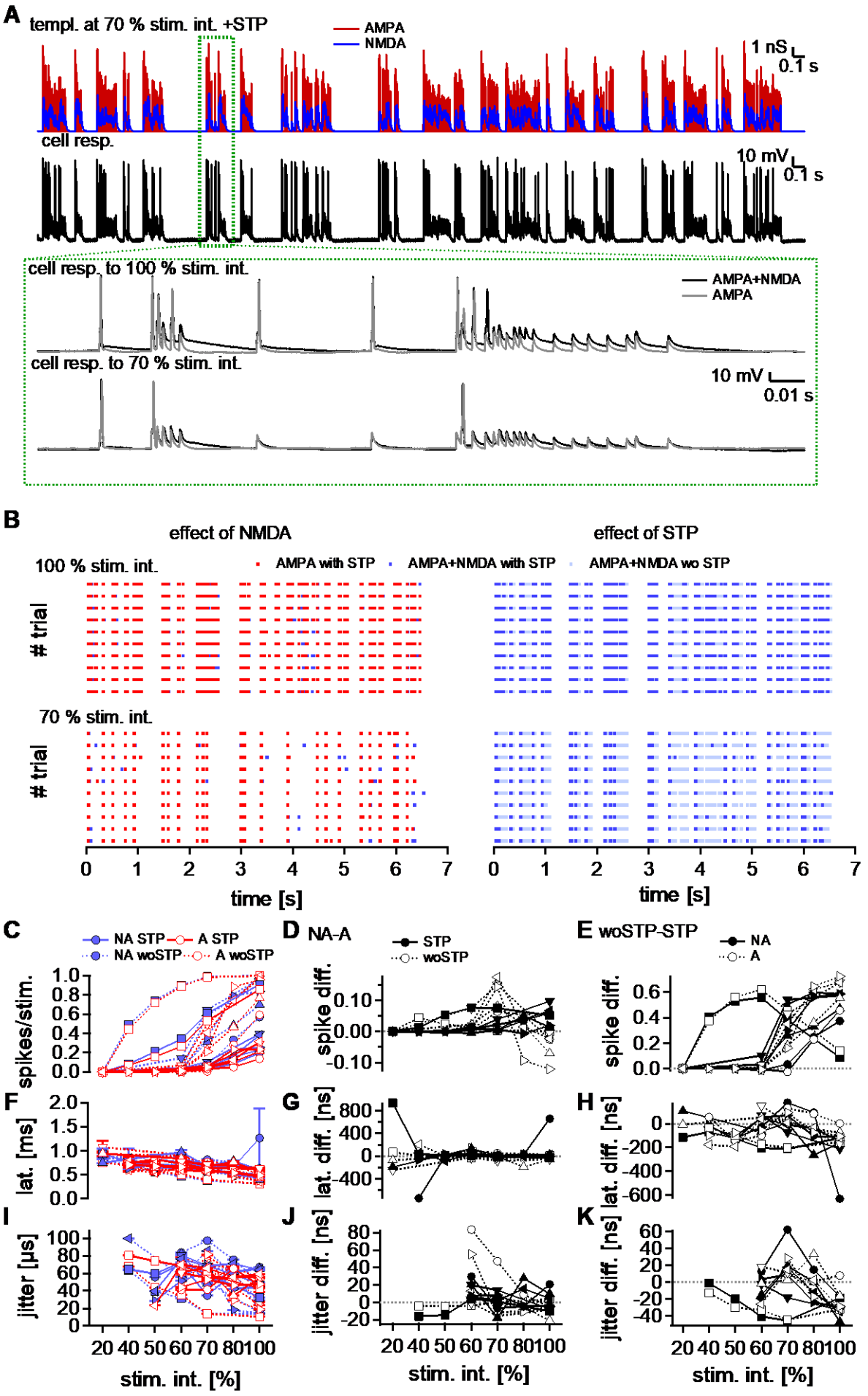
A
templ. at 70 % stim. int. +STP
AMPA
NMDA
1 nS
0.1 s
cell resp.
10 mV
0.1 s
cell resp. to 100 % stim. int.
AMPA+NMDA
AMPA
cell resp. to 70 % stim. int.
10 mV
0.01 s
B
effect of NMDA
effect of STP
100 % stim. int.
AMPA with STP
AMPA+NMDA with STP
AMPA+NMDA wo STP
trial
70 % stim. int.
time [s]
C
NA STP
A STP
NA woSTP
A woSTP
spikes/stim.
D NA-A
STP
woSTP
spike diff.
E woSTP-STP
NA
A
spike diff.
F
lat. [ms]
G
lat. diff. [ns]
H
lat. diff. [ns]
I
jitter [µs]
J
jitter diff. [ns]
K
jitter diff. [ns]
stim. int. [%]

Fig. 11: Stimulation intensity and NMDA impact temporal precision in a PrDF stimulus. **A:** exemplary PrDF template [nS] at 70% intensity (*top*) for AMPA (*red*) and NMDA (*blue*) with STP and appropriate cell response (*bottom,* [Vm]) recorded with 1.2 mM extracellular $CaCl_2$. *Green dashed box*: Zoom in to a voltage response section to a 100% (*top*) and 70% stimulus (*bottom*) when recorded with AMPA and NMDA together (*black*) or with AMPA alone (*grey*). **B:** effect of NMDA (*left*) and STP (*right*) on AP occurrence throughout the train stimulus for trial 1-10 when stimulated with 100% (*top*) and 70% (*bottom*) exemplary shown for one representative cell. **C-K:** Temporal precision evaluated by spikes per stimulus (*top*, **C**), average latency (*middle,* [ms], **F**) and jitter (*bottom,* [µs], **I**) when stimulated with AMPA alone (*red*) or AMPA and NMDA together (*blue*) with (*solid line*) or without STP (*dashed line*) for single cells (*single cells with different markers*), with calculations for NMDA- (*middle*, **D, G, J**) and STP impact (*right*, **E, H, K**), plotted against stimulation intensity [%]. N = 6. SEM.

On this basis, 50% firing level, number of APs at high frequency steady state and the stimulation frequency, where the minimal amount of APs was elicited for the first time during the stimulus (notch frequency), were extracted (Fig. 12). At first glance, supra-threshold response events are maximal at 10.92 ± 1.4 Hz. Increase in average stimulation frequency decreases the average amount of APs, whereby the slope of the decrease appears to be affected by chosen stimulation paradigms (Fig. 12A). At 40% intensity, 50% firing level is reached at 7.58 to 313.21 Hz across cells. Increasing intensity to 100% shifts 50% firing level to higher frequencies of 15.98 up to 582.84 Hz. Averaging 50% firing level across cells for each stimulation paradigm reveals significant difference when stimulated with or without STP. NMDA conductance has no significant effect on the 50% firing level (paired two-tailed WMP test or paired two-tailed t-test: NA vs NA STP: W = 45.0, p = 0.004, number of pairs = 9; A vs A STP: W = 36.0, p = 0.008, number of pairs = 8; NA STP vs A STP: W = -8.0, ns., number of pairs = 11; NA vs A: t(9) = 1.31, ns., number of pairs = 10; Fig. 12B). Further investigation of frequency dependent spiking behaviour was done by extracting the impact of NMDA conductance and STP. Consequent outcome reveals a shift of 50% firing level to higher stimulation frequencies at all stimulation intensities when stimulated with NMDA, except of when stimulated with 80 or 100% intensity. Due to the low sample size, statistical analysis was not feasible to test for this observation (Fig. 12C). Additionally, the 50% firing level is shifted towards higher frequencies in the absence of STP, which is reflected in the positive values of 146.97 up to 555.33 Hz frequency shift (Fig. 12D).

To examine the AP generation at high frequencies, the cell responses to the last three and thus most high frequency bins of 611.96 ± 1.5, 639.44 ± 1.6 and 660.47 ± 1.0 Hz were pooled. The outcome shows the average amount of APs per stimulus across these three high frequency bins. Obtained results reveal an increase of elicited APs at high frequencies with increasing stimulation intensity until at 100% intensity a maximum of on average 0.05 to 1.9 generated APs per stimulus is reached. Averaging across cells for each of the four stimulation paradigms indicates no significant impact of stimulus paradigm on high frequency firing (paired two-tailed WMP test: NA vs NA STP: W = -52.0, ns., A vs A STP: W = -10.0, ns.; NA STP vs A STP: W = -67.0, ns.; NA vs A: W = -56.0, ns.; number of pairs = 34 for all conditions; Fig. 12E). However, separate analysis hints towards no apparent effect of NMDA (Fig. 12F) but, towards an increase in elicited APs in the absence of STP (Fig. 12G).

The notch frequency increases with increasing stimulation intensity, starting at 10.92 Hz for 20%, until the maximum is reached mostly at 70, 80 or 100% stimulation intensity. Averaging the notch frequency across all cells for each stimulation paradigm reveals a significant increase when cells were stimulated without STP compared to stimulation with STP, whereas NMDA contribution has no significant effect (paired two-tailed WMP test: NA vs NA STP: W = 251.0, p = 0.0008, A vs A STP: W = 233.0, p<0.0001; NA STP vs A STP: W = -54.0, ns.; NA vs A: W = -9.0, ns.; number of pairs = 34 for all conditions; Fig. 12H). In line with this finding, separate analysis reveals no effect of NMDA on notch frequency (Fig. 12I), but a shift of notch frequency towards the higher end of the frequency range when STP is absent (Fig. 12J). Taken together, results hint towards a marginal role of NMDA conductance for AP generation

at high stimulation frequencies. Furthermore, data point towards the assumption that STP might affect spiking behaviour at low and high stimulation frequencies (Fig. 12D+G), whereby this result must be treated with caution, since history dependence has not been taken into account in this experimental analysis.

Frequency dependent temporal integration. As shown in the PrDF experiments, cells can generate high frequency output of up to 660.8 Hz, even though the amount of elicited APs was reduced compared to when stimulated with lower frequencies. This suggests that VNLL cells tend to follow these high frequencies on the PP level, rather than on the continuous stimulation level. Thus, in the following, supra-threshold temporal integration and limitations of the spike generator were investigated on a PP level. Voltage responses to PPs of identical amplitude and ISIs from 10 to 2000 Hz was recorded in GC and evaluated in dependence of stimulation frequency, -intensity and EPSC component contribution. Between PPs, the cell was given enough time to recover.

Results reveal an impact of stimulation frequency and –intensity on AP generation on a PP level (Fig. 13), which is supported at high stimulation intensity (Fig. 13A). Data reveal that the required stimulation intensity for PPs to elicit at least one AP decreases with stimulation frequency. Furthermore, discrimination between two pulses is limited at extremely high stimulation frequencies, which is reflected in the inability to produce more than one AP, even at high stimulation intensity (Fig. 13B). When stimulated with AMPA and NMDA conductance together, the average required stimulation intensity to elicit one AP decreases continuously from 600 Hz on, until at 2000 Hz, 22.62 ± 1.8% are sufficient to elicit one AP. This means a significant decrease in average required stimulation intensity from 800 Hz on, referred to when stimulated with 10 Hz (paired two-tailed WMP test or paired two-tailed t-test: 10 to 50 Hz: $t(12) = 0.21$, ns.; 10 to 100 Hz: $t(12) = 0.32$, ns.; 10 to 200 Hz: $t(12) = 1.11$, ns.; 10 to 300 Hz: $t(12) = 0.21$, ns.; 10 to 400 Hz: $t(12) = 0.89$, ns.; 10 to 500 Hz: $t(12) = 0.13$, ns.; 10 to 600 Hz: $t(12) = 1.58$, ns.; 10 to 700 Hz: $t(12) = 2.14$, ns.; 10 to 800 Hz: $t(12) = 3.21$, $p = 0.008$; 10 to 900 Hz: $t(12) = 4.01$, $p = 0.002$; 10 to 1000 Hz: $t(12) = 5.55$, $p = 0.0001$; 10 to 1200 Hz: $t(12) = 7.32$, $p<0.0001$; 10 to 1400 Hz: $t(12) = 7.78$, $p<0.0001$; 10 to 1600 Hz: $t(12) = 10.32$, $p<0.0001$; 10 to 1800 Hz: $W = -91.0$, $p = 0.0002$; 10 to 2000 Hz: $t(12) = 13.70$, $p<0.0001$, $n = 13$ for all frequencies). Contribution of NMDA conductance has no effect on the average required stimulation intensity (paired two-tailed WMP test or paired two-tailed t-test: 10 Hz: $t(12) = 1.1$, ns.; 50 Hz: $t(12) = 1.1$, ns.; 100 Hz: $t(12) = 1.1$, ns.; 200 Hz: $t(12) = 1.1$, ns.; 300 Hz: $t(12) = 0.11$, ns.; 400 Hz: $t(12) = 0.19$, ns.; 500 Hz: $t(12) = 0.23$, ns.; 600 Hz: $t(12) = 1.48$, ns.; 700 Hz: $t(12) = 0.53$, ns.; 800 Hz: $t(12) = 1.21$, ns.; 900 Hz: $t(12) = 2.65$, $p = 0.02$; 1000 Hz: $t(12) = 1.54$, ns.; 1200 Hz: $t(12) = 0.82$, ns.; 1400 Hz: $t(12) = 1.81$, ns.; 1600 Hz: $t(12) = 1.0$, ns.; 1800 Hz: $W = 11.0$, ns.; 2000 Hz: $t(12) = 2.31$, $p = 0.04$; $n = 13$ for all frequencies; Fig. 13C). In order to transition firing from one to two APs, the required stimulation intensity increase is frequency dependent. The average required PP stimulation frequency to fire for both stimuli is thereby limited to PPs between 444.44 ± 62.6 and 1261 ± 61.5 Hz, since lower frequencies consistently fired either none or two APs, whereas higher frequencies were incapable of firing more than one AP.

The average required PP frequency to fire two distinct APs increases with stimulation intensity. When stimulated with AMPA and NMDA conductance together, low PP frequency of 477.78 ± 61.9 Hz requires the lowest stimulation intensity of 40%, which increases with PP frequency without exception until it reaches its maximum.

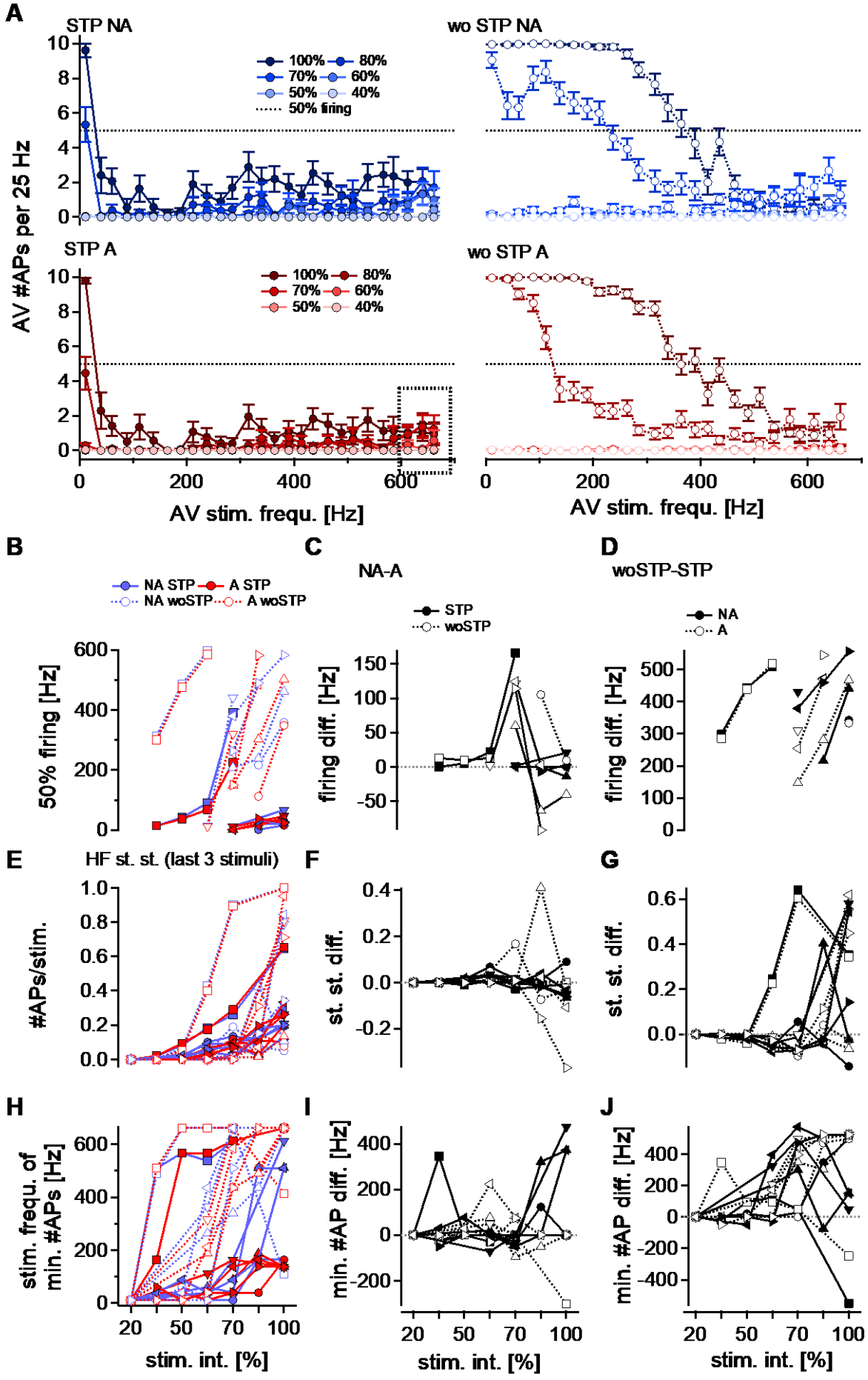
A
STP NA
wo STP NA
STP A
wo STP A
100%
80%
70%
60%
50%
40%
50% firing
AV #APs per 25 Hz
AV stim. frequ. [Hz]
B
NA STP
A STP
NA woSTP
A woSTP
50% firing [Hz]
C
NA-A
STP
woSTP
firing diff. [Hz]
D
woSTP-STP
NA
A
firing diff. [Hz]
E
HF st. st. (last 3 stimuli)
#APs/stim.
F
st. st. diff.
G
st. st. diff.
H
stim. frequ. of min. #APs [Hz]
stim. int. [%]
I
min. #AP diff. [Hz]
stim. int. [%]
J
min. #AP diff. [Hz]
stim. int. [%]

Fig. 12: Frequency and intensity in concert impact AP generation in a PrDF stimulus. **A:** average amount of elicited APs over 10 repetitions in response to a PrDF stimulus of various intensities [%] when stimulated with AMPA and NMDA together (*top*) or AMPA alone (*bottom*) with (*left*) or without STP (*right*), plotted against stimulation frequency bundles of 25 Hz, exemplary shown for one cell. *Green dashed line*: 50% firing level. D*ashed box:* high frequency range. **B-J:** AP generation characteristics: 50% firing level [Hz] (**B**), amount of elicited APs per stimulus at high frequencies (**E**) and notch frequency [Hz] (**H**) for single cells (*single cells with different markers*) when stimulated with AMPA alone (*red*) or AMPA and NMDA together (*blue*), with (*solid line*) or without STP (*dashed line*) respectively, with calculations for NMDA- (**C, F, I**) and STP impact (**D, G, J**), plotted against stimulation intensity [%]. N = 6. SEM.

This means a significant increase in required stimulation intensity from 50% stimulation intensity on, referred to when stimulated with 40% (paired two-tailed WMP test or paired two-tailed t-test: 50-80, 100, 150%: $t(8) \geq 7.25$, $p<0.0001$; 90, 110-140%: $W = 45.0$, $p = 0.004$; $n = 9$ for all intensities). Again, the contribution of NMDA conductance has no effect on the required stimulation intensity to elicit two APs (paired two-tailed WMP test or paired two-tailed t-test: 40%: $t(8) = 2.0$, ns; 50%: $t(11) = 0.0$, ns.; 60%: $W = 0.0$, ns.; 70%: $t(12) = 1.0$, ns.; 80%: $W = 1.0$, ns.; 90%: $W = 0.0$, ns.; 100%: $t(12) = 1.0$, ns.; 110%: $W = 4.0$, ns.; 120%: $W = 3.0$, ns.; 130%: $W = 0.0$, ns.; 140%: $W = -1.0$, ns.; 150%: $W = -1.0$, ns., $n = 13$ for all intensities except 40% $n = 9$, 50% $n = 12$; Fig. 13D). Taken together, results reveal an impact of stimulation intensity and -frequency of PPs on temporal integration. The spike generator in VNLL cells can produce APs even up to 2000 Hz. Since stimulus discrimination for PPs is feasible until 1260 Hz at 150% stimulation intensity and since stimulus discrimination during ongoing stimulation of 333 Hz with STP requires more than 100% to faithfully generate APs throughout the train stimulus, results might suggest that two inputs are required to drive faithful spiking at the VNLL endbulb for these stimulation conditions.

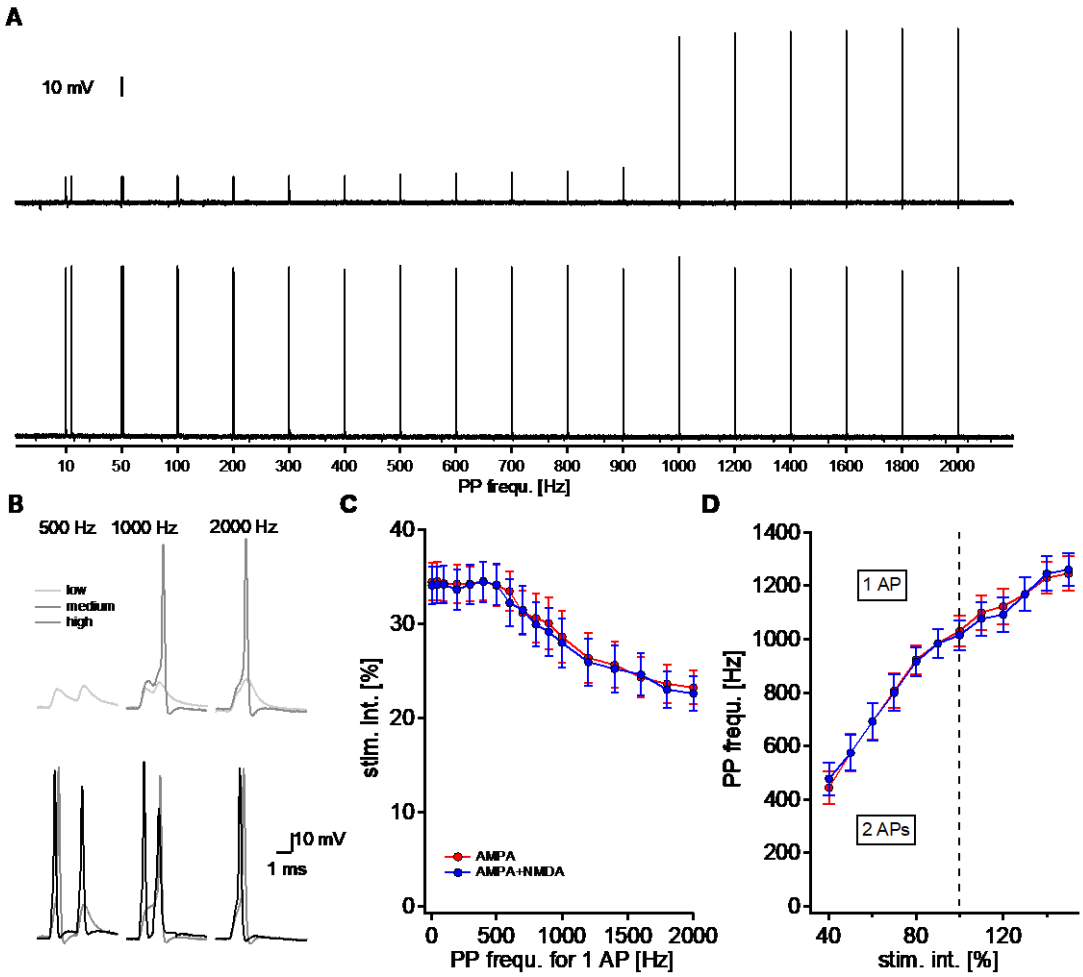

Fig. 13: AP integration in PP stimulation arrangement depends on stimulation frequency and –intensity, not on NMDA mediated currents. **A:** Exemplary voltage response to paired pulse (PP) stimuli of various frequencies (10, 50, 100, 200, 300, 400, 500, 600, 700, 800, 900, 1000, 1200, 1400, 1600, 1800 and 2000 Hz) for low (*top*) and high input conductance (*bottom*). **B:** Exemplary voltage response to 500 (*left*), 1000 (*middle*) and 2000 Hz PP ratio (*left*) to stimuli eliciting sub-threshold response (*light grey*), one AP (*dark grey*) and two APs (*black*). **C:** Required average stimulation intensity [%] to elicit one AP for all PP frequencies [Hz] when stimulated with AMPA alone (*red*) or with AMPA and NMDA together (*blue*). **D:** AP generation plotted as a function of average PP stimulation frequency [Hz] and stimulation intensity [%], revealing the transition in firing from one AP to two APs.

DISCUSSION

The purpose of this project was the examination of synaptic mechanisms underlying accurate information transfer at the VNLL endbulb in the auditory brainstem of hearing Mongolian gerbils. AMPA- and NMDAR mediated currents were identified as solely contributors to synaptic EPSCs. These EPSCs undergo frequency dependent STP, which in turn impacts postsynaptic output generation regarding temporal precision of supra-threshold responses.

EPSC components at the VNLL endbulb. Pharmacological VC experiments manifested the bi-exponential shape of the EPSC decay at the VNLL endbulb at holding potentials resembling the cells' resting potential. This study identified AMPA- and NMDAR mediated currents as exclusive mediators of these EPSCs, AMPARs mediating the fast, and NMDARs mediating the slow EPSC component. This finding is consistent with published data revealing bi-exponential decay in the AMPA mediated EPSCs in MNTB- and VNLL neurons of juvenile gerbils (Berger and Meyer et al., 2014). Bi-exponentially

decaying EPSCs have further been reported in neurons of other brainstem regions such as in stellate- and bushy cells (BCs) of the AVCN in mice (Chanda and Xu-Friedman, 2010) as well as at the calyx of Held in rats (Yamashita et al., 2003). Surprisingly, in this study, pharmacological CPP experiments revealed, besides NMDAR blockage, decreased AMPAR mediated peak current amplitudes. This suggests unspecific binding of CPP to AMPARs. The outward rectifying current-voltage relationship in AMPARs likely results from a higher Ca^{2+} permeability of these channels due to a reduced amount of the edited GluR2 subunit, in combination with intracellular blockage of AMPARs by endogenous polyamines. If GluR2, in the edited form, would be present, the current-voltage relationship would behave linearly, since the neutrally charged glutamine in the GluR2 RNA would have changed to positively charged arginine in a transmembrane domain in GluR2 (see Wisden and Seeburg 1993 for review; Sommer et al., 1991). This positive charge, introduced into the channel pore, would impede the flow of divalent ions through the channel (see Jonas and Burnashev, 1995 for review; Swanson et al., 1997).

The contribution of AMPA- and NMDAR mediated currents in EPSC shape in the auditory brainstem is not limited to the VNLL endbulb, but has, e.g., been shown at the calyx of Held in the MNTB in juvenile gerbils (Berger and Meyer et al., 2014), in the DNLL in young and adult gerbils (Siveke et al., 2018; Ammer et al., 2012; Wu and Kelly, 1996) and adult rats (Fu et al., 1997) and in the IC of adult rats (Zhang and Kelly, 2001). This abundance of AMPA- and NMDAR mediated currents in various nuclei within the auditory brainstem suggests their importance for auditory processing in these brain regions. Interestingly, kinetics of the fast AMPA component resembles data from other studies, whereas the decay times of the slow component deviate. EPSC decay times of 0.3 ms for τ_1 and 3.0 ms for τ_2 at -83 mV resemble those observed in other studies, reporting approximately 0.3 ms at the VNLL endbulb of mature gerbils, whereby in contrast to the present study, single-exponential functions were applied for EPSC decay fitting (Baumann and Koch, 2017, Caspari et al., 2015). More comparable studies using bi-exponential fitting function, verify values at least for τ_1 in juvenile gerbils, yet with exceeding τ_2 values (Berger and Meyer et al., 2014). Other studies rather reveal the immense difference in VNLL decay times to those in the AVCN of mice (Chanda and Xu-Friedman, 2010) or the MNTB in juvenile gerbils (Berger and Meyer et al., 2014). This might originate from age differences in used gerbils, and the developmental changes in the AMPAR subunit composition (Caicedo and Eybalin, 1999), in NMDAR mediated currents (Pliss et al., 2009; Irfan et al., 2005) as well as in neuronal morphology (Mainen and Sejnowski, 1996). Taken together, similar to EPSCs in other auditory nuclei, data illustrate the participation of two kinetic types of glutamatergic ionotropic receptor mediated currents in EPSCs at the VNLL endbulb.

In the present study, small amounts of NMDAR mediated currents were present even at hyperpolarised membrane voltage levels up to -93 mV. Within the SOC and the LL of the auditory brainstem, similar amounts of NMDAR mediated currents at hyperpolarised membrane voltage levels have, for example, been reported in juvenile gerbil and nearly adult rat DNLL neurons (Porres et al., 2011; Fu et al., 1997). Larger currents were observed in juvenile mouse MNTB neurons (Joshi et al., 2007), perhaps due to still immature developmental states of this structure in mice at that age compared to juvenile gerbil DNLL neurons. Beyond that, these small NMDAR mediated currents at hyperpolarised levels have been reported in previous studies outside the auditory brainstem (Pliss et al,. 2009; Slutsky et al., 2004; Gauck and Jaeger, 2003; Mayer et al., 1984). Yet the role of these NMDAR mediated currents remains unclear so far. Probably, they occur due to constant incomplete Mg^{2+} block (Espinosa and Kavalali, 2009). Differences in the Mg^{2+} block of heteromeric NMDAR channels are influenced by elements of the NR2 subunit of these receptors, which determine the Mg^{2+} sensitivity of the receptors (Kuner and Schoepfer, 1996). Incomplete Mg^{2+} block might support synaptic plasticity

and stabilisation of synaptic functions over comparatively long time periods of minutes and hours (Sutton et al., 2006; Slutsky et al., 2004; Murphy et al., 1994).

Frequency dependent STP of EPSCs. EPSCs at the VNLL endbulb undergo frequency dependent STP, corresponding to previously reported STP for neurons in the AVCN in mice (Chanda and Xu-Friedman, 2010; Yang and Xu-Friedman, 2009), in the MNTB in juvenile rats (Taschenberger and von Gersdorff, 2000), in the LSO as well as at hippocampal synapses in young and adult mice (Krächan et al., 2017), in the MSO in adult gerbils (Couchman et al., 2010), in VNLL neurons in young and adult mice (Baumann and Koch, 2017; Caspari et al., 2015), in DNLL neurons in adult gerbils (Porres et al., 2011), as well as for inhibitory currents for in LSO neurons in young and adult gerbils (Walcher et al., 2011). Although all studies, including this work, report STP, the course of STP differs. This study indicates both frequency dependent short-term facilitation (STF) and STD, facilitation occurring from 100 Hz on and above. In contrast, most cited studies concerning this matter exclusively report frequency dependent STD, except of few additional studies dealing with STP in neurons of the MNTB of juvenile rats and the AVCN in mice, where facilitation occurred at the same stimulation frequencies as in the present study (Taschenberger et al., 2016; Wang and Manis, 2008; Taschenberger and von Gersdorff, 2000). This discrepancy might be grounded in different extracellular $CaCl_2$ concentration, with high $CaCl_2$ associated with higher presynaptic vesicle release probability and a weaker STF. Across cited studies, extracellular $CaCl_2$ ranged from 1.5 to 2 mM, whereas in the present study, 1.2 mM was used for train experiments. This supports the hypothesised influence of extracellular $CaCl_2$ on STF presence. The differences in STF expression might, furthermore, be linked to a variety in the pool size of superprimed vesicles (VC_s), which show high mean release probability especially at high stimulation frequencies, compared to normal primed VCs (Taschenberger et al., 2016). This difference in release readiness might, in case of lower pool size in VC_s, lead to weaker or no facilitation in EPSCs.

For the STD, published work supports the finding of frequency dependent STD throughout ongoing stimulation, becoming stronger with increasing stimulation frequency (Baumann and Koch, 2017; Caspari et al., 2015; Porres et al., 2011; Chanda and Xu-Friedman, 2010; Taschenberger and von Gersdorff, 2000) and probably suppressing inputs of high activity which carry less accurate temporal information (Yang and Xu-Friedman, 2009). Furthermore, reported steady state depression in vVNLL neurons of mature mice resembles the depression rate in this study, both approximating 0.5 in response to a 100 Hz train stimulus (Caspari et al., 2015). Discrepancy in steady state depression among other cited studies might be grounded in the variable NMDAR mediated current proportion in EPSCs and the related variation in build-up current size during ongoing stimulus (Pliss et al., 2009). Furthermore, a certain degree in variability of depression has been documented at endbulbs on BCs in the AVCN of mice (Yang and Xu-Friedman, 2009), which might be traced to receptor desensitisation (Xu-Friedman and Regehr, 2003; Trussell et al., 1993) or vesicle depletion (Wang and Manis, 2008; Yang and Xu-Friedman, 2008).

In accordance with the present data, where NMDAR mediated currents were shown to accumulate in a frequency dependent manner, this build-up current during ongoing stimulation has, e.g., been described in the AVCN of mice (Pliss et al., 2009), and might explain increased τ_w values at high stimulation frequencies at the end of an ongoing stimulus in the present study: The slow NMDAR mediated EPSC component accumulates from 100 Hz stimulation frequency on, despite increased AMPA depression at high frequencies (Pliss et al., 2009). Moreover, frequency dependent build-up has been reported *in vivo* for inhibitory currents in the gerbil DNLL, which probably supports long-lasting activation of postsynaptic receptors (Ammer et al., 2015; Porres et al., 2011). Perhaps, build-up currents in the VNLL target similar functions, and support prolonged activation of postsynaptic receptors. The generated output could then provide prolonged inhibition to subsequent structures

such as the iINLL, iDNLL and especially iIC (Moore and Trussell, 2017; Kelly et al., 2009; Tanaka et al., 1985; Willard and Martin, 1983; Zook and Casseday, 1982). On the whole, AMPA- and NMDAR mediated currents at the VNLL endbulb show frequency dependent STP during ongoing stimulation.

Effect of frequency dependent NMDA contribution on postsynaptic spike generation. Obtained data show that the frequency dependent NMDAR mediated build-up current supports postsynaptic AP generation above 100 Hz stimulation frequency. Additionally, the number of elicited APs increases with the AMPAR mediated input conductance. Thus, since AMPAR related input conductance depresses during ongoing stimulation, and in compliance with earlier studies, the amount of elicited APs per cycle is limited when stimulated with AMPA alone and increased when NMDAR mediated currents are involved (Siveke et al., 2018; Porres et al., 2011; Pliss et al., 2009; Harsch and Robinson, 2000). The here and elsewhere reported reaching of a plateau during summation of NMDAR mediated currents above 100 Hz (Pliss et al., 2009), might be one requirement for the cell to easier follow these frequencies due to sustained increased input conductance at the postsynaptic membrane. Presumably, the higher amount of NMDAR mediated build-up current proportion in the EPSCs maintains the membrane potential close to firing threshold and lowers the current threshold for postsynaptic AP generation (Pliss et al., 2009; Yang and Xu-Friedman, 2009). Interestingly, a similar role of NMDAR mediated currents for postsynaptic output generation during ongoing stimulation has been reported for neural responses in the superior paraolivary nucleus. Here, NMDAR mediated currents can build up over time and accelerate the timing of supra-threshold voltage responses. This auditory brainstem nucleus is located in the SOC, and provides offset responses to the IC (Rajaram et al., 2019). Altogether, kinetics of NMDAR mediated currents seem to be a key feature for promoting spike generation during intermediate and high frequency ongoing stimulation.

Spike limitation during ongoing stimulation. Despite NMDA conductance, the ability of VNLL neurons to spike at every pulse during an ongoing stimulus is limited to 333 Hz, which might be attributed to the degree of frequency dependent STP (Porres et al., 2011), since eliminating STP from the stimulation paradigm lifted this frequency limitation in this study. Most likely, this spike limitation reduces continuous firing exclusively to physiologically relevant levels. An upper frequency limit for continuous spiking has, for instance, also been reported in an *in vivo* study which observed spiking cessation in response to AM sound stimulation frequencies exceeding 300 Hz in adult rat VNLL neurons (Zhang and Kelly, 2006). Together with the *in vitro* comparatively low frequency intrinsic resonance of 10 to 60 Hz in VNLL neurons (Fischer et al., 2018), data point towards a functionality of VNLL neurons in the transmission of neuronal signals in response to low frequency modulated sound envelopes as they occur in conspecific gerbil vocalisation (Ter-Mekaelian et al., 2012). Additionally, this study shows that, on the PP level, VNLL cells can discriminate frequencies up to 1261 Hz, when stimulated with enough intensity, rendering them faithful onset responders to these frequencies.

Role of NMDAR conductance and STP in temporal precision. Data of this study verifies the highly temporal precise discharge patterns of VNLL neurons reported in previous papers (Recio-Spinoso and Joris, 2014; Liu et al., 2014; Zhang and Kelly, 2006; Taschenberger and von Gersdorff, 2000), whereby both jitter and latency increase during ongoing stimulation of constant intermediate and high frequency and in the presence of STP. This dependence of temporal precision on stimulation history is supported by previous data (Baumann and Koch, 2017; Pliss et al., 2009). These changes in accuracy of supra-threshold responses with ongoing stimulation and in dependence of STP probably arise from changes in input conductance during ongoing stimulation and with STP (Chanda et al., 2010; Yang and Xu-Friedman, 2009). As shown here, the AMPAR mediated current size depresses with pulse number at high frequencies, resulting in lower amount of AMPAR mediated input conductance. Breaking down the impact on temporal precision to the AMPAR mediated input conductance alone clearly reveals

more accurate cell responses at high input conductance and hence at the initial part of an ongoing stimulus of distinct frequency. The dependence of supra-threshold response accuracy on input strength was also confirmed during PrDF stimulation.
Importantly, interpretation of the results from the PrDF experiment requires caution since the history dependence of neuronal response has not been taken into account. Since in train experiments of distinct frequencies a history dependence of output generation and temporal precision for supra-threshold voltage responses has been shown, it has to be assumed that this history impact also holds in response to PrDF stimulation. To obtain reliable results, further PrDF experiments and analyses have to be performed.
The high temporal precision and related high input conductance might be promoted by increased amounts of SVs fusing with the presynaptic membrane and the resulting increased quantal content that is released into the synaptic cleft (Krächan et al., 2017). Beyond that, NMDAR mediated currents marginally affect temporal precision as well, which has also been shown *in vitro* and *in vivo* in the DNLL of adult gerbils (Siveke et al., 2018). The increased jitter of supra-threshold responses during ongoing stimulation of constant high frequency stimulation as well as during strong PrDF stimulation, might assume that temporal precision during ongoing stimulation is less essential, compared to the spike generation at all.
For the biological system STP might provide fast and faithful onset-inhibition to subsequent structures by facilitating high frequency inputs on the PP level, and wipe out broadband onset noise during ongoing stimulation (Spencer et al., 2015). Broadband onset noise occurs in response to abrupt onset sounds or tone bursts. OCA cells are known to preferentially respond to such short tone bursts (Rhode et al., 1983), and provide the here out resulting excitatory input to VNLL cells, which then in turn suppress the broadband onset noise on the IC level. In addition, the inhibition of VNLL cells provided to the IC might determine directional preferences of frequency modulations by determining the timing of relative latency between excitation and inhibition in the IC, or shaping input waveforms, as it has been proposed *in vivo* in bats (Gittelman and Pollak, 2011).

CONCLUSION

Bi-exponential decaying EPSCs in adult gerbil VNLL neurons are exclusively driven by AMPA- and NMDARs, with AMPARs driving the fast and NMDARs driving the slow component. Thereby, EPSCs undergo frequency dependent STP in the form of STF for paired pulses followed by STD during ongoing stimulation. Postsynaptic AP generation primarily depends on input conductance and is supported by NMDAR mediated currents during ongoing stimulation of intermediate and high frequencies. Thereby temporal precision of supra-threshold voltage responses primarily depends on the AMPA mediated input conductance and is infuenced by the frequency dependent contribution of NMDAR mediated currents. STP might on the one hand support faithful onset inhibition provided to the iINLL, iDNLL and iIC. On the other hand, STP suppresses broadband onset noise supplied by cells in the OCA. Furthermore, NMDA supports faithful firing during high frequency ongoing stimulation, providing prolonged inhibition to downstream structures. Altogether, results provide evidence concerning a functionality of the inhibitory output of VNLL neurons in coding for sound envelopes in conspecific vocalisation.

GRANTS

Funds for this project were provided by the Deutsche Forschungsgemeinschaft (DFG: FE 789/6-1; AOBJ: 622960). L. Fischer and N. Kladisios were funded by the DFG (FE 789/6-1 and FE 789/7-1).

AUTHOR CONTRIBUTIONS

F.F. and C.L. conception, design and fund raising for research; L.F. and N.K. performed electrophysiological experiments; M.R. and C.L. performed computational modelling; L.F., N.K., F.F., and C.L. analysed data; L.F., N.K., F.F., and C.L. interpreted results of experiments; L.F., N.K., and F.F. prepared figures; L.F. and F.F. drafted manuscript.

CONFLICT OF INTEREST

The authors declare no competing financial interests.

ACKNOWLEDGEMENT

The authors thank Elisabeth M. M. Meyer for setting up the conductance-clamp setup and for help in the Boltzmann function application.

REFERENCES

Adams, J. C. (1997). "Projections from octopus cells of the posteroventral cochlear nucleus to the ventral nucleus of the lateral lemniscus in cat and human." Auditory Neuroscience **3**(4): 335-350.
Ammer, J. J., et al. (2012). "Late postnatal development of intrinsic and synaptic properties promotes fast and precise signaling in the dorsal nucleus of the lateral lemniscus." J Neurophysiol **107**(4): 1172-1185.
Ammer, J. J., et al. (2015). "Activity-dependent transmission and integration control the timescales of auditory processing at an inhibitory synapse." Curr Biol **25**(12): 1562-1572.
Axmacher, N. and R. Miles (2004). "Intrinsic cellular currents and the temporal precision of EPSP-action potential coupling in CA1 pyramidal cells." J Physiol **555**(Pt 3): 713-725.
Baumann, V. J. and U. Koch (2017). "Perinatal nicotine exposure impairs the maturation of glutamatergic inputs in the auditory brainstem." J Physiol **595**(11): 3573-3590.
Berger, C., et al. (2014). "Large somatic synapses on neurons in the ventral lateral lemniscus work in pairs." J Neurosci **34**(9): 3237-3246.
Budinger, E., et al. (2000). "Functional organization of auditory cortex in the Mongolian gerbil (Meriones unguiculatus). IV. Connections with anatomically characterized subcortical structures." Eur J Neurosci **12**(7): 2452-2474.
Caicedo, A. and M. Eybalin (1999). "Glutamate receptor phenotypes in the auditory brainstem and mid-brain of the developing rat." Eur J Neurosci **11**(1): 51-74.
Caspari, F., et al. (2015). "Heterogeneity of Intrinsic and Synaptic Properties of Neurons in the Ventral and Dorsal Parts of the Ventral Nucleus of the Lateral Lemniscus." Front Neural Circuits **9**: 74.
Chanda, S. and M. A. Xu-Friedman (2010). "A low-affinity antagonist reveals saturation and desensitization in mature synapses in the auditory brain stem." J Neurophysiol **103**(4): 1915-1926.
Cook, D. L., et al. (2003). "Synaptic depression in the localization of sound." Nature **421**(6918): 66-70.
Covey, E. and J. H. Casseday (1986). "Connectional basis for frequency representation in the nuclei of the lateral lemniscus of the bat Eptesicus fuscus." J Neurosci **6**(10): 2926-2940.
Covey, E. and J. H. Casseday (1991). "The monaural nuclei of the lateral lemniscus in an echolocating bat: parallel pathways for analyzing temporal features of sound." J Neurosci **11**(11): 3456-3470.
Dzubay, J. A. and C. E. Jahr (1996). "Kinetics of NMDA channel opening." J Neurosci **16**(13): 4129-4134.
Espinosa, F. and E. T. Kavalali (2009). "NMDA receptor activation by spontaneous glutamatergic neurotransmission." J Neurophysiol **101**(5): 2290-2296.
Fischer, L., et al. (2018). "Resonance Properties in Auditory Brainstem Neurons." Front Cell Neurosci **12**: 8.

Franzen, D. L., et al. (2015). "Development and modulation of intrinsic membrane properties control the temporal precision of auditory brain stem neurons." J Neurophysiol **113**(2): 524-536.
Friauf, E. and J. Ostwald (1988). "Divergent projections of physiologically characterized rat ventral cochlear nucleus neurons as shown by intra-axonal injection of horseradish peroxidase." Exp Brain Res **73**(2): 263-284.
Fu, X. W., et al. (1997). "Synaptic excitation in the dorsal nucleus of the lateral lemniscus: whole-cell patch-clamp recordings from rat brain slice." Neuroscience **78**(3): 815-827.
Gauck, V. and D. Jaeger (2003). "The contribution of NMDA and AMPA conductances to the control of spiking in neurons of the deep cerebellar nuclei." J Neurosci **23**(22): 8109-8118.
Geiger, J. R., et al. (1995). "Relative abundance of subunit mRNAs determines gating and Ca2+ permeability of AMPA receptors in principal neurons and interneurons in rat CNS." Neuron **15**(1): 193-204.
Gittelman, J. X. and G. D. Pollak (2011). "It's about time: how input timing is used and not used to create emergent properties in the auditory system." J Neurosci **31**(7): 2576-2583.
Irfan, N., et al. (2005). "Synaptic transmission mediated by ionotropic glutamate, glycine and GABA receptors in the rat's ventral nucleus of the lateral lemniscus." Hear Res **203**(1-2): 159-171.
Johnson, J. W. and P. Ascher (1987). "Glycine potentiates the NMDA response in cultured mouse brain neurons." Nature **325**(6104): 529-531.
Joshi, I., et al. (2007). "Coincident activation of metabotropic glutamate receptors and NMDA receptors (NMDARs) downregulates perisynaptic/extrasynaptic NMDARs and enhances high-fidelity neurotransmission at the developing calyx of Held synapse." J Neurosci **27**(37): 9989-9999.
Kelly, J. B., et al. (2009). "Anatomical projections of the nuclei of the lateral lemniscus in the albino rat (Rattus norvegicus)." J Comp Neurol **512**(4): 573-593.
Krachan, E. G., et al. (2017). "Synaptic reliability and temporal precision are achieved via high quantal content and effective replenishment: auditory brainstem versus hippocampus." J Physiol **595**(3): 839-864.
Kuba, H., et al. (2002). "Synaptic depression improves coincidence detection in the nucleus laminaris in brainstem slices of the chick embryo." Eur J Neurosci **15**(6): 984-990.
Kuner, T. and R. Schoepfer (1996). "Multiple structural elements determine subunit specificity of Mg2+ block in NMDA receptor channels." J Neurosci **16**(11): 3549-3558.
Liu, H. H., et al. (2014). "Acoustic signal characteristic detection by neurons in ventral nucleus of the lateral lemniscus in mice." Dongwuxue Yanjiu **35**(6): 500-509.
Mayer, M. L., et al. (1984). "Voltage-dependent block by Mg2+ of NMDA responses in spinal cord neurones." Nature **309**(5965): 261-263.
Moore, L. A. and L. O. Trussell (2017). "Corelease of Inhibitory Neurotransmitters in the Mouse Auditory Midbrain." J Neurosci **37**(39): 9453-9464.
Murphy, T. H., et al. (1994). "Differential regulation of calcium/calmodulin-dependent protein kinase II and p42 MAP kinase activity by synaptic transmission." J Neurosci **14**(3 Pt 1): 1320-1331.
Mylius, J., et al. (2013). "Subcortical auditory structures in the Mongolian gerbil: I. Golgi architecture." J Comp Neurol **521**(6): 1289-1321.
Nowak, L., et al. (1984). "Magnesium gates glutamate-activated channels in mouse central neurones." Nature **307**(5950): 462-465.
Oertel, D., et al. (2000). "Detection of synchrony in the activity of auditory nerve fibers by octopus cells of the mammalian cochlear nucleus." Proc Natl Acad Sci U S A **97**(22): 11773-11779.
Pinheiro, P. S., et al. (2013). "Selective block of postsynaptic kainate receptors reveals their function at hippocampal mossy fiber synapses." Cereb Cortex **23**(2): 323-331.
Pliss, L., et al. (2009). "Context-dependent effects of NMDA receptors on precise timing information at the endbulb of Held in the cochlear nucleus." J Neurophysiol **102**(5): 2627-2637.
Porres, C. P., et al. (2011). "NMDA Currents Modulate the Synaptic Input-Output Functions of Neurons in the Dorsal Nucleus of the Lateral Lemniscus in Mongolian Gerbils." Journal of Neuroscience **31**(12): 4511-4523.
Rajaram, E., et al. (2019). "Slow NMDA-Mediated Excitation Accelerates Offset-Response Latencies Generated via a Post-Inhibitory Rebound Mechanism." eNeuro **6**(3).
Recio-Spinoso, A. and P. X. Joris (2014). "Temporal properties of responses to sound in the ventral nucleus of the lateral lemniscus." J Neurophysiol **111**(4): 817-835.
Rhode, W. S., et al. (1983). "Physiological response properties of cells labeled intracellularly with horseradish peroxidase in cat ventral cochlear nucleus." J Comp Neurol **213**(4): 448-463.
Saint Marie, R. L., et al. (1997). "Patterns of gamma-aminobutyric acid and glycine immunoreactivities reflect structural and functional differences of the cat lateral lemniscal nuclei." J Comp Neurol **389**(2): 264-276.
Schofield, B. R. and N. B. Cant (1997). "Ventral nucleus of the lateral lemniscus in guinea pigs: cytoarchitecture and inputs from the cochlear nucleus." J Comp Neurol **379**(3): 363-385.

Siveke, I., et al. (2018). "Electrogenic N-methyl-D-aspartate receptor signaling enhances binaural responses in the adult brainstem." Eur J Neurosci **47**(7): 858-865.
Slutsky, I., et al. (2004). "Enhancement of synaptic plasticity through chronically reduced Ca2+ flux during uncorrelated activity." Neuron **44**(5): 835-849.
Sommer, B., et al. (1991). "RNA editing in brain controls a determinant of ion flow in glutamate-gated channels." Cell **67**(1): 11-19.
Spencer, M. J., et al. (2015). "Broadband onset inhibition can suppress spectral splatter in the auditory brainstem." PLoS One **10**(5): e0126500.
Sutton, M. A., et al. (2006). "Miniature neurotransmission stabilizes synaptic function via tonic suppression of local dendritic protein synthesis." Cell **125**(4): 785-799.
Swanson, G. T., et al. (1997). "Single-channel properties of recombinant AMPA receptors depend on RNA editing, splice variation, and subunit composition." J Neurosci **17**(1): 58-69.
Tanaka, K., et al. (1985). "The organization of neurons in the nucleus of the lateral lemniscus projecting to the superior and inferior colliculi in the rat." Brain Res **341**(2): 252-260.
Taschenberger, H. and H. von Gersdorff (2000). "Fine-tuning an auditory synapse for speed and fidelity: developmental changes in presynaptic waveform, EPSC kinetics, and synaptic plasticity." J Neurosci **20**(24): 9162-9173.
Taschenberger, H., et al. (2016). "Superpriming of synaptic vesicles as a common basis for intersynapse variability and modulation of synaptic strength." Proc Natl Acad Sci U S A **113**(31): E4548-4557.
Ter-Mikaelian, M., et al. (2012). "Vocal behavior of the Mongolian gerbil in a seminatural enclosure." Behaviour **149**(5): 461-492.
Trussell, L. O., et al. (1993). "Desensitization of AMPA receptors upon multiquantal neurotransmitter release." Neuron **10**(6): 1185-1196.
Walcher, J., et al. (2011). "Comparative posthearing development of inhibitory inputs to the lateral superior olive in gerbils and mice." J Neurophysiol **106**(3): 1443-1453.
Wang, Y. and P. B. Manis (2008). "Short-term synaptic depression and recovery at the mature mammalian endbulb of Held synapse in mice." J Neurophysiol **100**(3): 1255-1264.
Willard, F. H. and G. F. Martin (1983). "The auditory brainstem nuclei and some of their projections to the inferior colliculus in the North American opossum." Neuroscience **10**(4): 1203-1232.
Wisden, W. and P. H. Seeburg (1993). "Mammalian ionotropic glutamate receptors." Curr Opin Neurobiol **3**(3): 291-298.
Wu, S. H. and J. B. Kelly (1996). "In vitro brain slice studies of the rat's dorsal nucleus of the lateral lemniscus. III. synaptic pharmacology." J Neurophysiol **75**(3): 1271-1282.
Xu-Friedman, M. A. and W. G. Regehr (2003). "Ultrastructural contributions to desensitization at cerebellar mossy fiber to granule cell synapses." J Neurosci **23**(6): 2182-2192.
Yamashita, T., et al. (2003). "Developmental increase in vesicular glutamate content does not cause saturation of AMPA receptors at the calyx of held synapse." Journal of Neuroscience **23**(9): 3633-3638.
Yang, H. and M. A. Xu-Friedman (2009). "Impact of synaptic depression on spike timing at the endbulb of Held." J Neurophysiol **102**(3): 1699-1710.
Yang, Y., et al. (2015). "High-speed dynamic-clamp interface." J Neurophysiol **113**(7): 2713-2720.
Zhang, H. and J. B. Kelly (2001). "AMPA and NMDA receptors regulate responses of neurons in the rat's inferior colliculus." J Neurophysiol **86**(2): 871-880.
Zhang, H. and J. B. Kelly (2006). "Responses of neurons in the rat's ventral nucleus of the lateral lemniscus to amplitude-modulated tones." J Neurophysiol **96**(6): 2905-2914.
Zook, J. M. and J. H. Casseday (1982). "Origin of ascending projections to inferior colliculus in the mustache bat, Pteronotus parnellii." J Comp Neurol **207**(1): 14-28.

GENERAL DISCUSSION

This thesis comprises three studies, all investigating biophysically and synaptically evoked input-output functions in the CNS by performing *in vitro* intracellular and whole-cell somatic recordings in neurons of invertebrates and vertebrates. The main model organisms representing these subphyla were the European medicinal leech *H. medicinalis* for invertebrates and the Mongolian gerbil *M. unguiculatus* for vertebrates.

In general, this thesis reveals intrinsic frequency tuning as a universal principle for central filtering of sensory signals. The first two studies in this thesis indicate that intrinsic frequency tuning allows for segregation of tactile and acoustic sensory inputs in the mechano-sensory system in leech as well as in the mammalian hearing system. Moreover, in a third study, VNLL neurons in the auditory brainstem were further investigated regarding the physiological basis of temporally precise information processing.

For the first two studies, mechano-sensory neurons in leech and neurons in the mammalian auditory brainstem were investigated regarding neuronal intrinsic frequency tuning. Intrinsically frequency tuned neurons should respond selectively to specific frequency ranges of membrane voltage or current oscillations. With respect to this objective, recordings of somata responses to sinusoidal current injections of variable frequency and intensity were performed. Both studies together reveal frequency dependent behaviour in all recorded neurons on the sub- and supra-threshold voltage level.

Frequency filters in mechano-sensory neurons of the leech. In accordance with previously reported data, three different types of mechano-sensory neurons were identified in the leech segmental ganglia: N-, T-, and P-cells (Kretzberg et al., 2016; Kristan et al., 2005; Pinato and Torre, 2000; Mar and Drapeau, 1996; Blackshaw et al., 1982; Baylor Yau 1976; Jansen and Nicholls, 1973; Van Essen, 1973; Baylor and Nicholls, 1969a and b; Nicholls and Baylor, 1968). Excitability profiles revealed different intrinsic frequency tuning across these cell types, with low-pass filter properties in N-cells, band-pass filter properties in T-cells, and high-pass filter properties in P-cells (Fischer et al., 2017). This is an essential feature, especially for P- and N-cells, which both respond to intermediate and high tactile stimulation intensities, with some response overlap (Kretzberg et al., 2016; Pinato and Torre, 2000; Lewis and Kristan, 1998; Nicholls and Baylor, 1968). Intrinsic frequency tuning supports the generation of neuron specific filters for supra-threshold firing rates in order to segregate this overlapping information. These filter properties might, therefore, support the assignment of mechano-sensory information into a central neuronal filter bank in the leech. Importantly, in this analysis, frequency dependent tuning was based on the rate of supra-threshold events in the neurons in response to appropriate stimulation paradigms. It is noteworthy that, besides AP rate, temporal response features

also might be used for sensory input segregation, such as the first-spike timing of fast and temporally more precise T-cells (Pirschel and Kretzberg, 2016; Thomson and Kristan, 2006). In addition to intrinsic frequency tuning, central discrimination of mechano-sensory information is further influenced by the stimulation intensity (Fischer et al., 2017). An impact of intrinsic tuning to specific tactile stimulation intensities has been investigated numerous times before (Kretzberg et al., 2016; Mar and Drapeau, 1996; Blackshaw et al., 1982; Jansen and Nicholls, 1973; Van Essen, 1973; Baylor and Nicholls, 1969a) and, thus, supports the assumption that it is a mixture of intrinsic tuning forms, which contribute and determine the biophysical output generation of neurons in the CNS in invertebrates.

Taken together, multiplexed coding across neuron types in concert with different intrinsic neuronal tuning on the frequency and intensity level likely support filter banks and central stimulus discrimination in the leech. Importantly, it has to be considered that data in this study were obtained by intracellular soma recordings. Assuming that differences in peripheral and somatic voltage signalling is primarily based on compartment size rather than on active membrane properties, somatic excitability profiles allow useful insights into the biophysical input-output functions of neurons in the invertebrate CNS.

Subthreshold membrane resonance in mammalian auditory brainstem neurons. Besides frequency dependent supra-threshold output generation, intrinsic frequency tuning was shown to be also expressed on the subthreshold level, in the form of subthreshold membrane resonance, which is suggested as a further feature for neuronal discrimination (see Izhikevich, 2001 and Hutcheon and Yarom, 2000 for review; Puil et al., 1986). Subthreshold membrane resonance is based on membrane potential oscillations, which in turn depend on the repertoire of involved voltage gated ion channels, and supports neuronal response to specific frequencies (see Hutcheon and Yarom, 2000 for review). It is well-studied across rodents, amphibians, and birds (Beraneck et al., 2003; Ris et al., 2001; Av-Ron and Vidal, 1999; du Lac and Lisberger, 1995). In this thesis, the resonance frequency (R_f) was determined in five neuronal populations in the mammalian auditory brainstem. They all perform different tasks in the computation of temporally precise acoustic information. Interestingly, R_f was expressed in a low frequency membrane hyperpolarising trough and a high frequency membrane depolarising peak. This is in accordance with earlier resonance data, for instance, in frog vestibular neurons (Beraneck et al., 2007). Apart from that, so far, previous studies assigned both the hyperpolarising and depolarising R_f to similar stimulation frequencies, for instance, in mesencephalic and cortical neurons, in granule cells of the olfactory bulb, and in neurons of the MSO and LSO in various rodents (Hu et al., 2016; Remme et al., 2014; Boehlen et al., 2013; Hsiao et al., 2009; Wu et al., 2005). In the present study, the focus was put on the depolarising part, which facilitates AP generation at the resonance peak. In accordance with a recent study, the R_f in steady state R_0 was determined solely by the steady state membrane time constant (τ_s) (Schneider et al., 2011) and, thus, by the

instantaneous input resistance R_{ZAP} of the neuron. The second study of this thesis additionally revealed the main parameter determining R_f, which is the parameter β, the effective relaxation rate, which in turn is determined by the subthreshold activity of voltage gated ion channels and, hence, correlates to the leakiness of the cell membrane: leaky membranes lead to high R_f, whereas non-leaky membranes lead to low R_f.

Neuron population specific R_f and its functionality. For the biological system this means that R_f is intrinsic to neurons with fast τ_s and absent if τ_s exceeds 0.42/β (Fischer et al., 2018). This study indicates that neurons in the auditory brainstem that act as coincidence detectors on the circuit level have low τ_s values and, thus, show comparatively high R_f. In the mature gerbil MSO, R_f extended to values of up to 500 Hz, whereas in the mature mouse and rat LSO, R_f was maximally 200 Hz. Thus, the here obtained R_f in LSO neurons exceeded earlier data from LSO neurons in nearly mature guinea pigs, where the R_f was limited to approximately 100 Hz (Remme et al., 2014). This discrepancy can be explained by differences in the developmental states and, thus, by differences in either cell R_m or C_m. Since the R_m in LSO and MSO neurons in Remme et al. (2014) was similar to the R_m in LSO neurons of mice in the present study, here the differences in R_f are more likely based on a larger C_m in LSO and MSO neurons in Remme et al. (2014) compared to mouse LSO neurons in the present study. Furthermore, Remme et al. (2014) reported a specific arrangement of resonant principal LSO and MSO neurons, with the occurrence of resonant neurons decreasing from the lateral to the medial limb of the LSO, i.e. along the tonotopic axis from the low to the high frequency end. This arrangement could not be confirmed in the present study.

MSO and LSO neurons are involved in binaural pathways, detecting ITDs and ILDs in the millisecond range (see Grothe et al., 2010 for review; Brand et al., 2002; Yin and Chan, 1990). For mature MSO neurons, the R_f of 100 Hz and above matches the frequency range of phase-locked inputs of several 100 Hz provided by neurons of the CN (Joris et al., 1994) and, thus, might boost the cell response to these input frequencies. For LSO neurons, the stated R_f suggests larger time window requirements for faithful integration compared to MSO neurons. Taken together, the data point towards the encoding of the envelope of sound structures by LSO neurons, whereas MSO neurons code for the fine structure of sounds. For the VNLL, neurons show comparatively low R_f, suggesting that they probably code for low frequency sound envelopes (Zhang and Kelly, 2006a).

Interestingly, MSO and LSO neurons function as coincidence detectors on the circuit level and act as biophysical integrators on the cellular level. The extraordinary small τ_s, which is generally mediated by small R_m (Scott et al., 2005), enables integration of inputs over extremely small time windows in the microsecond range (see Grothe et al., 2003 and Golding and Oertel, 2012 for review; Myoga et al., 2014). Further, precise but slower integrators are located in the DNLL and VNLL, where neurons integrate inputs in the millisecond range (Recio-Spinoso and Joris, 2014; Pecka et al., 2007; Zhang and

Kelly, 2006a; Adams 1997; Covey and Casseday, 1991). Thereby, the width of the integration time window is determined by involved subthreshold currents (Fricker and Miles, 2000). The firing pattern is determined by passive membrane properties, which in turn are traced back to, for example, cell morphology (Mainen and Sejnowski, 1996) and involved voltage gated ion channels (see Johnston et al., 2010 for review; Fricker and Miles, 2000; Gittelman and Tempel, 2006).

Influence of postnatal development on R_f. R_f in the mammalian auditory brainstem undergoes developmental changes. Juvenile neurons revealed lower R_f compared to mature neurons, which probably allows for postnatal developmental refinement as described in the LSO (Kotak and Sanes, 2000 and 2014). The here observed age dependent R_f shift is in line with previous studies in gerbils, which showed postnatal developmental changes in gerbil MSO neurons after hearing onset, regarding synaptic current kinetics, transmitter release synchrony, postsynaptic potentials, passive membrane properties, and changes in axon projections to MSO neurons (Werthat et al., 2008; Chirila et al., 2007; Magnusson et al., 2005; Scott et al., 2005). Unfortunately, the developmental aspect was only examined in MSO neurons in this thesis.

In the LSO, postnatal changes in R_f would have been expected due to previously reported postnatal developmental electrophysiological changes in gerbil and rat LSO neurons around hearing onset. Neurons revealed increased synaptic peak current amplitudes, decreased decay times, and increased synaptic conductance (Scott et al., 2005; Kim and Kandler, 2003) after hearing onset. These changes could enhance the biophysical temporal precision in the mature state. Also, neurons in the gerbil and mouse VNLL have been documented to undergo postsynaptic development regarding membrane properties at rest and during activity (Franzen et al., 2015) and regarding EPSC amplitudes (Baumann and Koch, 2017). In rat hippocampal neurons, postnatal development is associated with changes in K^+ channel subtype expression patterns (Falk et al., 2003; Spigelman et al., 1992). All in all, changes of membrane properties at rest and during activation as well as alterations in K^+ channel expression might be main mediators for neuronal maturation (Franzen et al., 2015; Ammer et al., 2012; Scott et al., 2005). Taken together, both, the frequency dependent behaviour in leech mechano-sensory neurons and mammalian auditory brainstem neurons, reveal the universality of neuronal intrinsic frequency tuning mechanisms across neuron populations and indicate its role for central stimulus discrimination and for temporal processing adjustment in neurons.

Cellular basis for intrinsic frequency tuning in mechano-sensory neurons of the leech. Besides cellular morphology (Mainen and Seinowski, 1996), involved ionic conductance (Franzen et al., 2015; Ratté et al., 2013) presumably promotes intrinsic filtering. One possible actor promoting filter bank generation in leech neurons is the K^+ conductance which has been documented and characterised numerous times before (see Rudy, 1988 for review; Chandy and Gutman, 1993). D-type K^+ conductance is known to drive the repolarisation phase of APs (see Scheuer et al., 2011 and Rudy, 1988 for review). The

contribution of fast D-type K^+ channels and strong hyperpolarisation gated conductance possibly promotes fast voltage gating in the leech P-cells (Gerard et al., 2012; Steward et al., 1989). Slow voltage gating in N-cells might be supported by the extended after-hyperpolarisation of APs (Schlue, 1976). However, the exact physiology for the cell type specific firing behaviour at mechano-sensory neurons of the leech remains unclear and needs further investigations.

Cellular basis for subthreshold membrane resonance. The physiological basis for high frequency depolarising subthreshold membrane resonance in LSO and MSO neurons might involve inward and outward currents mediated by low threshold activated K_v1 channels, which have been identified in these brainstem nuclei (Fischl et al., 2016; Mathews et al., 2010; Scott et al., 2005; Barnes-Davies et al., 2004; Svirskis et al., 2002). Beyond K^+ mediated conductance, also Na mediated conductance could affect intrinsic frequency tuning, since Na channels have, for instance, been shown to undergo gating kinetic modulations, dependent on the β-subunit composition, which can influence, for example, the opening and closing speed of these channels (Schreibmayer et al., 1994; Bennett et al., 1993; Gershon et al., 1992; Li et al., 1992). Furthermore, slow inactivating Na^+ currents have been shown to amplify resonance behaviour in rat mesencephalic neurons (Wu et al., 2005).

For the low frequency hyperpolarising subthreshold resonance in auditory brainstem neurons, HCN channels have already been shown to drive subthreshold membrane activity in vertebrates and invertebrates, mainly mediating the I_h current (see Biel et al., 2009; Hutcheon and Yarom, 2000 and Pape, 1996 for review; Gerard et al., 2012; Hassfurth et al., 2009; Wu et al., 2005). HCN channels as mediator of the low frequency hyperpolarising resonance in MSO neurons have been firstly described in a comparative study across rodents (Fischer et al., 2018). Besides subthreshold membrane resonance (Hu et al., 2016; Boehlen et al., 2013), the functionality of HCN channel mediated currents are attributed to a huge variety of tasks in different biological systems, which can be condensed to the stabilisation of membrane potential and rhythmogenesis (see Biel et al., 2009 for review; Meuth et al., 2006; Ludwig et al., 2003; Pape, 1996; McCormick and Pape, 1990). For VNLL neurons, the ionic mechanism for subthreshold membrane resonance is unclear so far.

AMPA- and NMDARs mediate bi-exponentially decaying EPSC at the VNLL endbulb. Synaptic transmission at the chemical synapse is influenced by various factors. For instance, enzymes can support synaptic plasticity and, thus, alter neuronal excitability (Nelson et al., 2005). Furthermore, different kinetics of involved membrane ion channels and different expression levels of genes for receptor subunits can influence synaptic transmission (Wu et al., 2005; Dzubay and Jahr, 1996; Geiger et al., 1995). To elucidate the biophysical basis for temporally precise information processing in neurons involved in auditory processing, the third study in this thesis examined synaptic EPSCs at the VNLL endbulb in the auditory brainstem. EPSCs are strikingly fast, even faster than the rapid AMPAR mediated EPSCs at the MNTB (Berger and Meyer et al., 2014; Couchman et al., 2011). This is probably

due to differences in the calyx endbulb morphology (Berger and Meyer et al., 2014; Xu-Friedman and Regehr, 2004) or in glutamate content that is released into the synaptic cleft. Thus, neurons in the VNLL constitute an interesting target area for the inspection of mechanisms underlying temporally extremely precise information processing.

Physiological examination in this study revealed the bi-exponential shape of EPSCs, similar to EPSCs in other auditory brainstem nuclei (Berger and Meyer et al., 2014; Chanda and Xu-Friedman, 2010; Yamashita et al., 2003). The bi-exponential EPSC shape is mediated by glutamate. In line with this, the excitatory function of glutamate driven currents has already been documented multiple times in the mammalian CNS (e.g. Pinheiro et al., 2012; Geiger et al., 1995; Johnson and Ascher, 1987; Mayer et al., 1984; Nowak et al., 1984) and especially at the VNLL endbulb (Caspari et al., 2015; Berger and Meyer et al., 2014). In this study, AMPARs were attributed to the fast, whereas NMDARs were attributed to the slow EPSC component. This is in line with earlier data, which characterised the two ionotropic glutamate receptor types and their mediated synaptic currents (Dzubay and Jahr, 1996; Geiger et al., 1995; Johnson and Ascher, 1987; Mayer et al., 1984; Nowak et al., 1984). Thereby, EPSC decay times have been shown to vary with age, which in turn is linked to age dependent receptor subunit composition and current changes (Pliss et al., 2009; Irfan et al., 2005; Caicedo and Eybalin, 1999).

Frequency dependent STP during ongoing stimulation in VNLL neurons. In line with published data, EPSCs in VNLL neurons of the gerbil from this thesis underwent frequency dependent STP, comprising frequency dependent STF and frequency dependent STD, both increasing with stimulation frequency (Krächan et al., 2017; Baumann and Koch, 2017; Taschenberger et al., 2016; Caspari et al., 2015; Porres et al., 2011; Walcher et al., 2011; Chanda and Xu-Friedmann, 2010; Yang and Xu-Friedman, 2009; Wang and Manis, 2008; Cook et al., 2003; Kuba et al., 2002; Chung et al., 2002; Taschenberger and Gersdorff, 2000). Also in line with earlier data, STF occurred at the initial part of ongoing stimulation frequencies from 100 Hz on (Wang and Manis, 2008; Taschenberger and von Gersdorff, 2000). STF probably promotes fast and faithful AP generation on the PP level at the stimulus onset. STD, a more well-studied feature of STP, might be traced back to synaptic mechanisms such as receptor desensitisation (Xu-Friedman and Regehr, 2003; Trussell et al., 1993) or vesicle depletion (Wang and Manis, 2008; Yang and Xu-Friedman, 2008). STD probably functions as a suppressor of high activity inputs, which carry less precise timing information (Spencer et al., 2015; Yang and Xu-Friedman, 2009; Nayagam et al., 2005; Chung et al., 2002; Fortune and Rose, 2000) and, thus, filters received information at physiologically relevant levels. Consequently, STD might improve coincidence detection (Cook et al., 2003; Kuba et al., 2002) and control synaptic gain on the level of the IC (see Rothman et al., 2009 for review). Overall, this third study emphasises the assumption that STP functions as a temporal filter for central sensory processing, comprising high-pass filter properties using STF on the paired pulse level,

and low-pass filter properties using STD on the level of ongoing stimulation (see Fortune and Rose, 2001 and 2002 for review).

Frequency dependent NMDAR mediated build-up currents in VNLL neurons. In this study, NMDAR mediated build-up currents were documented during ongoing stimulation from 100 Hz on. This build-up current supports AP generation, which complies with previous data where the number of elicited APs during synaptic stimulation was increased at these frequencies when NMDARs were involved in synaptic transmission (Siveke et al., 2018; Porres et al., 2011; Pliss et al., 2009; Harsch and Robinson, 2000). The NMDAR mediated build-up currents likely counteract STD from 100 Hz on by holding the membrane potential close to firing threshold and, thus, promoting the postsynaptic AP generation. The resulting neuronal signal, which is then provided to downstream neurons in the iINLL, iDNLL, and especially in the iIC, might provide prolonged inhibition (Moore and Trussell, 2017; Kelly et al., 2009; Tanaka et al., 1985; Willard and Martin, 1983; Zook and Casseday, 1982).

Spike limitation in VNLL neurons. The faithfulness of spiking during ongoing stimulation *in vitro* is limited to 333 Hz, which is in line with the described, low R_f in these neurons (Fischer et al., 2018). Also, *in vivo* experiments revealed a spike limitation in rat VNLL neurons in case the modulation frequency of AM stimulation exceeded 300 Hz (Zhang and Kelly, 2006a). The *in vitro* spike limitation in gerbil VNLL neurons might result from presynaptic mechanisms, since an elimination of frequency dependent STP from the stimulation paradigm removed this limitation and indicated the functionality of the postsynaptic spike generator in response to current injections of 400 Hz (see VNLL Manuscript). Taken together, frequency dependent STP might limit the firing of VNLL neurons to physiologically relevant levels. This spike limitation to comparatively low stimulation frequencies below 400 Hz suggests that these neurons transmit information of comparatively low frequency AM sound envelopes, like they have been recently identified in conspecific vocalisation sounds of gerbils (Ter-Mekaelian et al., 2012).

Temporal precision of supra-threshold responses in VNLL neurons. For the temporal precision of supra-threshold responses, both jitter and latency are remarkably low, which is in line with *in vivo* observations (Recio-Spinoso and Joris, 2014; Liu et al., 2014; Zhang and Kelly, 2006a and b; Covey and Casseday, 1986 and 1991), revealing the high degree of temporally precise onset firing of VNLL neurons. In compliance with data on temporal precision of supra-threshold responses in mouse AVCN neurons, the underlying input conductance has been shown to define jitter and latency of postsynaptic APs during ongoing stimulation (Chanda and Xu-Friedman, 2010; Yang and Xu-Friedman, 2009). In accordance with data from mouse AVCN and VNLL neurons and gerbil DNLL neurons, a small effect on AP precision is attributed to NMDAR mediated currents (Siveke et al., 2018; Baumann and Koch, 2017; Pliss et al., 2009). The reduced accuracy of supra-threshold responses during ongoing stimulation

suggests a lower importance of temporal precision compared to the information transfer itself during ongoing stimulation.

Functionality of precise information processing in the VNLL for downstream neurons. STP probably provides secure onset spiking in VNLL neurons and subsequent onset inhibition to downstream neurons in the iINLL, iDNLL, and iIC (Moore and Trussell, 2017; Kelly et al., 2009; Tanaka et al., 1985; Willard and Martin, 1983; Zook and Casseday, 1982). Furthermore, during ongoing stimulation from 100 Hz on, NMDAR mediated build-up currents at the VNLL endbulb can counteract STD and support AP generation in the VNLL neuron and thereby provide prolonged inhibition to iINLL, iDNLL, and iIC neurons, to suppress broadband onset noise on the level of these downstream structures (Spencer et al., 2015). The resulting inhibition delivered to the IC could have diverse functions, such as determination of directional preferences of frequency modulations or shaping input waveforms (Gittelman and Pollak, 2011), enhancing the dynamic range of excitation integration, and threshold reduction for physiologically relevant excitatory inputs to the IC.

Taken together, neuronal intrinsic frequency tuning was proven as a universal principle for central sensory filtering in the CNS across sensory systems in both invertebrates and vertebrates. Intrinsic tuning is expressed on the sub- and supra-threshold voltage level and differs according to its function within the appropriate biological system. Overall, for the auditory system in gerbils and probably other mammals, results point towards the conclusion that the VNLL endbulb structure is a beneficial system component for the initial detection of salient sounds and that it is implemented in the transmission of information of low frequency AM envelopes.

CONCLUSION

Intrinsic frequency tuning in neurons supports central segregation of sensory inputs. The universality of this feature extends across different sensory systems in various species comprising invertebrates and vertebrates. Thereby, frequency tuning occurs on the sub- and supra-threshold voltage level in form of frequency dependent AP rate and subthreshold membrane resonance, which both differ with neuron type and function within the respective system. The physiological basis for intrinsic frequency tuning is attributed to contributing ionic conductance mediated by different involved ion channels. This physiological basis applies to temporally precise information transfer at the VNLL endbulb in the mammalian auditory brainstem: frequency dependent EPSC component contribution and STP, and the related frequency dependent postsynaptic input conductance influence postsynaptic AP generation, providing fast and secure onset and potentially prolonged inhibition to downstream structures.

OUTLOOK

So far, frequency dependent temporal processing at the VNLL endbulb was revealed in the form of subthreshold membrane potential resonance. Together with the observed frequency dependent EPSC component contribution and STP during ongoing temporally precise information processing at the gerbil VNLL endbulb, it is assumed that VNLL neurons are implicated in the transmission of low frequency AM sound envelopes. Such low frequency AM sound envelopes occur during gerbil vocalisation (Ter-Mekaelian et al., 2012) and are a characteristic feature for salient vocalisation in humans (Arnal et al., 2015). To test whether VNLL neurons code for these features in conspecific vocalisations, the final experiment will investigate supra-threshold firing patterns in response to gerbil vocalisations. For this, gerbil vocalisations need to be recorded and fed into an octopus cell model (programmed by M.R. and C.L.). Since the octopus cells provide the main source for excitatory glutamatergic input to VNLL neurons, this model can then mimic the excitatory input conductance, which is provided to VNLL neurons, in response to monaural contralateral conspecific stimulation. GC recordings will then elucidate, whether VNLL neurons transmit information of conspecific vocalisations.

REFERENCES

Ache, B. W. and J. M. Young (2005). "Olfaction: diverse species, conserved principles." Neuron **48**(3): 417-430.
Adams, J. C. (1997). "Projections from octopus cells of the posteroventral cochlear nucleus to the ventral nucleus of the lateral lemniscus in cat and human." Auditory Neuroscience **3**(4): 335-350.
Agmon-Snir, H. (1995). "A novel theoretical approach to the analysis of dendritic transients." Biophys J **69**(5): 1633-1656.
Agren, G., et al. (1989). "Ecology and Social-Behavior of Mongolian Gerbils, Meriones-Unguiculatus, at Xilinhot, Inner-Mongolia, China." Animal Behaviour **37**: 11-27.
Ammer, J. J., et al. (2012). "Late postnatal development of intrinsic and synaptic properties promotes fast and precise signaling in the dorsal nucleus of the lateral lemniscus." J Neurophysiol **107**(4): 1172-1185.
Ammer, J. J., et al. (2015). "Activity-dependent transmission and integration control the timescales of auditory processing at an inhibitory synapse." Curr Biol **25**(12): 1562-1572.
Arnal, L. H., et al. (2015). "Human screams occupy a privileged niche in the communication soundscape." Curr Biol **25**(15): 2051-2056.
Ashida, G. and C. E. Carr (2011). "Sound localization: Jeffress and beyond." Curr Opin Neurobiol **21**(5): 745-751.
Av-Ron, E. and P. P. Vidal (1999). "Intrinsic membrane properties and dynamics of medial vestibular neurons: a simulation." Biol Cybern **80**(6): 383-392.
Barnes-Davies, M., et al. (2004). "Kv1 currents mediate a gradient of principal neuron excitability across the tonotopic axis in the rat lateral superior olive." Eur J Neurosci **19**(2): 325-333.
Batra, R. (2006). "Responses of neurons in the ventral nucleus of the lateral lemniscus to sinusoidally amplitude modulated tones." J Neurophysiol **96**(5): 2388-2398.
Baumann, V. J. and U. Koch (2017). "Perinatal nicotine exposure impairs the maturation of glutamatergic inputs in the auditory brainstem." J Physiol **595**(11): 3573-3590.
Baylor, D. A. and J. G. Nicholls (1969a). "After-effects of nerve impulses on signalling in the central nervous system of the leech." J Physiol **203**(3): 571-589.
Baylor, D. A. and J. G. Nicholls (1969b). "Chemical and electrical synaptic connexions between cutaneous mechanoreceptor neurones in the central nervous system of the leech." J Physiol **203**(3): 591-609.
Bean, B. P. (2007). "The action potential in mammalian central neurons." Nat Rev Neurosci **8**(6): 451-465.
Beiderbeck, B., et al. (2018). "Precisely timed inhibition facilitates action potential firing for spatial coding in the auditory brainstem." Nat Commun **9**(1): 1771.
Bennett, P. B., Jr., et al. (1993). "A molecular basis for gating mode transitions in human skeletal muscle Na+ channels." FEBS Lett **326**(1-3): 21-24.
Benson, C. G. and N. B. Cant (2008). "The ventral nucleus of the lateral lemniscus of the gerbil (Meriones unguiculatus): organization of connections with the cochlear nucleus and the inferior colliculus." J Comp Neurol **510**(6): 673-690.
Beraneck, M., et al. (2003). "Long-term plasticity of ipsilesional medial vestibular nucleus neurons after unilateral labyrinthectomy." J Neurophysiol **90**(1): 184-203.
Beraneck, M., et al. (2007). "Differential intrinsic response dynamics determine synaptic signal processing in frog vestibular neurons." J Neurosci **27**(16): 4283-4296.
Berger, C., et al. (2014). "Large somatic synapses on neurons in the ventral lateral lemniscus work in pairs." J Neurosci **34**(9): 3237-3246.
Biacabe, B., et al. (2001). "Functional anatomy of auditory brainstem nuclei: application to the anatomical basis of brainstem auditory evoked potentials." Auris Nasus Larynx **28**(1): 85-94.
Biel, M., et al. (2009). "Hyperpolarization-activated cation channels: from genes to function." Physiol Rev **89**(3): 847-885.
Blackshaw, S. E. (1981). "Morphology and distribution of touch cell terminals in the skin of the leech." J Physiol **320**: 219-228.
Blackshaw, S. E., et al. (1982). "Physiological responses, receptive fields and terminal arborizations of nociceptive cells in the leech." J Physiol **326**: 251-260.

Boehlen, A., et al. (2013). "Contribution of near-threshold currents to intrinsic oscillatory activity in rat medial entorhinal cortex layer II stellate cells." J Neurophysiol **109**(2): 445-463.
Boudreau, J. C. and C. Tsuchitani (1968). "Binaural interaction in the cat superior olive S segment." J Neurophysiol **31**(3): 442-454.
Brand, A., et al. (2002). "Precise inhibition is essential for microsecond interaural time difference coding." Nature **417**(6888): 543-547.
Brew, H. M. and I. D. Forsythe (1995). "Two voltage-dependent K+ conductances with complementary functions in postsynaptic integration at a central auditory synapse." J Neurosci **15**(12): 8011-8022.
Brown, G. L., et al. (1936). "Reactions of the normal mammalian muscle to acetylcholine and to eserine." J Physiol **87**(4): 394-424.
Budinger, E., et al. (2000). "Functional organization of auditory cortex in the Mongolian gerbil (Meriones unguiculatus). IV. Connections with anatomically characterized subcortical structures." Eur J Neurosci **12**(7): 2452-2474.
Burrows, M. and P. L. Newland (1993). "Correlation between the receptive fields of locust interneurons, their dendritic morphology, and the central projections of mechanosensory neurons." J Comp Neurol **329**(3): 412-426.
Burrows, M. and P. L. Newland (1994). "Convergence of mechanosensory afferents from different classes of exteroceptors onto spiking local interneurons in the locust." J Neurosci **14**(5 Pt 2): 3341-3350.
Caicedo, A. and M. Eybalin (1999). "Glutamate receptor phenotypes in the auditory brainstem and mid-brain of the developing rat." Eur J Neurosci **11**(1): 51-74.
Camardo, J., et al. (1983). "Identified Aplysia neurons form specific chemical synapses in culture." J Neurosci **3**(12): 2614-2620.
Caporale, N. and Y. Dan (2008). "Spike timing-dependent plasticity: a Hebbian learning rule." Annu Rev Neurosci **31**: 25-46.
Carlton, T. and A. Mcvean (1995). "The Role of Touch, Pressure and Nociceptive Mechanoreceptors of the Leech in Unrestrained Behavior." Journal of Comparative Physiology a-Neuroethology Sensory Neural and Behavioral Physiology **177**(6): 781-791.
Caspari, F., et al. (2015). "Heterogeneity of Intrinsic and Synaptic Properties of Neurons in the Ventral and Dorsal Parts of the Ventral Nucleus of the Lateral Lemniscus." Front Neural Circuits **9**: 74.
Catterall, W. A. (2000). "From ionic currents to molecular mechanisms: the structure and function of voltage-gated sodium channels." Neuron **26**(1): 13-25.
Chanda, S. and M. A. Xu-Friedman (2010). "A low-affinity antagonist reveals saturation and desensitization in mature synapses in the auditory brain stem." J Neurophysiol **103**(4): 1915-1926.
Chandy, K. G. and G. A. Gutman (1993). "Nomenclature for mammalian potassium channel genes." Trends Pharmacol Sci **14**(12): 434.
Cheal, M. L. (1986). "The gerbil: a unique model for research on aging." Exp Aging Res **12**(1): 3-21.
Chirila, F. V., et al. (2007). "Development of gerbil medial superior olive: integration of temporally delayed excitation and inhibition at physiological temperature." J Physiol **584**(Pt 1): 167-190.
Chung, S., et al. (2002). "Short-term depression at thalamocortical synapses contributes to rapid adaptation of cortical sensory responses in vivo." Neuron **34**(3): 437-446.
Cook, D. L., et al. (2003). "Synaptic depression in the localization of sound." Nature **421**(6918): 66-70.
Cossart, R., et al. (2002). "Quantal release of glutamate generates pure kainate and mixed AMPA/kainate EPSCs in hippocampal neurons." Neuron **35**(1): 147-159.
Couchman, K., et al. (2010). "Medial superior olivary neurons receive surprisingly few excitatory and inhibitory inputs with balanced strength and short-term dynamics." J Neurosci **30**(50): 17111-17121.
Couchman, K., et al. (2012). "Functional localization of neurotransmitter receptors and synaptic inputs to mature neurons of the medial superior olive." J Neurophysiol **107**(4): 1186-1198.
Covey, E. and J. H. Casseday (1986). "Connectional basis for frequency representation in the nuclei of the lateral lemniscus of the bat Eptesicus fuscus." J Neurosci **6**(10): 2926-2940.
Covey, E. and J. H. Casseday (1991). "The monaural nuclei of the lateral lemniscus in an echolocating bat: parallel pathways for analyzing temporal features of sound." J Neurosci **11**(11): 3456-3470.
Crill, W. E. (1996). "Persistent sodium current in mammalian central neurons." Annu Rev Physiol **58**: 349-362.

Dale, H. H., et al. (1936). "Release of acetylcholine at voluntary motor nerve endings." J Physiol **86**(4): 353-380.
Deitmer, J. W. and W. R. Schlue (1981). "Measurements of the Intracellular Potassium Activity of Retzius Cells in the Leech Central Nervous-System." Journal of Experimental Biology **91**(Apr): 87-101.
du Lac, S. and S. G. Lisberger (1995). "Cellular processing of temporal information in medial vestibular nucleus neurons." J Neurosci **15**(12): 8000-8010.
Dzubay, J. A. and C. E. Jahr (1996). "Kinetics of NMDA channel opening." J Neurosci **16**(13): 4129-4134.
Encke, J. and W. Hemmert (2018). "Extraction of Inter-Aural Time Differences Using a Spiking Neuron Network Model of the Medial Superior Olive." Front Neurosci **12**: 140.
Falk, T., et al. (2003). "Developmental regulation of the A-type potassium-channel current in hippocampal neurons: role of the Kvbeta 1.1 subunit." Neuroscience **120**(2): 387-404.
Felmy, F. (2019). The Nuclei of the Lateral Lemniscus. The Oxford Handbook of the Auditory Brainstem. K. Kandler, Oxford University Press
Femy, F. and T. Kunzel (2014). "Giant synapses in the central auditory system." Neuroforum **20**(3): 240-249.
Fioravante, D. and W. G. Regehr (2011). "Short-term forms of presynaptic plasticity." Curr Opin Neurobiol **21**(2): 269-274.
Fischer, L., et al. (2018). "Resonance Properties in Auditory Brainstem Neurons." Front Cell Neurosci **12**: 8.
Fischer, L., et al. (2017). "Intrinsic frequency response patterns in mechano-sensory neurons of the leech." Biol Open **6**(7): 993-999.
Fischl, M. J., et al. (2016). "Physiology and anatomy of neurons in the medial superior olive of the mouse." J Neurophysiol **116**(6): 2676-2688.
Fitzpatrick, D. C., et al. (2000). "Neural sensitivity to interaural time differences: beyond the Jeffress model." J Neurosci **20**(4): 1605-1615.
Fortune, E. S. and G. J. Rose (2000). "Short-term synaptic plasticity contributes to the temporal filtering of electrosensory information." J Neurosci **20**(18): 7122-7130.
Fortune, E. S. and G. J. Rose (2001). "Short-term synaptic plasticity as a temporal filter." Trends Neurosci **24**(7): 381-385.
Fortune, E. S. and G. J. Rose (2002). "Roles for short-term synaptic plasticity in behavior." J Physiol Paris **96**(5-6): 539-545.
Franzen, D. L., et al. (2015). "Development and modulation of intrinsic membrane properties control the temporal precision of auditory brain stem neurons." J Neurophysiol **113**(2): 524-536.
French, A. S. and E. J. Sanders (1981). "The mechanosensory apparatus of the femoral tactile spine of the cockroach, Periplaneta americana." Cell Tissue Res **219**(1): 53-68.
Friauf, E. and J. Ostwald (1988). "Divergent projections of physiologically characterized rat ventral cochlear nucleus neurons as shown by intra-axonal injection of horseradish peroxidase." Exp Brain Res **73**(2): 263-284.
Fricker, D. and R. Miles (2000). "EPSP amplification and the precision of spike timing in hippocampal neurons." Neuron **28**(2): 559-569.
Fu, X. W., et al. (1997). "Synaptic excitation in the dorsal nucleus of the lateral lemniscus: whole-cell patch-clamp recordings from rat brain slice." Neuroscience **78**(3): 815-827.
Furukawa, H. (2012). "Structure and function of glutamate receptor amino terminal domains." J Physiol **590**(1): 63-72.
Geiger, J. R., et al. (1995). "Relative abundance of subunit mRNAs determines gating and Ca2+ permeability of AMPA receptors in principal neurons and interneurons in rat CNS." Neuron **15**(1): 193-204.
Gerard, E., et al. (2012). "Functional properties and cell type specific distribution of I(h) channels in leech neurons." J Exp Biol **215**(Pt 2): 227-238.
Gershon, E., et al. (1992). "Protein kinase A reduces voltage-dependent Na+ current in Xenopus oocytes." J Neurosci **12**(10): 3743-3752.
Gillespie, D. C., et al. (2005). "Inhibitory synapses in the developing auditory system are glutamatergic." Nat Neurosci **8**(3): 332-338.
Gittelman, J. X. and B. L. Tempel (2006). "Kv1.1-containing channels are critical for temporal precision during spike initiation." J Neurophysiol **96**(3): 1203-1214.
Gleich Otto and Strutz Jürgen (2012). The Mongolian Gerbil as a Model for the Analysis of Peripheral and

Central Age-Dependent Hearing Loss, Hearing Loss, Dr. Sadaf Naz (Ed.), ISBN: 978-953-51-0366-0, InTech, Available from: http://www.intechopen.com/books/hearing-loss/the-mongolian-gerbil-as-a-model-for-theanalysis-of-peripheral-and-central-age-dependent-hearing-los

Goldberg, J. M. and P. B. Brown (1969). "Response of binaural neurons of dog superior olivary complex to dichotic tonal stimuli: some physiological mechanisms of sound localization." J Neurophysiol **32**(4): 613-636.

Golding, N. L. and D. Oertel (2012). "Synaptic integration in dendrites: exceptional need for speed." J Physiol **590**(22): 5563-5569.

Grothe, B. and M. Pecka (2014). "The natural history of sound localization in mammals--a story of neuronal inhibition." Front Neural Circuits **8**: 116.

Grothe, B., et al. (2010). "Mechanisms of sound localization in mammals." Physiol Rev **90**(3): 983-1012.

Grothe, B. and D. H. Sanes (1994). "Synaptic inhibition influences the temporal coding properties of medial superior olivary neurons: an in vitro study." J Neurosci **14**(3 Pt 2): 1701-1709.

Harsch, A. and H. P. Robinson (2000). "Postsynaptic variability of firing in rat cortical neurons: the roles of input synchronization and synaptic NMDA receptor conductance." J Neurosci **20**(16): 6181-6192.

Hassfurth, B., et al. (2009). "Sensory deprivation regulates the development of the hyperpolarization-activated current in auditory brainstem neurons." Eur J Neurosci **30**(7): 1227-1238.

Heffner, H. E. and R. S. Heffner (2007). "Hearing ranges of laboratory animals." J Am Assoc Lab Anim Sci **46**(1): 20-22.

Hermann, J., et al. (2007). "Synaptic transmission at the calyx of Held under in vivo like activity levels." J Neurophysiol **98**(2): 807-820.

Hildebrand, J. G. and G. M. Shepherd (1997). "Mechanisms of olfactory discrimination: converging evidence for common principles across phyla." Annu Rev Neurosci **20**: 595-631.

Hodgkin, A. L. and A. F. Huxley (1952). "A quantitative description of membrane current and its application to conduction and excitation in nerve." J Physiol **117**(4): 500-544.

Hopson, J. A. (1950). "The Origin of the Mammalian Middle Ear." Am. Zoologist **6**: 437-450.

Hsiao, C. F., et al. (2009). "Participation of Kv1 channels in control of membrane excitability and burst generation in mesencephalic V neurons." J Neurophysiol **101**(3): 1407-1418.

Hu, R., et al. (2016). "Hyperpolarization-Activated Currents and Subthreshold Resonance in Granule Cells of the Olfactory Bulb." eNeuro **3**(5).

Hutcheon, B. and Y. Yarom (2000). "Resonance, oscillation and the intrinsic frequency preferences of neurons." Trends Neurosci **23**(5): 216-222.

Irfan, N., et al. (2005). "Synaptic transmission mediated by ionotropic glutamate, glycine and GABA receptors in the rat's ventral nucleus of the lateral lemniscus." Hear Res **203**(1-2): 159-171.

Ito, T., et al. (2011). "Expression of Glutamate and Inhibitory Amino Acid Vesicular Transporters in the Rodent Auditory Brainstem." Journal of Comparative Neurology **519**(2): 316-340.

Izhikevich, E. M. (2001). "Resonate-and-fire neurons." Neural Netw **14**(6-7): 883-894.

Jansen, J. K. and J. G. Nicholls (1973). "Conductance changes, an electrogenic pump and the hyperpolarization of leech neurones following impulses." J Physiol **229**(3): 635-655.

Johnson, J. W. and P. Ascher (1987). "Glycine potentiates the NMDA response in cultured mouse brain neurons." Nature **325**(6104): 529-531.

Johnston, J., et al. (2010). "Going native: voltage-gated potassium channels controlling neuronal excitability." J Physiol **588**(Pt 17): 3187-3200.

Jones, S. W. (1989). "On the resting potential of isolated frog sympathetic neurons." Neuron **3**(2): 153-161.

Joris, P. X., et al. (1994). "Enhancement of neural synchronization in the anteroventral cochlear nucleus. I. Responses to tones at the characteristic frequency." J Neurophysiol **71**(3): 1022-1036.

Kandler, K., et al. (2009). "Tonotopic reorganization of developing auditory brainstem circuits." Nat Neurosci **12**(6): 711-717.

Kandler, K. and E. Friauf (1993). "Pre- and postnatal development of efferent connections of the cochlear nucleus in the rat." J Comp Neurol **328**(2): 161-184.

Kaplan, J. H. (2002). "Biochemistry of Na,K-ATPase." Annu Rev Biochem **71**: 511-535.

Kelly, J. B. and S. A. Kidd (2000). "NMDA and AMPA receptors in the dorsal nucleus of the lateral lemniscus shape binaural responses in rat inferior colliculus." J Neurophysiol **83**(3): 1403-1414.
Kelly, J. B., et al. (2009). "Anatomical projections of the nuclei of the lateral lemniscus in the albino rat (Rattus norvegicus)." J Comp Neurol **512**(4): 573-593.
Khurana, S., et al. (2012). "An essential role for modulation of hyperpolarization-activated current in the development of binaural temporal precision." J Neurosci **32**(8): 2814-2823.
Killion, M. C. and P. Dallos (1979). "Impedance Matching by the Combined Effects of the Outer and Middle-Ear." Journal of the Acoustical Society of America **66**(2): 599-602.
Kim, G. and K. Kandler (2003). "Elimination and strengthening of glycinergic/GABAergic connections during tonotopic map formation." Nat Neurosci **6**(3): 282-290.
Koppl, C. (2009). "Evolution of sound localisation in land vertebrates." Curr Biol **19**(15): R635-639.
Kopp-Scheinpflug, C., et al. (2003). "The medial nucleus of the trapezoid body in the gerbil is more than a relay: comparison of pre- and postsynaptic activity." J Assoc Res Otolaryngol **4**(1): 1-23.
Kotak, V. C., et al. (1998). "A developmental shift from GABAergic to glycinergic transmission in the central auditory system." J Neurosci **18**(12): 4646-4655.
Kotak, V. C. and D. H. Sanes (2000). "Long-lasting inhibitory synaptic depression is age- and calcium-dependent." J Neurosci **20**(15): 5820-5826.
Kotak, V. C. and D. H. Sanes (2014). "Developmental expression of inhibitory synaptic long-term potentiation in the lateral superior olive." Front Neural Circuits **8**: 67.
Kowalski, J., et al. (2016). "Intrinsic membrane properties determine hippocampal differential firing pattern in vivo in anesthetized rats." Hippocampus **26**(5): 668-682.
Krachan, E. G., et al. (2017). "Synaptic reliability and temporal precision are achieved via high quantal content and effective replenishment: auditory brainstem versus hippocampus." J Physiol **595**(3): 839-864.
Kretzberg, J., et al. (2016). "Encoding of Tactile Stimuli by Mechanoreceptors and Interneurons of the Medicinal Leech." Front Physiol **7**: 506.
Kristan, W. B., Jr., et al. (2005). "Neuronal control of leech behavior." Prog Neurobiol **76**(5): 279-327.
Krnjevic, K. (1974). "Chemical Nature of Synaptic Transmission in Vertebrates." Physiol Rev **54**(2): 418-540.
Kuba, H., et al. (2002). "Synaptic depression improves coincidence detection in the nucleus laminaris in brainstem slices of the chick embryo." Eur J Neurosci **15**(6): 984-990.
Kullmann, P. H. and K. Kandler (2008). "Dendritic Ca2+ responses in neonatal lateral superior olive neurons elicited by glycinergic/GABAergic synapses and action potentials." Neuroscience **154**(1): 338-345.
Kuo, S. P., et al. (2012). "Intrinsic and synaptic properties of vertical cells of the mouse dorsal cochlear nucleus." J Neurophysiol **108**(4): 1186-1198.
Leao, K. E., et al. (2011). "Modulation of dendritic synaptic processing in the lateral superior olive by hyperpolarization-activated currents." Eur J Neurosci **33**(8): 1462-1470.
Lewis, J. E. and W. B. Kristan, Jr. (1998). "Representation of touch location by a population of leech sensory neurons." J Neurophysiol **80**(5): 2584-2592.
Li, M., et al. (1992). "Functional modulation of brain sodium channels by cAMP-dependent phosphorylation." Neuron **8**(6): 1151-1159.
Lisman, J. (1989). "A mechanism for the Hebb and the anti-Hebb processes underlying learning and memory." Proc Natl Acad Sci U S A **86**(23): 9574-9578.
Liu, H. H., et al. (2014). "Acoustic signal characteristic detection by neurons in ventral nucleus of the lateral lemniscus in mice." Dongwuxue Yanjiu **35**(6): 500-509.
Lu, W., et al. (2009). "Subunit composition of synaptic AMPA receptors revealed by a single-cell genetic approach." Neuron **62**(2): 254-268.
Ludwig, A., et al. (2003). "Absence epilepsy and sinus dysrhythmia in mice lacking the pacemaker channel HCN2." EMBO J **22**(2): 216-224.
Luscher, C. and R. C. Malenka (2012). "NMDA receptor-dependent long-term potentiation and long-term depression (LTP/LTD)." Cold Spring Harb Perspect Biol **4**(6).
Magnusson, A. K., et al. (2005). "Maturation of glycinergic inhibition in the gerbil medial superior olive after hearing onset." J Physiol **568**(Pt 2): 497-512.

Mainen, Z. F. and T. J. Sejnowski (1996). "Influence of dendritic structure on firing pattern in model neocortical neurons." Nature **382**(6589): 363-366.

Malmierca, M. S., et al. (1998). "Anatomic evidence of a three-dimensional mosaic pattern of tonotopic organization in the ventral complex of the lateral lemniscus in cat." Journal of Neuroscience **18**(24): 10603-10618.

Mar, A. and P. Drapeau (1996). "Modulation of conduction block in leech mechanosensory neurons." J Neurosci **16**(14): 4335-4343.

Masaki, H., et al. (2004). "The functional locus of the lateralized readiness potential." Psychophysiology **41**(2): 220-230.

Mathews, P. J., et al. (2010). "Control of submillisecond synaptic timing in binaural coincidence detectors by K(v)1 channels." Nat Neurosci **13**(5): 601-609.

Mayer, M. L., et al. (1984). "Voltage-dependent block by Mg2+ of NMDA responses in spinal cord neurones." Nature **309**(5965): 261-263.

McCormick, D. A. and H. C. Pape (1990). "Noradrenergic and serotonergic modulation of a hyperpolarization-activated cation current in thalamic relay neurones." J Physiol **431**: 319-342.

Meuth, S. G., et al. (2006). "Membrane resting potential of thalamocortical relay neurons is shaped by the interaction among TASK3 and HCN2 channels." J Neurophysiol **96**(3): 1517-1529.

Miyasho, T., et al. (2001). "Low-threshold potassium channels and a low-threshold calcium channel regulate Ca2+ spike firing in the dendrites of cerebellar Purkinje neurons: a modeling study." Brain Res **891**(1-2): 106-115.

Moore, L. A. and L. O. Trussell (2017). "Corelease of Inhibitory Neurotransmitters in the Mouse Auditory Midbrain." J Neurosci **37**(39): 9453-9464.

Moore, L. E. and J. T. Buchanan (1993). "The effects of neurotransmitters on the integrative properties of spinal neurons in the lamprey." J Exp Biol **175**: 89-114.

Mylius, J., et al. (2013). "Subcortical auditory structures in the Mongolian gerbil: I. Golgi architecture." J Comp Neurol **521**(6): 1289-1321.

Myoga, M. H., et al. (2014). "Glycinergic inhibition tunes coincidence detection in the auditory brainstem." Nat Commun **5**: 3790.

Nabekura, J., et al. (2004). "Developmental switch from GABA to glycine release in single central synaptic terminals." Nat Neurosci **7**(1): 17-23.

Nabel, A. L., et al. (2019). "Distinct Distribution Patterns of Potassium Channel Sub-Units in Somato-Dendritic Compartments of Neurons of the Medial Superior Olive." Frontiers in Cellular Neuroscience **13**.

Nayagam, D. A., et al. (2005). "Powerful, onset inhibition in the ventral nucleus of the lateral lemniscus." J Neurophysiol **94**(2): 1651-1654.

Nelson, A. B., et al. (2005). "Decreases in CaMKII activity trigger persistent potentiation of intrinsic excitability in spontaneously firing vestibular nucleus neurons." Neuron **46**(4): 623-631.

Nelson, R. J., et al. (1980). "Representations of the body surface in postcentral parietal cortex of Macaca fascicularis." J Comp Neurol **192**(4): 611-643.

Nicholls, J. and B. G. Wallace (1978). "Modulation of transmission at an inhibitory synapse in the central nervous system of the leech." J Physiol **281**: 157-170.

Nicholls, J. G. and D. A. Baylor (1968). "Specific modalities and receptive fields of sensory neurons in CNS of the leech." J Neurophysiol **31**(5): 740-756.

Nishimaki, T., et al. (2007). "Reduction of metabotropic glutamate receptor-mediated heterosynaptic inhibition of developing MNTB-LSO inhibitory synapses." Eur J Neurosci **26**(2): 323-330.

Nowak, L., et al. (1984). "Magnesium gates glutamate-activated channels in mouse central neurones." Nature **307**(5950): 462-465.

Pape, H. C. (1996). "Queer current and pacemaker: the hyperpolarization-activated cation current in neurons." Annu Rev Physiol **58**: 299-327.

Pecka, M., et al. (2007). "Inhibiting the inhibition: a neuronal network for sound localization in reverberant environments." J Neurosci **27**(7): 1782-1790.

Peters, A. and S. L. Palay (1996). "The morphology of synapses." J Neurocytol **25**(12): 687-700.

Pfaff, C., et al. (2019). "The vertebrate middle and inner ear: A short overview." J Morphol **280**(8): 1098-1105.

Pickles, J. O. (2015). "Auditory pathways: anatomy and physiology." Handb Clin Neurol **129**: 3-25.

Pinato, G. and V. Torre (2000). "Coding and adaptation during mechanical stimulation in the leech nervous system." J Physiol **529 Pt 3**: 747-762.

Pinheiro, P. S., et al. (2013). "Selective block of postsynaptic kainate receptors reveals their function at hippocampal mossy fiber synapses." Cereb Cortex **23**(2): 323-331.

Pirschel, F. and J. Kretzberg (2016). "Multiplexed Population Coding of Stimulus Properties by Leech Mechanosensory Cells." J Neurosci **36**(13): 3636-3647.

Pliss, L., et al. (2009). "Context-dependent effects of NMDA receptors on precise timing information at the endbulb of Held in the cochlear nucleus." J Neurophysiol **102**(5): 2627-2637.

Pollak, G. D., et al. (2011). "Inhibitory projections from the ventral nucleus of the lateral lemniscus and superior paraolivary nucleus create directional selectivity of frequency modulations in the inferior colliculus: a comparison of bats with other mammals." Hear Res **273**(1-2): 134-144.

Porres, C. P., et al. (2011). "NMDA Currents Modulate the Synaptic Input-Output Functions of Neurons in the Dorsal Nucleus of the Lateral Lemniscus in Mongolian Gerbils." Journal of Neuroscience **31**(12): 4511-4523.

Proctor, R., Vu, K. (2006). Stimulus-Response Compatibility Principles - Data, Theory and Application, CRC Press Taylor & Francis Group.

Puil, E., et al. (1986). "Quantification of membrane properties of trigeminal root ganglion neurons in guinea pigs." J Neurophysiol **55**(5): 995-1016.

Pumplin, D. W. and T. S. Reese (1978). "Membrane ultrastructure of the giant synapse of the squid Loligo pealei." Neuroscience **3**(8): 685-696.

Radojcic, T. and V. W. Pentreath (1979). "Invertebrate glia." Prog Neurobiol **12**(2): 115-179.

Raeside, J. R. (2011). "A proving of Hydrophis cyanocinctus. 1959." Homeopathy **100**(1-2): 62-72.

Rall, W. (1959). "Branching dendritic trees and motoneuron membrane resistivity." Exp Neurol **1**: 491-527.

Ranjan, R., et al. (2019). "A Kinetic Map of the Homomeric Voltage-Gated Potassium Channel (Kv) Family." Frontiers in Cellular Neuroscience **13**.

Rash, J. E., et al. (2013). "Molecular and functional asymmetry at a vertebrate electrical synapse." Neuron **79**(5): 957-969.

Ratte, S., et al. (2013). "Impact of neuronal properties on network coding: roles of spike initiation dynamics and robust synchrony transfer." Neuron **78**(5): 758-772.

Recio-Spinoso, A. and P. X. Joris (2014). "Temporal properties of responses to sound in the ventral nucleus of the lateral lemniscus." J Neurophysiol **111**(4): 817-835.

Remme, M. W. H., et al. (2014). "Subthreshold resonance properties contribute to the efficient coding of auditory spatial cues." Proceedings of the National Academy of Sciences of the United States of America **111**(22): E2339-E2348.

Rhode, W. S., et al. (1983). "Physiological response properties of cells labeled intracellularly with horseradish peroxidase in cat ventral cochlear nucleus." J Comp Neurol **213**(4): 448-463.

Ris, L., et al. (2001). "Resonance of spike discharge modulation in neurons of the guinea pig medial vestibular nucleus." J Neurophysiol **86**(2): 703-716.

Rodriguez, M. J., et al. (2004). "Modulation of mechanosensory responses by motoneurons that regulate skin surface topology in the leech." J Neurophysiol **91**(5): 2366-2375.

Rosenberger, M. H., et al. (2003). "Expression of the Kv1.1 ion channel subunit in the auditory brainstem of the big brown bat, Eptesicus fuscus." J Comp Neurol **462**(1): 101-120.

Rothman, J. S., et al. (2009). "Synaptic depression enables neuronal gain control." Nature **457**(7232): 1015-1018.

Rudy, B. (1988). "Diversity and ubiquity of K channels." Neuroscience **25**(3): 729-749.

Ryugo, D. K. and S. Sento (1991). "Synaptic connections of the auditory nerve in cats: relationship between endbulbs of held and spherical bushy cells." J Comp Neurol **305**(1): 35-48.

Saint Marie, R. L., et al. (1997). "Patterns of gamma-aminobutyric acid and glycine immunoreactivities reflect structural and functional differences of the cat lateral lemniscal nuclei." J Comp Neurol **389**(2): 264-276.

Sanchez, J. T., et al. (2007). "Contribution of NMDA and AMPA receptors to temporal patterning of auditory responses in the inferior colliculus." J Neurosci **27**(8): 1954-1963.

Sanes, D. H. and V. Siverls (1991). "Development and specificity of inhibitory terminal arborizations in the central nervous system." J Neurobiol **22**(8): 837-854.

Scheuer, T. (2011). "Regulation of sodium channel activity by phosphorylation." Semin Cell Dev Biol **22**(2): 160-165.

Schlue, W. R. (1976). "Sensory neurons in leech central nervous system: changes in potassium conductance an excitation threshold." J Neurophysiol **39**(6): 1184-1192.

Schneider, A. D., et al. (2011). "In vivo conditions induce faithful encoding of stimuli by reducing nonlinear synchronization in vestibular sensory neurons." PLoS Comput Biol **7**(7): e1002120.

Schofield, B. R. and N. B. Cant (1997). "Ventral nucleus of the lateral lemniscus in guinea pigs: cytoarchitecture and inputs from the cochlear nucleus." J Comp Neurol **379**(3): 363-385.

Schreibmayer, W., et al. (1994). "Mechanism of modulation of single sodium channels from skeletal muscle by the beta 1-subunit from rat brain." Pflugers Arch **426**(3-4): 360-362.

Scott, L. L., et al. (2005). "Posthearing developmental refinement of temporal processing in principal neurons of the medial superior olive." J Neurosci **25**(35): 7887-7895.

Segev, I. (1992). "Single Neuron Models - Oversimple, Complex and Reduced." Trends Neurosci **15**(11): 414-421.

Sillar, K. T. P., L.D. (2016). The Neuroethology of Predation and Escape, WILEY Blackwell.

Siveke, I., et al. (2018). "Electrogenic N-methyl-D-aspartate receptor signaling enhances binaural responses in the adult brainstem." Eur J Neurosci **47**(7): 858-865.

Skou, J. C. (1957). "The influence of some cations on an adenosine triphosphatase from peripheral nerves." Biochim Biophys Acta **23**(2): 394-401.

Skou, J. C. (1965). "Enzymatic Basis for Active Transport of Na+ and K+ across Cell Membrane." Physiol Rev **45**: 596-617.

Smith, P. H., et al. (2005). "Acoustic stria: anatomy of physiologically characterized cells and their axonal projection patterns." J Comp Neurol **482**(4): 349-371.

Spangler, K. M., et al. (1985). "The projections of principal cells of the medial nucleus of the trapezoid body in the cat." J Comp Neurol **238**(3): 249-262.

Spencer, M. J., et al. (2015). "Broadband onset inhibition can suppress spectral splatter in the auditory brainstem." PLoS One **10**(5): e0126500.

Spigelman, I., et al. (1992). "Patch-clamp study of postnatal development of CA1 neurons in rat hippocampal slices: membrane excitability and K+ currents." J Neurophysiol **68**(1): 55-69.

Spruston, N., et al. (1994). "Dendritic attenuation of synaptic potentials and currents: the role of passive membrane properties." Trends Neurosci **17**(4): 161-166.

Stephen, R. O. and H. C. Bennetclark (1982). "The Anatomical and Mechanical Basis of Stimulation and Frequency-Analysis in the Locust Ear." Journal of Experimental Biology **99**(Aug): 279-&.

Sterenborg, J. C., et al. (2010). "Lateral olivocochlear (LOC) neurons of the mouse LSO receive excitatory and inhibitory synaptic inputs with slower kinetics than LSO principal neurons." Hear Res **270**(1-2): 119-126.

Stewart, R. R., et al. (1989). "Na+, K+ and Ca2+ currents in identified leech neurones in culture." J Exp Biol **141**: 1-20.

Stuart, A. E. (1970). "Physiological and morphological properties of motoneurones in the central nervous system of the leech." J Physiol **209**(3): 627-646.

Stuermer, I. W., et al. (2003). "Intraspecific allometric comparison of laboratory gerbils with Mongolian gerbils trapped in the wild indicates domestication in Meriones unguiculatus (Milne-Edwards, 1867) (Rodentia : Gerbillinae)." Zoologischer Anzeiger **242**(3): 249-266.

Stuhmer, W., et al. (1989). "Structural parts involved in activation and inactivation of the sodium channel." Nature **339**(6226): 597-603.

Sung, C. H. and J. Z. Chuang (2010). "The cell biology of vision." J Cell Biol **190**(6): 953-963.

Svirskis, G., et al. (2002). "Enhancement of signal-to-noise ratio and phase locking for small inputs by a low-threshold outward current in auditory neurons." J Neurosci **22**(24): 11019-11025.

Tanaka, K., et al. (1985). "The organization of neurons in the nucleus of the lateral lemniscus projecting to the superior and inferior colliculi in the rat." Brain Res **341**(2): 252-260.

Taschenberger, H. and H. von Gersdorff (2000). "Fine-tuning an auditory synapse for speed and fidelity: developmental changes in presynaptic waveform, EPSC kinetics, and synaptic plasticity." J Neurosci **20**(24): 9162-9173.

Taschenberger, H., et al. (2016). "Superpriming of synaptic vesicles as a common basis for intersynapse variability and modulation of synaptic strength." Proc Natl Acad Sci U S A **113**(31): E4548-4557.

Ter-Mikaelian, M., et al. (2012). "Vocal behavior of the Mongolian gerbil in a seminatural enclosure." Behaviour **149**(5): 461-492.

Thomson, E. E. and W. B. Kristan (2006). "Encoding and decoding touch location in the leech CNS." J Neurosci **26**(30): 8009-8016.

Tollin, D. J. (2003). "The lateral superior olive: a functional role in sound source localization." Neuroscientist **9**(2): 127-143.

Tollin, D. J. and T. C. Yin (2005). "Interaural phase and level difference sensitivity in low-frequency neurons in the lateral superior olive." J Neurosci **25**(46): 10648-10657.

Toth, K., et al. (2000). "Differential mechanisms of transmission at three types of mossy fiber synapse." J Neurosci **20**(22): 8279-8289.

Turrigiano, G. G. and S. B. Nelson (2004). "Homeostatic plasticity in the developing nervous system." Nat Rev Neurosci **5**(2): 97-107.

Van Essen, D. C. (1973). "The contribution of membrane hyperpolarization to adaptation and conduction block in sensory neurones of the leech." J Physiol **230**(3): 509-534.

Waiblinger, E. and B. Konig (2004). "Refinement of gerbil housing and husbandry in the laboratory." Altern Lab Anim **32 Suppl 1A**: 163-169.

Walcher, J., et al. (2011). "Comparative posthearing development of inhibitory inputs to the lateral superior olive in gerbils and mice." J Neurophysiol **106**(3): 1443-1453.

Wang, Y. and P. B. Manis (2008). "Short-term synaptic depression and recovery at the mature mammalian endbulb of Held synapse in mice." J Neurophysiol **100**(3): 1255-1264.

Werthat, F., et al. (2008). "Experience-dependent refinement of the inhibitory axons projecting to the medial superior olive." Dev Neurobiol **68**(13): 1454-1462.

Willard, F. H. and G. F. Martin (1983). "The auditory brainstem nuclei and some of their projections to the inferior colliculus in the North American opossum." Neuroscience **10**(4): 1203-1232.

Wu, N., et al. (2005). "Persistent sodium currents in mesencephalic v neurons participate in burst generation and control of membrane excitability." J Neurophysiol **93**(5): 2710-2722.

Wu, S. H. and J. B. Kelly (1996). "In vitro brain slice studies of the rat's dorsal nucleus of the lateral lemniscus. III. synaptic pharmacology." J Neurophysiol **75**(3): 1271-1282.

Xu-Friedman, M. A. and W. G. Regehr (2004). "Structural contributions to short-term synaptic plasticity." Physiol Rev **84**(1): 69-85.

Yamashita, T., et al. (2003). "Developmental increase in vesicular glutamate content does not cause saturation of AMPA receptors at the calyx of held synapse." Journal of Neuroscience **23**(9): 3633-3638.

Yang, H. and M. A. Xu-Friedman (2009). "Impact of synaptic depression on spike timing at the endbulb of Held." J Neurophysiol **102**(3): 1699-1710.

Yau, K. W. (1976). "Physiological properties and receptive fields of mechanosensory neurones in the head ganglion of the leech: comparison with homologous cells in segmental ganglia." J Physiol **263**(3): 489-512.

Yin, T. C. and J. C. Chan (1990). "Interaural time sensitivity in medial superior olive of cat." J Neurophysiol **64**(2): 465-488.

Zemankovics, R., et al. (2010). "Differences in subthreshold resonance of hippocampal pyramidal cells and interneurons: the role of h-current and passive membrane characteristics." J Physiol **588**(Pt 12): 2109-2132.

Zhang, H. and J. B. Kelly (2001). "AMPA and NMDA receptors regulate responses of neurons in the rat's inferior colliculus." J Neurophysiol **86**(2): 871-880.

Zhang, H. and J. B. Kelly (2006a). "Responses of neurons in the rat's ventral nucleus of the lateral lemniscus to amplitude-modulated tones." J Neurophysiol **96**(6): 2905-2914.

Zhang, H. and J. B. Kelly (2006b). "Responses of neurons in the rat's ventral nucleus of the lateral lemniscus to monaural and binaural tone bursts." J Neurophysiol **95**(4): 2501-2512.

Zook, J. M. and J. H. Casseday (1982). "Origin of ascending projections to inferior colliculus in the mustache bat, Pteronotus parnellii." J Comp Neurol **207**(1): 14-28.

Zucker, R. S. and W. G. Regehr (2002). "Short-term synaptic plasticity." Annu Rev Physiol **64**: 355-405.

AFFIDAVIT

I herewith declare that I autonomously carried out the PhD-thesis entitled „Input-Output Functions of Sensory Neurons in the Central Nervous System with Focus on the Physiological Basis underlying Information Transfer in the VNLL“.

No third party has been used.

I did not receive any assistance in return for payment by consulting agencies or any other person. No one received any kind of payment for direct or indirect assistance in correlation to the content of the submitted thesis.

I conducted the project at the following institution: Institute of Zoology, University of Veterinary Medicine Hannover.

The thesis has not been submitted elsewhere for an exam, as thesis or for evaluation in a similar context.

I hereby affirm the above statements to be complete and true to the best of my knowledge.

_____

ACKNOWLEDGEMENT

Sincere gratitude is owed to my first supervisor Prof. Dr. Felix Felmy. I would like to thank you for giving me the opportunity to work on this great project, for continuous support and motivation during the experimental and writing process, and for giving me the opportunity to meet excellent people who work in this research field. For me, you have been an outstanding mentor. Secondly, I would like to thank Prof. Dr. Anaclet Ngezahayo and Prof. Dr. Evgeni Ponimaskin as members of my supervision group. Your helpful comments and advice allowed me to think more outside the box and to improve my research.

In addition, I thank our collaboration partners at the LMU in Munich, Prof. Dr. Christian Leibold and Michael Rebhan, for providing your programming skills and your expertise for this project. Moreover, thanks go to Dr. Frank Scherbarth, Dr. Boris Chagnaud, and Prof. Dr. Andreas Herz for support and helpful comments on the leech paper.

Further I would like to express many thanks to my colleague Nikolaos Kladisios for your numerous helpful comments and discussions on my project. I had a great time with you as an office and laboratory mate and enjoyed our productive time in the institute. Furthermore, I would like to thank Alexandra Benn for her technical support in the lab.

My thanks also go to Jennifer Wittkowski, for the refreshing and amusing coffee breaks we had. Further, I would like to thank my temporary colleagues Elisabeth Meyer and Anna Sternberg. I will remember the time you spent at our institute as amazingly livid and motivating. Furthermore, I would like to thank the animal care takers for their work.

Beyond that, I would like to thank my friends and fellow PhD students Rebecca Möller, Sarah Schwarz, and Teresa Wenhart for giving me a good time in Hannover. Furthermore, I would like to express sincere appreciation to Daniel Schmidtke. Thank you so much for your ongoing support.

Finally, very special thanks go to my family. I cannot express how thankful I am to have you standing behind me. Your support for my academic career and our mutual visits in Stuttgart and Hannover gave me the perseverance for this PhD project.